

Electronic Thesis and Dissertation Repository

8-26-2019 2:00 PM

Development of a Computational Method for Assessing Static Field Induced Torque on Medical Implants

Xiao Fan Ding
The University of Western Ontario

Supervisor
Chronik, Blaine A.
The University of Western Ontario

Graduate Program in Medical Biophysics
A thesis submitted in partial fulfillment of the requirements for the degree in Master of Science
© Xiao Fan Ding 2019

Follow this and additional works at: <https://ir.lib.uwo.ca/etd>



Part of the [Medical Biophysics Commons](#)

Recommended Citation

Ding, Xiao Fan, "Development of a Computational Method for Assessing Static Field Induced Torque on Medical Implants" (2019). *Electronic Thesis and Dissertation Repository*. 6452.
<https://ir.lib.uwo.ca/etd/6452>

This Dissertation/Thesis is brought to you for free and open access by Scholarship@Western. It has been accepted for inclusion in Electronic Thesis and Dissertation Repository by an authorized administrator of Scholarship@Western. For more information, please contact wlsadmin@uwo.ca.

Abstract

The objective of this thesis is the development of a computational method for finding the torque induced on an object when placed in the static magnetic field of an MR scanner. As a preliminary step, the classic EM problems of a sphere and infinitely long cylinder of linear material was modeled in commercially available simulation software. Upon verification of the parameters implemented, the second step is the simulation of simple objects with realistic material properties, stainless-steel cylinders. Physical cylinders were machined to match those in the simulations and underwent the ASTM standard method for measuring induced torque. An adjacent study that was also performed was finding the measurement uncertainty in a prototype ASTM abiding apparatus, separate from the one used for experimental verification.

It was found that the sphere and infinitely long cylinder models differed less than 5% from the analytical solutions. Implementing the correct material properties, magnetic susceptibility in particular, to the grades of stainless-steel used in this study was particularly challenging. However, when the experimentally measured results were used to find the necessary susceptibility values for the computational methods, it was found to be in agreement with literature values. The following computationally-found torque values agreed within 10% difference from the experimentally measured values. The induced torque increased linearly with the length of the cylinders and the square of magnetic susceptibility.

In the uncertainty analysis of the torque measurement apparatus described in ASTM F2213-17, it was found that the apparatus described in the ‘Pulley Method’ offered a lower instrument uncertainty than the apparatus described in the ‘Torsional Spring Method’. This study emphasized on the contribution of static friction and is important to consider should the apparatus be used in the future to verify computational results.

Keywords: Magnetic Resonance Imaging; Static Field; Magnetic Field; Magnetic Flux; Magnetically Induced Torque; Implantable Medical Devices; Stainless-steel; Cylinder; Sphere; Linear Material; MR Safety; MR Environment; Magnetic Susceptibility; ASTM; COMSOL

Summary for Lay Audience

Magnetic Resonance Imaging (MRI) is a method of visualizing the inside of the human body by using a variety of magnets to create a complex electromagnetic environment, or MR environment, contained within the scanning room. Since the 1990s, MRI has seen widespread adoption around the world and has since received a reputation being a safe imaging method due, in part, to the intense scrutiny that MRI technicians place on what is allowed into the scanning room.

A common signage at any MRI site is the warning that ‘The Magnet is Always On’. When foreign material, anything not already contributing to the MR environment, enter the MRI site, it may interact with the magnetic fields being generated. Material of any kind have magnetic properties. Pure iron for example, can fly across the scanning room, like a projectile, due to the displacement force exerted on it by the scanner’s magnetic fields. Human tissue, on the other hand, is so weakly magnetic that they appear to be inert until extremely high magnetic field strengths, far above what is currently clinically approved.

A significant population of patients who may benefit from MRI exams are those living with medical implants. However, the magnetic properties of the implant are not always known. Testing for implant safety is often laborious since implants often have many components allowing for innumerable configurations making it impractical to rely on experimental testing alone. Therefore, the objective of this thesis is the development of the capability to assess medical implants quickly and accurately by computational means. The particular interaction explored in this thesis is the induced rotational force on an implant from the magnetic field generated by the main magnet.

Co-Authorship Statement

It is the intention of the author to publish the work presented in Chapter 2 co-authored by Xiao Fan Ding, William B. Handler, and Blaine A. Chronik. William Handler offered assistance and suggestions in to the development of the computational methods used as well as data analysis. William Handler and Blaine Chronik reviewed the written work. Blaine Chronik aided in apparatus setup and taking measurements for validation of simulations and was responsible for overall supervision of the study. Development of the computational methods, production of scripts, measurements, analysis, and writing was performed by Xiao Fan Ding.

The work presented in Chapter 3 was submitted and accepted as an abstract to the international Society of Magnetic Resonance in Medicine (ISMRM) ¹. This body of work was presented as a digital poster at ISMRM 2019 and it is the intention of the author to publish this work co-authored by Xiao Fan Ding, William B. Handler, and Blaine A. Chronik. William Handler offered assistance and suggestions on improvements in the data analysis. William Handler and Blaine Chronik reviewed the written work. Blaine Chronik was responsible for overall supervision. Apparatus setup, measurements, writing, and analysis was performed by Xiao Fan Ding.

¹ Ding, X., Handler, W. B., & Chronik, B. A. (2018). Uncertainty Analysis of Torque Measurement Methods Described in ASTM F2213-17. In *ISMRM*. (1441). Montreal.

Acknowledgements

The work presented in this thesis could not have been completed without all those who have offered their guidance and support in my personal and professional development. I would like to use this space to give my acknowledgements to those people.

First and foremost, I must thank Dr. Blaine Chronik who has acted as my supervisor for the past two years. He gave me the opportunity to work at the xMR Labs and guided me through the trials and tribulations of academic research. In addition, I would like to acknowledge Dr. William Handler, the lead researcher at the xMR Labs and an indispensable source of knowledge through his intelligence, wit, and humour. Our interactions were few but each one worthwhile. I would also like to acknowledge my advisory committee, Dr. Tamie Poepping and Dr. Jean Theberge and The Ontario Research Fund, NSERC, and Canadian Foundation for Innovation as sources of funding.

Furthermore, I would like to acknowledge Frank van Sas, Brian Dalrymple, and Derek Gignac for the design and manufacturing of the apparatuses used throughout my research as well as machining of the stainless-steel rods. Not to mention, occasionally they would 3D print Star Wars figurines that I designed on a whim.

My experience with graduate school got off to a rough start. When at my lowest, I could always count on my lab mates to raise my spirits. On my first day I was in the company of Christopher Brown, Amgad Louka, Eric Lessard, Kieffer Davieau, and Arjama Halder. Along the way Diego Martinez and John Adams joined our group. I know without a doubt that I will forever cherish the friendships I've made in the past two years.

Last but not least, I must thank my family. My father is the intellectual of my family and my greatest inspiration in seeking higher education. My mother is my greatest source of encouragement and continually supports me in all aspects of life. My sister is ten years my junior and still at the age with grandiose dreams and ambitions. Watching my sister has helped me keep my own dreams and ambitions alive.

Table of Contents	Page
Abstract	ii
Summary for Lay Audience	iii
Co-Authorship Statement	iv
Acknowledgements	v
Table of Contents	vi
List of Figures and Tables	x
List of Symbols and Abbreviations	xii
Chapter 1: Introduction	1
1.1 Motivation	2
1.2 Research Objective	4
1.3 MR Systems	4
1.3.1 The Main Magnet	8
1.3.2 The Gradient Coils	11
1.3.3 The Radiofrequency Coils	14
1.3.4 The Electromagnetic Environment of an MRI System	17
1.3.5 The Screening Process for Patients Entering the MR Environment	19
1.4 Medical Devices	22
1.4.1 Electromagnetic Material Properties	24
1.4.2 Interactions with an MR Scanner	26
1.4.2.1 Radiofrequency Interactions	27
1.4.2.2 Gradient Interactions	29
1.4.2.3 Magnetically Induced Displacement Force	31
1.4.2.4 Magnetically Induced Torque	33
1.5 Electromagnetic Interactions Relevant to Torque	35
1.5.1 A Sphere of Linear Magnetic Material	36
1.5.2 An Infinitely Long Cylinder of Linear Magnetic Material	38
1.5.3 Force and Torque on a Magnetic Dipole Moment	39
1.6 Regulatory Environment	39
1.6.1 How Large Families of Implants Are Assessed	41
1.6.2 ASTM Methods for Device Interactions in MR	42
1.6.3 ASTM Methods for Torque Assessment	43
1.7 Thesis Overview	47
1.8 References	48

Chapter 2: Computational Evaluation of Stainless-Steel Cylinders for Static Field Induced Torque	54
2.1 Introduction	55
2.2 Theory	56
2.2.1 Magnetic Field Inside and Outside of a Sphere	59
2.2.2 Magnetic Field Inside and Outside of an Infinitely Long Cylinder	59
2.2.3 The Force on a Magnetic Dipole Moment	60
2.2.4 The Volume Magnetic Susceptibility of Stainless-Steel Alloys	60
2.3 Methods	63
2.3.1 Part 1: Verification of Parameters for Simulating Linear Magnetic Material in a Static Magnetic Field	63
2.3.2 Part 2: Simulation of Stainless-Steel Rods in a Static and Uniform Magnetic Field.....	66
2.3.2.1 Computational Setup	67
2.3.2.2 Experimental Setup	70
2.4 Results	75
2.4.1 Part 1: 3D Slice Plots from COMSOL and Analytical Plots MATLAB	75
2.4.2 Part 1: Verification with Analytical Solution	78
2.4.3 Part 2: Finding the Magnetic Susceptibilities of the Stainless-Steel Cylinders	80
2.4.4 Part 2: Experimentally Measured Induced Torque	82
2.5 Conclusion.....	84
2.5.1 Validity of Using FEM to Find the Field Inside and Outside of Objects of Linear Magnetic Material	84
2.5.2 Verification of Computational Method to Calculate the Torque Induced on Stainless-Steel Cylinders from the Static Field of an MR Scanner	84
2.6 References.....	86

Chapter 3: Uncertainty Analysis of Torque Measurement Methods Described in ASTM F2213-17 88

3.1	Introduction	89
3.2	Theory	90
3.2.1	Error Propagation in the Torsional Spring Method	90
3.2.2	Error Propagation in the Pulley Method	91
3.2.3	Sources of Measurement Uncertainty	92
3.3	Methods	93
3.4	Results	96
3.5	Conclusion	99
3.6	References	100

Chapter 4: Thesis Summary, Future Directions, and Conclusion 101

4.1	Thesis Summary	101
4.1.1	Chapter 2 Summary	101
4.1.2	Chapter 3 Summary	102
4.2	Future Directions	102
4.1.1	Investigate Torque Induced on Better Characterized Material	102
4.1.2	Extend Computational Torque and Force Models to More Complex Objects	102
4.1.3	Investigate Eddy Current Torque	103
4.1.4	Automating Computational Processes	103
4.1.5	Investigate Very Long Objects Experiencing Interactions in Tandem	104
4.1.6	Extend Uncertainty Analysis of Rotating Test Platforms	104
4.3	Conclusion	105

Appendix A: Derivation of Equations	106
A.1 Spherical and cylindrical coordinates	107
A.2 Finding the magnetic flux density inside and outside of a sphere of linear material with the external field along z-direction	108
A.3 Finding the magnetic flux density inside and outside of an infinitely long cylinder of linear material with the external field perpendicular to the cylinder	111
A.4 Finding the static field induced torque on a sphere	113
Appendix B: Certificate of Tests for Stainless Steel Rods	115
B.1 Stainless steel 316 rod, diameter of 0.5 in. and length of 1 ft.	115
B.2 Stainless steel 316 rod, diameter of 0.25 in. and length of 1 ft.	117
B.3 Stainless steel 304 rod, diameter of 0.5 in. and length of 1 ft.	119
B.4 Stainless steel 304 rod, diameter of 0.25 in. and length of 1 ft.	121
Appendix C: Calibration Reports for Laboratory Equipment	123
C.1 MR03-025 Force Sensor (Mark-10 Co., Copiague, USA)	123
C.2 SPX123 Laboratory Balance (Ohaus Co., Parsippany, USA)	124
Appendix D: Permission to Use Copyrighted Figures	126
D.1 Allen D. Elster of MRIquestions.com	126
D.2 Standards Council of Canada Letter of Agreement	127
D.3 John Wiley and Sons License Terms and Conditions	129
D.4 ASTM International License Terms and Conditions	133
D.5 Cambridge University Press License Cover Sheet	139
Curriculum Vitae	142

List of Figures and Tables

Figure	Page
1.3-1	The components of an MR system 6
1.3-2	Cross-sectional view of an MR system 7
1.3-3	Applying shims to the main magnet 10
1.3-4	Main magnet coil windings and active shielding 10
1.3-5	Positioning of RF, gradient, and main magnet coils 13
1.3-6	Trapezoidal gradient pulse shape 14
1.3-7	Birdcage and surface coils 16
1.3-8	Saddle and birdcage coil designs 17
1.3-9	The MR environment within 5 Gauss 19
1.3-10	ACR zoning recommendation for MR suites 21
1.4-1	ASTM symbols for MR safe, unsafe, and conditional 23
1.4-2	Spectrum of magnetic susceptibility 26
1.4-3	Device interactions from static, gradient, and RF fields 27
1.4-4	Schematic of the deflection test method for static field induced force 32
2-1	Orientation of the external magnetic field 58
2-2	Sphere and cylinder models in COMSOL 64
2-3	Meshed sphere and cylinder models in COMSOL 65
2-4	Set of cylinders in COMSOL 68
2-5	Positions of 3 cm long cylinder exported from COMSOL 70
2-6	Crank operated linear displacement mechanism 71
2-7	Machined stainless-steel cylinders 72
2-8	Rotating apparatus holding cylinders 73
2-9	Measurement setup in the MR suite 74
2-10	Magnetic flux plots from COMSOL 76
2-11	Magnetic flux plots based on analytical solution 77
2-12	Analysis of field inside and outside of sphere 78
2-13	Analysis of field inside and outside of cylinder 79
2-14	Plot of anticipated peak torque and magnetic susceptibility 80

3-1	Schematic diagram of apparatus from ASTM F2213-17	94
3-2	Schematic and photograph of apparatus designed for the pulley method	95
3-3	Propagation of errors for the ‘Torsional Spring’ and ‘Pulley’ methods	98
A-1	Spherical and cylindrical coordinates	107

Table		Page
2-1	Magnetic susceptibility values for stainless-steel alloys	61
2-2	ASTM composition requirements for SS304 and SS316	62
2-3	Equations for susceptibility curves	81
2-4	Measured peak torque values	82
2-5	Comparison of measured and simulated peak torque values	83
3-1	‘Break torque’ observations	97
3-2	Sources of instrument uncertainties	97

List of Symbols and Abbreviations

MR and MRI	Magnetic resonance and magnetic resonance imaging
CADTH	Canadian Agency for Drugs and Technologies in Health
OECD	Organization for Economic Co-operation and Development
ICDs	Implantable cardioverter defibrillators
RF	Radiofrequency
PNS	Peripheral nerve stimulation
FDA	Food and Drug Administration
NbTi	Niobium-titanium
LHe	Liquid helium
SNR	Signal-to-noise ratio
DSV	Diameter of spherical volume
B and B₀	Magnetic flux density ('B-field') and external magnetic flux density
H and H₀	Magnetic field strength ('H-field') and external magnetic field strength
EMF	Electromotive force
NMR	Nuclear magnetic resonance
ω_0	Larmor frequency
γ	Gyromagnetic ratio
M	Magnetization
SAR	Specific absorption rate
ACR	American College of Radiology
ISO	International Organization for Standardization
ASTM	ASTM International (formerly 'American Society for Testing and Materials')
CDRH	Center for Devices and Radiological Health
μ_m or μ	Permeability of the material
μ_0	Permeability of vacuum
μ_r	Relative permeability
χ_m or χ	Volume magnetic susceptibility
AIMDs	Active implanted medical devices
IEC	International Electrotechnical Commission

EPI	Echoplanar imaging
\mathbf{F}_m	Magnetically induced displacement force
\mathbf{m}	Magnetic dipole moment
M_s	Saturation magnetization
V and dV	Volume of device and volume of element
DUT	Device under testing
θ	Deflection angle
\mathbf{F}_g	Weight ('force due to gravity')
ρ	Density
\mathbf{g}	Acceleration due to gravity
N_n and N_t	Demagnetizing factor perpendicular to the plane of the device and demagnetizing factor in the plane of the device
W_T	Magneto-static energy per unit volume
α	Angle of the saturation magnetization with respect to the normal in plane of the device
R	Radius
τ	Torque
PMA	Premarket approval
NEMA	National Electrical Manufacturers Association
F and F_f	Force and frictional force
L	Longest dimension of device
μ	Coefficient of friction
θ_{repose}	Angle of repose
k	Torsional spring constant
$\Delta\theta$	Deflection angle in torsional spring method
FEM	Finite element method
SS 304 and SS 316	Stainless-steel grade 304 and 305
mfnc	Magnetic fields, no currents
PDE	Partial differential equations
IED	Infinite element domain

Chapter 1

Introduction

This thesis investigates the capacity to use computer simulations to predict the phenomenon of an induced torque on medical devices placed in a static and uniform magnetic field, such as those produced at the magnetic isocentre of an MR scanner. The phenomenon of magnetically induced torque is an aspect in the regulation of medical devices entering the commercial market. The motivation behind this thesis is first described through the current prevalence of MRI as an imaging modality and the usage of medical devices. The electromagnetic environment concerning medical devices is described through the technical details of a typical MRI scanner. This is followed by a description of material properties that a medical device may have and what interactions arise from foreign objects, inanimate and biological, entering an electromagnetic environment. Mathematical concepts of electricity and magnetism that are relevant to torque are then described for objects of simple geometries. An overview of the regulatory environment and standard testing methods for medical devices is presented. Finally, the last section contains an overview of the thesis.

1.1 Motivation

Magnetic Resonance Imaging (MRI) is a non-invasive and non-ionizing imaging modality that has seen annual growth in Canada and abroad. In Canada, three times as many MRI units were installed than decommissioned between 2012 and 2016, suggesting a trend of net growth in the future [2]. An estimated 1.86 million MRI examinations were performed in the 2017 to 2018 Canadian fiscal year, approximately 51 examinations per 1000 people, up from 1 million MR scans in 2007 [1]. Internationally, the Organization for Economic Co-operation and Development (OECD), an intergovernmental economic organization whose mission is to improve the economic and social well-being of people around the world, uses the number of MRI units and examinations as a metric for assessing quality of healthcare [3]. Amongst OECD members, there was an upwards trend in the number of MRI examinations between 1995 to 2017 [4].

The growth in the use of MRI has been in parallel with the growth in the implementation of permanent and semi-permanent implantable medical devices [5]. In 2003, over 370,000 implants of device-based therapies using implantable cardiac systems, pacemakers and implantable cardioverter defibrillators (ICDs), occurred in the United States [5]. In Canada, there were more than 120,000 patients and 15,000 patients living with pacemakers and ICDs respectively [6]. With the growth of these two phenomena, it is estimated that 50-75% of patients living with such an implant will require an MRI exam over the lifetime of their device [5].

During an MRI exam, the patient is exposed to strong, static, magnetic fields from the main magnet, \mathbf{B}_0 . In addition, there are also the radiofrequency (RF) fields and the spatially and temporally varying gradient magnetic fields. During an MRI scan, the patient (or parts of) is exposed to all these fields and the safety of the procedure has been a concern since the introduction of MRI as a clinical imaging modality. The gradient and RF fields require upper limits since there are known phenomena that may cause harm to a patient. From the gradients, there is peripheral nerve stimulation (PNS) while the RF fields cause tissue heating. However, apart from short-term discomfort, there has yet to be a known case where long-term irreversible patient injury was brought upon by the static field [7,17].

There have been no indications that fields as high as 16 T have an adverse effect on animal subjects, well above the 1.5 T to 3 T fields used in clinical scanners [7,8]. In 2017, the FDA approved the first clinical 7 T scanner limited to the head and extremities, arms and legs [55]. Although exposure to strong magnetic fields have not shown adverse effects on patients without medical implants, the same cannot be said for patients with medical implants.

As mentioned, up to 75% of patients living with medical implants may require an MR exam over the lifetime of their device however, there are concerns regarding safety when examining patients with medical implants. These concerns include, but are not limited to, magnetically induced displacement force and torque, gradient and RF induced heating, and gradient induced vibrations [9,10,11]. It becomes clear that the growth of MRI as a diagnostic tool together with the increased use of medical implants, there is a need to accurately and systematically test for the safety of such devices in the MR environment.

Commercially available medical implants need to be approved by a governing body to enter an MR scanner. To determine the risk that an implant poses, implants are subjected to experimental testing outlined by test standards for different interactions between implant and scanner. Test standards are available for investigating the following, but are not limited to, force torque from the static field, heating, vibrations, and voltages from the pulsed gradient coils, and heating from the RF coils [11,13-15]. The results from testing for each interaction are compiled to create a safety label that stipulate whether an implant is safe, unsafe, or conditional in an MR scanner [26]. This thesis focuses on magnetically induced torque.

For a single implant, it is reasonable to rely on physical testing to determine its risk in an MR scanner. However, in a family of implants where each serve a similar purpose but differ in the material, geometry, position, or orientation, there comes an innumerable amount of combinations. It becomes impractical to physically test for every conceivable configuration of even a single device. A simulation capable of accurately determining the interaction of an implant in an MR environment can alleviate the task of physical testing. The MR environment is defined to be the three-dimensional volume of space surrounding the MR magnet that contains both the Faraday shielded volume and the 5 Gauss line [26].

Therefore, it includes the uniform field inside the scanner, the static field gradient around the scanner, the pulsed gradients and RF fields as well.

1.2 Research Objective

The objective of this thesis was to design simulations capable of accurately determining the magnetically induced torque on entire families of medical implants in the MR environment. As previously mentioned, there are other possible interactions between the implant and the MR environment, those interactions are not discussed in this thesis. A simulation may alleviate the workload of assessing the safety of all the commercially available medical implants. Provided the static magnetic field along with the material, geometry, and orientation of the device being tested, the simulations should have the capacity to output the induced torque for any combination of the aforementioned parameters. The simulations are not intended to replace physical testing altogether, but rather, to go through the many configurations that exist and identify the ‘worst-case’ configurations. The identified worst-case configuration is then subjected to physical testing to identify the conditions for which it is safe for the implant to be present in the MR scanner.

1.3 MR Systems

A complete MR system is made up of many components working together to ultimately form an image. Figure 1.3-1 and 1.3-2 depict cross sections of a cylindrical MR scanners from the front and side respectively [16]. Modern 1.5 T and 3 T scanners use current-driven electromagnets while permanent magnets were used more often in the past in low field (< 0.35 T) scanners.

Permanent Magnets – The magnetic field of a permanent magnet is always present. Unlike current-driven magnets, permanent magnets supply a magnetic field for an indefinite amount of time with no cost to maintenance [17,19]. A common material used to produce permanent magnets is an alloy of aluminum, nickel, and cobalt known as alnico [16]. The use of permanent magnets is limited due to being extremely heavy and a maximum static field of less than 1 T [50].

Resistive Magnets – These are made up of coils of wire through which an electrical current is passed [17]. The field strength of resistive magnets is dependent on the current that passes through the coils. Resistive magnets are less limited by weight than permanent magnets but require much higher costs due to the large quantities of power required to maintain the magnetic field [16]. The maximum field strength of a system made from resistive magnets is typically 0.6 T due to its excessive power requirements [16,17].

Superconducting Magnets – Like resistive magnets, these are made up of coils of wire through which an electrical current is passed. The phenomenon of superconductivity occurs when certain materials conduct electricity with little to no electrical resistance when cooled below a critical temperature. Cryogenics are the substances used to supercool the coils. The cryostat is a device which houses the coils and cryogenics and maintains the extremely low temperatures for superconductivity. The material used in the large majority of MR scanners is niobium-titanium (NbTi), which becomes superconducting at approximately 10 K. A common cryogen used to supercool NbTi is liquid helium (LHe) which has a boiling point of 4.2 K [17,39]. Once a current has been established and the field has been ramped up, a superconducting magnet requires little to no additional power to maintain the magnetic field. Superconducting magnets are used in mid and high-field systems with field strengths greater than 0.35 T [17,18,41].

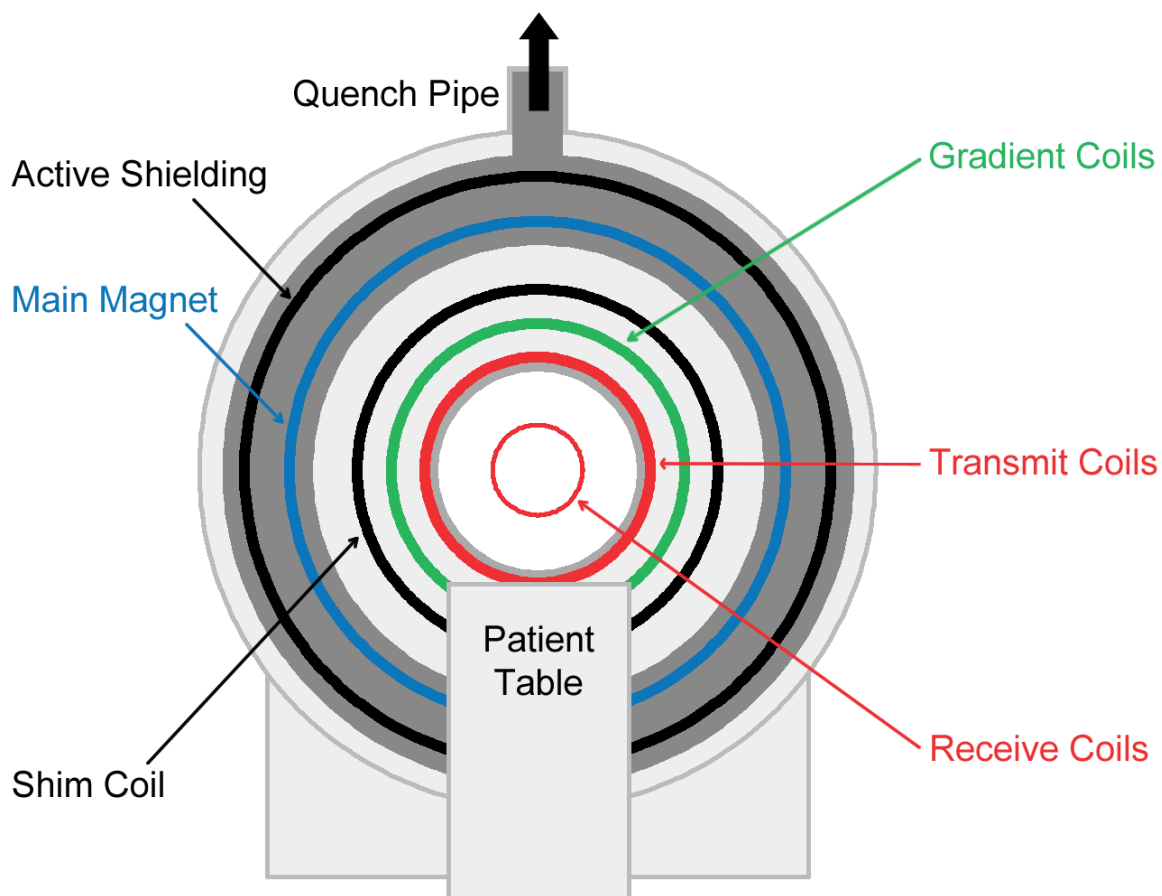


Figure 1.3-1: The components of a complete MR system. The patient table is used to position the patient into the bore. The main magnet shown is a superconducting magnet made up of a set of coils (blue) inside a cryogen bath (dark gray). The active shielding coils reduce the fringe fields around the magnet. The quench pipe is used to expel evaporated cryogens outside into the atmosphere. Shim coils are used to correct for field inhomogeneities and improve uniformity at the imaging region within the bore [16,17]. The RF transmit and receive coils (red) and gradient coils (green) are vital components that generate an image.

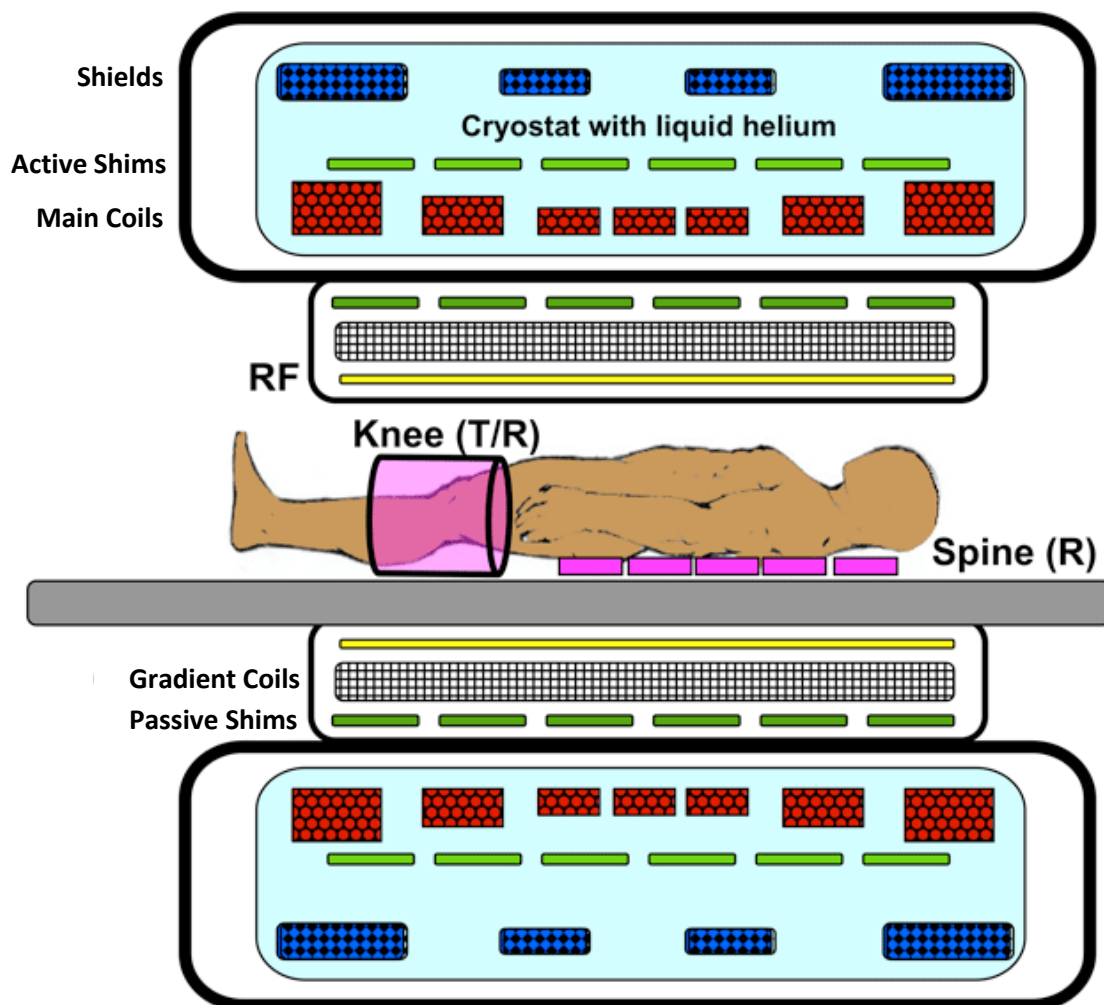


Figure 1.3-2: A cross-sectional view of an MRI scanner. The most exterior object is the main magnet which houses the main magnet coils (red), active shims (green), and active shielding (red) all submerged in liquid helium. Nested within the main magnet are gradient coils (b/w grid) and a set of passive shims (green). An RF transmit/receive coil (pink, left) is placed over the knees of the patient and a set of receive only coil array (pink, right) are placed below the spine. Courtesy of Allen D. Elster, MRIquestions.com.

1.3.1 The Main Magnet

The main magnet supplies the static magnetic field, \mathbf{B}_0 . This field is in the direction of the bore, where the patient lies. Low-field MRI magnets (less than 0.35 T) use a combination of resistive and permanent magnets. However, resistive magnets require large power consumption and permanent magnets have high installation cost [41]. Over time, low-field scanners have been replaced by 1.5 T scanners while studies that require greater resolution in MRI have been conducted using 7 T and 9.4 T [8,40,41]. The benefit of higher fields is the increased signal-to-noise ratio (SNR), a crucial aspect for image quality. Fields greater than 0.35 T require superconducting magnets, with 1.5 T scanners being the predominant field strength in the clinical setting, MRI is the largest commercial application of superconductivity [41].

In theory, superconducting magnets require no power to maintain once a current is established since zero electrical resistance means the current never dies out. In reality, imperfections in coil design add some resistance to the circuit and over time, there is a loss in magnetic field. Historically, the LHe used to supercool coil windings regularly evaporates into gas that needs to be expelled into the atmosphere requiring refills every 4.5 months [17,41,42]. Modern magnets have zero-boil off technology allowing helium gas to re-condense into LHe within the cryostat [41,42].

Ideally, the region of the scanner bore where the patient lies should have a completely homogeneous static field from the main magnet. Field homogeneity is measured in parts per million (ppm) over a certain diameter of spherical volume (DSV). The magnetic isocenter is the centre of the DSV. The requirement for commercial 1.5 T and 3 T magnets is a homogeneity on the order of 10 ppm of the static field over a 50 cm DSV [41]. For context, any two positions within ± 25 cm of the magnetic isocentre of the bore should not differ more than 1.5 μT or 3 μT on a 1.5 T or 3 T scanner respectively. The loss in field strength should be no more than 0.1 ppm per hour [41,42].

Due to design limitations however, the static field produced from a commercial magnet is not entirely homogeneous [17]. Standard commercial magnets may have inhomogeneities of up to a hundred ppm [41]. Reducing inhomogeneities is done through

passive and active shimming. In the absence of a patient, passive shimming is performed by placing ferromagnetic metal sheets, shims, in shim trays that are arranged along the circumference of the bore [41,43]. When field inhomogeneities arise from interactions between a patient and the static field, active shimming is used. Shim coils, either superconducting or resistive magnets, rely on a current to generate a magnetic field opposite to the inhomogeneities [17].

A quench refers to the loss of superconductivity, and consequentially the magnetic field, when the coil windings are raised above the critical temperature [17]. NbTi is superconducting at approximately 10 K and cooled in LHe at 4.7 K [17,39]. During a quench, the heat generated raises the temperature enough such that there is a large amount of boil-off of LHe [17]. The quench pipes are to guide the gas out of the building. Quenches can be accidental or intentional in emergencies, such as when there is a fire in the scanner room or when a patient is pinned to the scanner. The latter is a concern when ferromagnetic objects in the scanner room become a projectiles due to an induced force from the static field. In those events, the field needs to be turned off by an emergency quench [51].

Magnetic shielding is the process of reducing the size of the fringe fields, the stray fields produced by and surrounding the exterior of the main magnet [17]. The strength of the fringe fields decreases with distance but may interfere with sensitive electronic equipment [51]. Early unshielded magnets were placed inside large rooms to accommodate for fringe fields. Passive shielding methods incorporate iron or steel plates into the walls, ceiling, and floor of the magnetic room while self-shielding magnets use iron plates either attached to the outside of the cryostat or incorporated them into the magnet design [17,52]. Modern superconducting magnets for MRI are actively shielded and include an additional set of coils separate from the main coils that generate \mathbf{B}_0 . In actively shielded superconducting magnets, the fringe fields are suppressed within the cryostat where the shielding wires are superconducting as well. The industry standard requires the field outside of the scanning suite to not exceed 5 Gauss. It is assumed that at 5 Gauss, devices such as pacemakers, remain properly functional [17,41]. Pacemakers often include a magnetic switch that may be affected by the magnetic field strengths higher than 5 G.

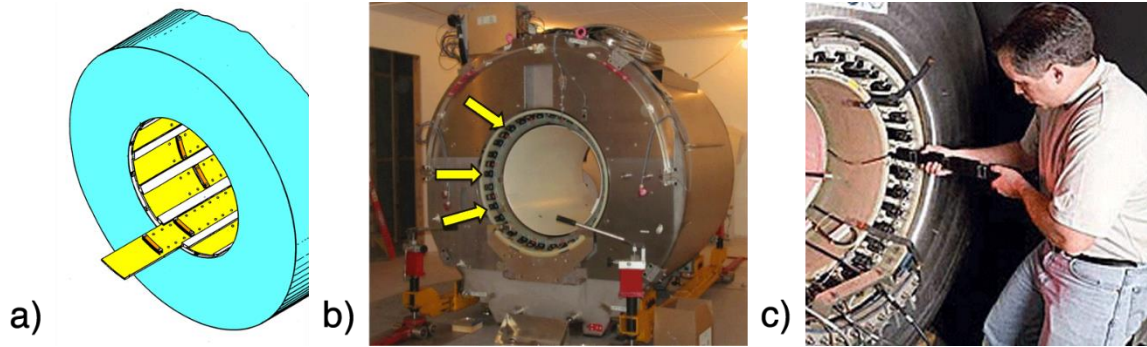


Figure 1.3-3: a) Diagram showing the arrangement of shim trays (yellow) along the inner bore of the magnet (blue). b) Photograph of shim trays arranged along the magnet bore. c) Positioning the shim tray. Courtesy of Allen D. Elster, MRIquestions.com.

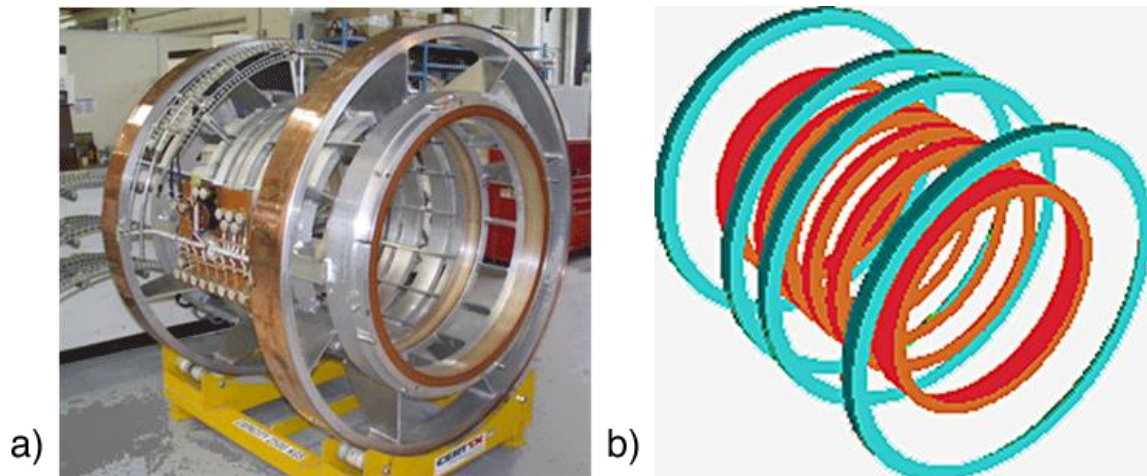


Figure 1.3-4: a) Main and shielding coils of a superconducting magnet before being enclosed in a cryostat. b) Shielding coils (blue) are in series with the main coil windings (orange) but carry current in the opposite direction. Courtesy of Allen D. Elster, MRIquestions.com.

1.3.2 The Gradient Coils

The purpose of the gradient magnetic fields from the gradient coils is to spatially encode the positions of the nuclei of the sample in the scanner by creating a variation in the Larmor frequency, the intrinsic precessional frequency of a magnetic dipole in an external magnetic field, as a function of position [36,49]. The cylindrical gradient coils are placed inside the bore and sit between the main magnet and the RF coils. The most common configuration used consists of three sets of coils used to generate three orthogonal fields G_x , G_y , and G_z that are pulsed intermittently [35,36]. The role of the gradient coils is to vary the z component of the static field, B_z , linearly along the Cartesian axes x , y , and z .

$$G_x = \frac{\partial B_z}{\partial x} \quad G_y = \frac{\partial B_z}{\partial y} \quad G_z = \frac{\partial B_z}{\partial z} \quad (1.3-1)$$

The gradients are resistive magnets and the fields are produced by passing a current through the wires arranged on a cylindrical surface. For clinical scanners the gradient strengths are on the order of mT per metre.

The variation in static magnetic field is achieved by superimposing the gradient fields on the static field [16,35]. Since the static field is in the direction of the bore, B_x and B_y are negligible and assumed to be zero. After the gradients have been applied, the field is still in the direction of the bore, but the field strength varies linearly along x , y , and z depending on the applied gradient. Before applying gradients, the static field is given the following,

$$\mathbf{B} = \begin{pmatrix} B_x \\ B_y \\ B_z \end{pmatrix} = \begin{pmatrix} 0 \\ 0 \\ B_0 \end{pmatrix} \quad (1.3-2)$$

Afterwards,

$$\mathbf{B} = \begin{pmatrix} 0 \\ 0 \\ B_0 + G_x x + G_y y + G_z z \end{pmatrix} \quad (1.3-3)$$

The gradient fields are not always present, they are pulsed intermittently and the rate at which they are pulsed have an operational limit that is in part determined by PNS

[36]. PNS is discussed in greater detail in section 1.4.2.2 on gradient interactions. In short, by Faraday's law of induction, a changing magnetic field will induce an electromotive force (EMF), measured in volts, across a conducting material [17,23]. The switching of the gradients can induce a voltage on nerves, conductive tissue in the human body [17]. The effect of stimulation occurs when the induced current exceeds the depolarization threshold of the nerve and initiates an action potential across the cell membrane [17,54].

As mentioned, the gradient fields are pulsed intermittently. By Faraday's law of induction, the rate of change of pulsed gradients can induce localized electric currents, eddy currents, in conductive material. Scanner components such as the shims, coils, cryostat, and scanner housing are all subject to induced eddy currents. One method to avoid or reduce eddy currents outside the imaging region is to use active shielding. This is accomplished by implanting an additional set of coils, shield coils, that are placed exterior to the gradient coils [36]. The wires of the shield coils are positioned such that the fields generated in between the gradient and shield coils cancel out [36,38].

Some characteristics of the gradient field produced are the amplitude, rise time, and slew rate [16]. The strength of the gradient, the gradient amplitude, are typically between 10 and 60 mT/m. The gradient amplitude directly affects image resolution. High gradient amplitudes are required for images with smaller field of views and thinner slice widths. The rise time is the time it takes for gradients to reach the gradient amplitude. Conversely, fall time is the time it takes for the gradient strength to fall from the gradient amplitude to zero. The rise time, and fall time, is usually expressed in microseconds with typical values from 1000 to 200 microseconds [17]. In order to maintain the same resolution and field of view, higher gradient amplitudes allow for shorter rise times. High speed imaging techniques require gradient amplitudes of 20 mT/m or higher. The slew rate is described as the strength of the gradient over distance and is calculated by dividing the gradient amplitude by the rise time [16,17]. Typical gradient slew rates for body coils are in the order of 150-200 T/m/s and can go above 400 T/m/s for head-only.

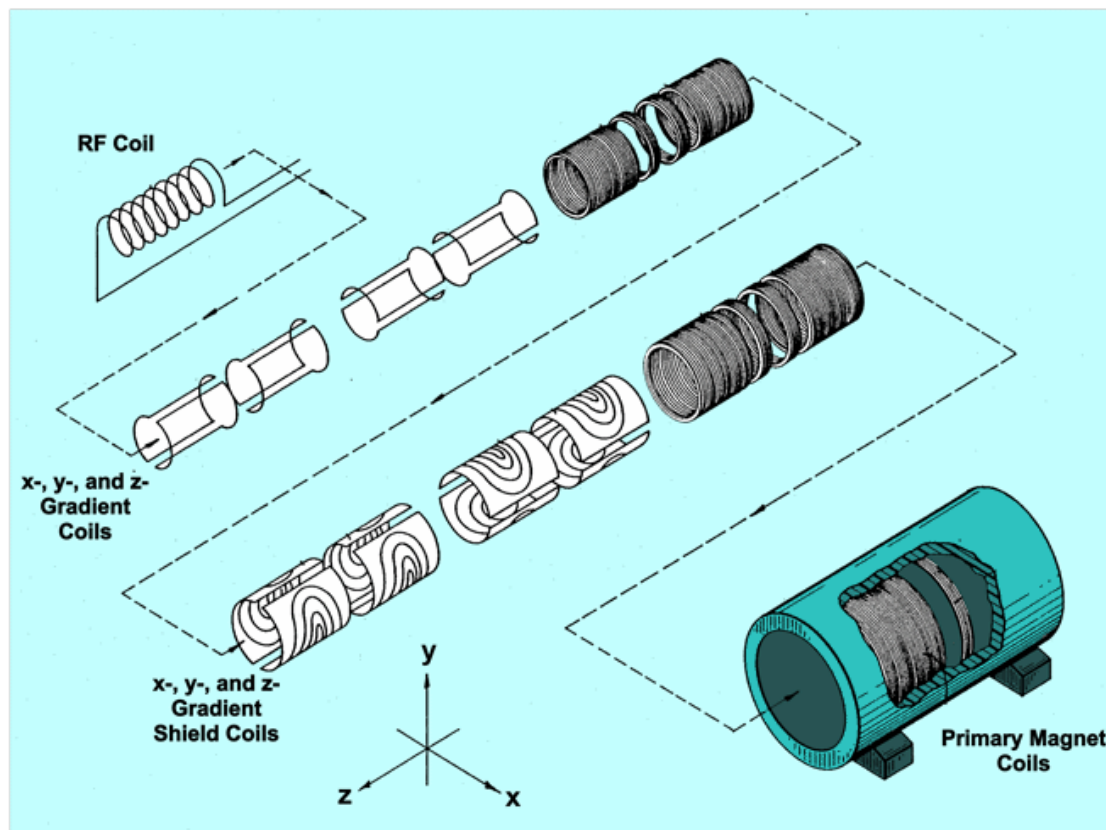


Figure 1.3-5: Positioning of RF coils, gradient coils, and actively shielded gradients in the MR scanner. The outermost structure is the main magnet. Placed within the main magnet are actively shielded gradients. Actively shielded gradients consist of primary (gradient) coils and secondary (shielding) coils. The RF coils are the smallest and are placed between the gradients and patient. Courtesy of Allen D. Elster, MRIquestions.com.

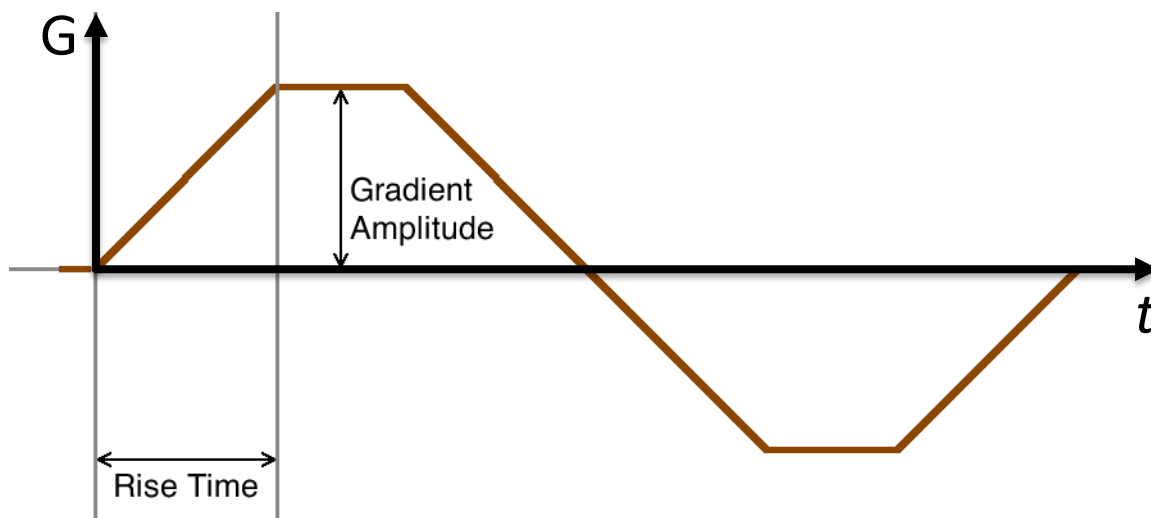


Figure 1.3-6: A gradient pulse in a trapezoidal shape. Moving from left to right, the strength of the gradient rises from zero to its max amplitude and maintains that amplitude for some time before falling to zero. The reverse then occurs, where the gradient strength falls to the min amplitude and rises to zero. Take for example, when the z-gradient is applied with a max amplitude of 10 mT/m (1 G/cm). Inside of a 120 cm long bore of a 3 T scanner, the field strength along z would vary from 2.994 T to 3 T at the isocentre and to 3.006 T. At the min amplitude of -10 mT/m, the field inside varies from 3.006 T to 2.994 T from end to end. The gradient then rises to zero. The rise and fall times in this figure are equal [16,17].

1.3.3 The Radiofrequency Coils

The physical phenomenon that MRI relies on to generate a signal from is nuclear magnetic resonance (NMR) [17]. NMR describes how nuclei aligned to an external magnetic field are exposed to an RF source at the resonant frequency, it will respond by producing a detectable electromagnetic signal [53]. The application of an RF source that exploits the phenomenon of resonance is termed excitation. In MRI, the nuclei that is often excited is hydrogen, whose nucleus consists of a single proton. The Larmor frequency, ω_0 , is an intrinsic property of nuclei with odd number of protons and neutrons. The Larmor

frequency is the frequency at which such a nuclear system precesses about an external magnetic field, \mathbf{B}_0 , and is directly proportional to \mathbf{B}_0 by the gyromagnetic ratio [49].

$$\omega_0 = \gamma B_0 \quad (1.3-4)$$

Excitation of the nuclei and detection of the signal produced is performed by the RF coils. The RF transmit coil send out short bursts of electromagnetic waves in the radio frequency range, known as an RF pulse, to excite the nuclei and the signal produced is detected by the RF receiver coil [16].

In the absence of an external field, the nuclear magnetic moments of the nuclei in a sample are aligned randomly resulting in no net magnetization, \mathbf{M} [16]. Classically, magnetization is described as net magnetic dipole in a volume [48]. The main magnet supplies the necessary external field, \mathbf{B}_0 , and subsequently generating some net magnetization aligned with \mathbf{B}_0 . Net magnetization, as with any other vector, can be separated into components. The longitudinal component, \mathbf{M}_z , is aligned with \mathbf{B}_0 while the transverse component, \mathbf{M}_{xy} , is in the plane formed by the remaining two directions [49]. With the use of gradients in addition to a strategically chosen and simultaneously applied RF pulse, a particular slab of material can be excited [16,47]. The \mathbf{M}_{xy} created by resonance can then be detected by a receiver coil [16].

The RF transmit coil produce a time varying RF field, denoted by \mathbf{B}_1 , that is perpendicular to \mathbf{B}_0 . The net magnetization, \mathbf{M} , is aligned with \mathbf{B}_0 until \mathbf{B}_1 is applied at the Larmor frequency and ‘tips’ \mathbf{M} away by some tip angle, α . The duration of the applied \mathbf{B}_1 field is short and typically in the millisecond range. It is for that reason that they are referred to as RF pulses. After excitation, the signal produced in response to the RF pulse are detected by a receiver coil [17]. To put it simply, it is known that by Ampere’s law, a magnetic field is generated when a current passes through a wire [23]. Conversely, by Faraday’s law, if a loop of wire is exposed to an oscillating field, a current is induced in the loop and the resulting voltage constitutes the MR signal [16,23]. The purpose of the receiver coil is to maximize signal detection while minimizing the noise, in other words, maximize SNR [17].

A volume coil can both transmit and receive and encompasses the entire anatomy for head, extremity, or whole-body imaging [16]. In horizontal bore MR systems, where \mathbf{B}_0 is oriented horizontally, the transmit coil is likely to be a saddle coil or birdcage coil design. In a saddle coil, six wires are arranged at 60° intervals. This is so that an approximate sinusoidally varying current around the surface can be achieved. The birdcage coil design improves homogeneity over the saddle coil by increasing the number of conductors. It consists of two conductive loops connected by an even number of conductive rungs [17]. Birdcage coils are capable of yielding uniform SNR over the entire imaging volume [16]. However, although volume coils provide greater uniformity in RF excitation, their large size produce images with lower SNR than other types of coils.

Surface coils tend to be receive-only and are used to improve SNR when imaging structures near the surface of the patient. In general, the closer the coil is to the structure under examination, the greater the SNR as the coil is closer to the signal emitting anatomy. There is also the benefit of shaping surface coils to fit easily near the anatomy since the loop is not restricted to a circle. However, the signal and noise received from surface coils only correspond to volume of area located around the coil. For a circular coil, the depth to which the coils can detect signal is proportional to the radius of the loop [16]. For example, a 10 cm diameter circular loop can image tissue up to 10 cm in length and to a depth of 5 cm. A coil array system uses multiple surface coils whose individual signals are combined to create one image with improved SNR and increased field of view. A drawback of surface coils is that smaller loops provide greater SNR at the cost of field of view. Array systems seek to benefit from greater sensitivity to signal and increased coverage.

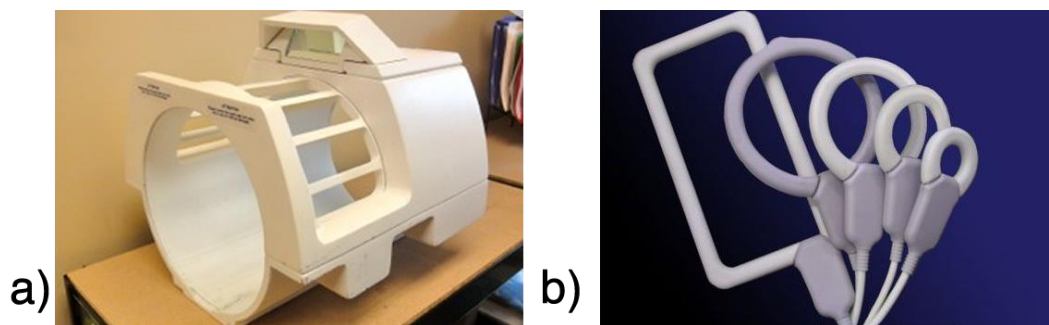


Figure 1.3-7: a) A transmit/receive birdcage coil. b) A variety of receive-only coils. Courtesy of Allen D. Elster, MRIquestions.com.

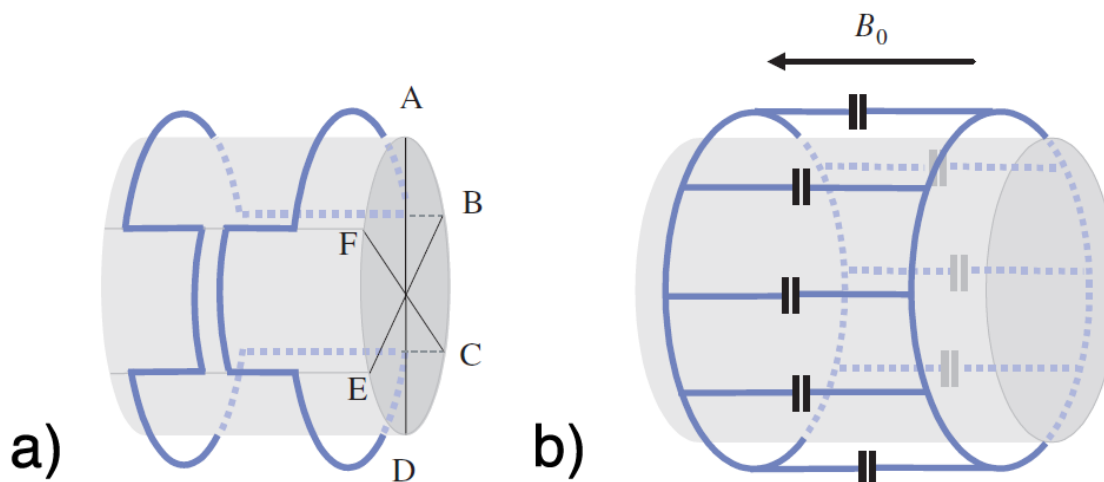


Figure 1.3-8: The saddle coil and birdcage coil designs of transmit/receive volume coils. a) Saddle coil where the current runs from point A to B and so forth until point F. To approximate for a sinusoidally varying current, the conductors at A and D carry zero current while it rises from . b) Birdcage coil consisting of two conductive loops connected by conductive rungs [17]. Reprinted with permission from Cambridge University Press, reference 17.

1.3.4 The Electromagnetic Environment of an MRI System

The electromagnetic environment of an MRI system, the MR environment, is defined as the volume of space within the 5 Gauss line that extends in all directions from the MR scanner. If the 5 Gauss line is within the Faraday shielded room, the entire room is considered to be the MR environment [15]. Surrounding the scanner, the MR environment is made up primarily of the fringe fields of the main magnet. Inside the scanner bore, the static field is always present while the switched gradients and RF pulses occur intermittently for imaging purposes. Understanding the interactions between foreign material, biological or otherwise, entering this environment is the objective of MRI safety and medical device testing.

When biological material such as human tissue is exposed to the MR environment, there are two potentially harmful effects that may occur. The first is heating in tissue due to exposure to RF pulses. The rate of change of the temperature is directly proportional to a quantity known as the specific absorption rate (SAR) which quantifies the power deposited into a mass of tissue by RF exposure and is measured in watts per kilogram. As a precaution, RF tissue heating is restricted to less than a single degree Celsius of the approved SAR limit by body area [9,17]. The second is PNS from the switched gradients [17,37]. Generally, PNS causes discomfort but is not harmful as modern scanners have stimulation monitor that alerts the operator/technician of the likelihood of PNS. It becomes hazardous when occurring on cardiac muscles however, cardiac stimulation requires 80 times the PNS threshold [17]. Extended exposure to the static field however, has shown no long-term adverse biological effects [6,17]. No biological effects have been observed in human subjects under 2 T while there have been reports of fatigue, headaches, and irritability on subjects exposed to fields greater than 2 T [16].

Interactions between medical implants and the MR environment will be discussed in greater detail in section 1.4.2. To summarize, there is a great variety of interactions that may occur when material enter the MR scanner. The static field may induce displacement force [15]. In particular, ferromagnetic objects can experience the projectile effect where the induced force is strong enough for the object to become airborne [16]. In addition, medical implants may also experience an induced torque from the static field, which is the only interaction being investigated in this thesis [14]. Recall that by Faraday's law, the rapidly changing gradients can induce eddy currents on conductive material [11,17]. Eddy currents lead to heating in the device enclosures, battery components, and the internal circuitry. When eddy currents are induced on planar surfaces, in combination with the static field, there is the possibility of induced vibrations [11]. RF induced heating can occur on passive and active implants which can in turn lead to temperature rises in area of tissue surround the implant [11,15]. In addition, all of the aforementioned interactions can in turn lead to device malfunction [11].

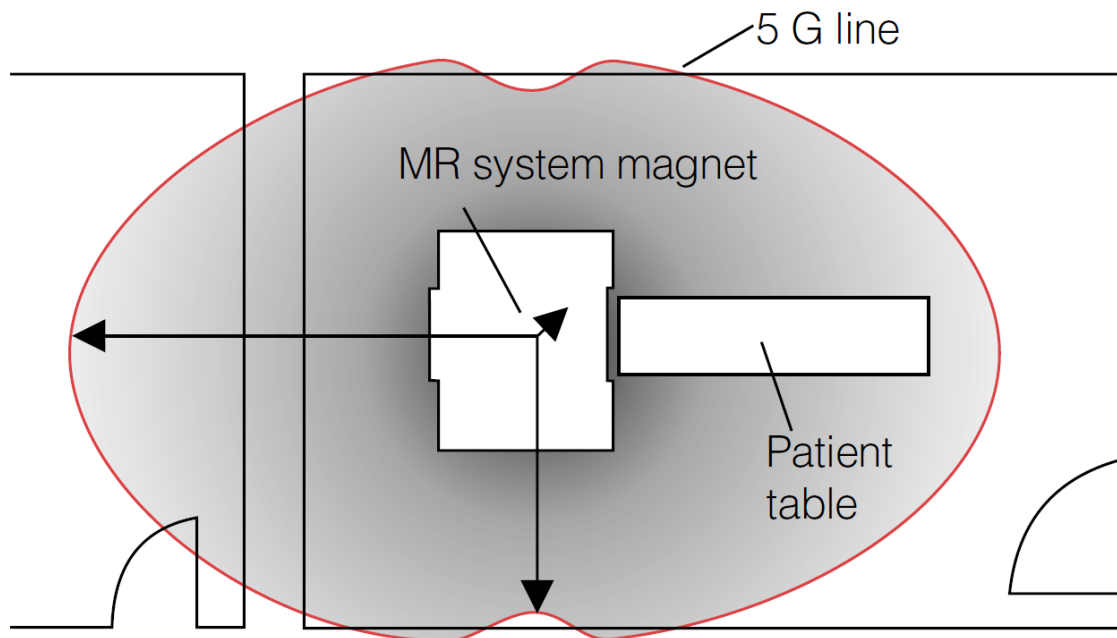


Figure 1.3-9: The electromagnetic environment of an MRI scanner, the MR environment, is defined to be the volume of space enclosed by the 5 Gauss line produced from the MR scanner. The 5G line extends in three dimensions around magnet bore [44]. Reprinted with permission from ECRI Institute, Plymouth Meeting, Pennsylvania.

1.3.5 The Screening Process for Patients Entering the MR Environment

The American College of Radiology developed the guidance document for safe MR practices. Though not a regulatory standard, the four zones model is widely used in the screening processes for individuals proceeding from the outside the MR facility in zone one to the scanner room in zone four [44-45]. The four zones are defined by the ACR as follows [45]:

Zone I – All areas freely accessible to the general public. This area is outside of the MR environment (no field higher than 5 G) and is uncontrolled and unregulated.

Zone II – This area is the interface between Zone I and Zone III. Patients are under supervision by MR personnel and are not free to move throughout Zone II at will. Patient screening and ferromagnetic detection occurs at this zone. Like Zone I, no field higher than 5 G in Zone II.

Zone III – This area is not freely accessible by unscreened non-MR personnel. Ferromagnetic objects or equipment in this area can result in serious injury or death as a result of interactions between individuals or equipment and the MR environment. All access to Zone III, which often provide access to Zone IV, is to be strictly physically restricted, controlled by, and under the supervision of MR personnel. Starting in Zone III, there begin to be fields higher than 5 G.

Zone IV – This is the room that contains the MR scanner and is accessed through Zone II or III. The highest field strengths are within this room and so, there is also the greatest risk. All ferromagnetic objects that have been identified to pose as a risk are excluded from this room.

The MR screening process is a multilevel process consisting of a preliminary interview followed by an MR screening form. The form contains questions to determine the medical history and metal exposure history of the patient. There are two levels of MR personnel. Level 1 personnel have passed minimal safety education and can work within zone 3 and level 2 personnel have received extensive training and education in the broader aspects of MR safety. Those who qualify to be level 2 personnel (i.e. MR technologists, radiologists, and certified MR physicists) are tasked with conducting physical examinations for signs of medical implants if the medical history of the patient cannot be obtained [44,45].

The use of ferromagnetic detectors should be for the purpose of detecting such objects external to the patient before they are brought to zone 4, they are not a replacement for the screening process. The ACR guidance document recommends against using conventional metal detectors since some MR conditional metals, such as aluminum and titanium, may trigger the metal detector alarm while ferromagnetic material in nonferromagnetic enclosures may not [44].

Before entering zone 3, any individual undergoing an MRI scan is required to remove all readily removable metallic personal items and devices on their body. The screening process should have ensured that all non-readily removable metallic items have been considered and have been identified as compatible in the MR environment. Any individual not undergoing an MR scan is subject to the same screening process before entering zone 3 or 4.

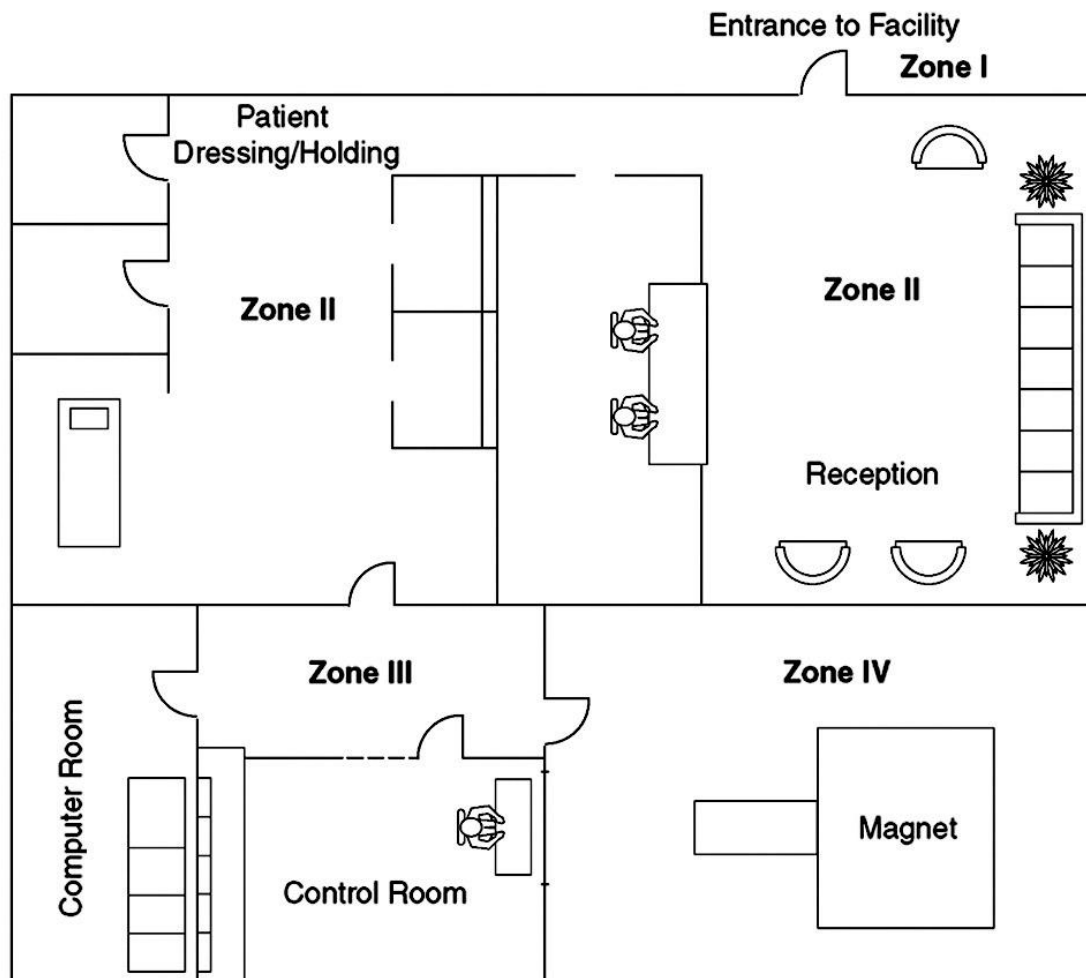


Figure 1.3-10: Sample floor plan illustrating the four zones system in a typical magnetic resonance suite published by the ACR [45]. Sometimes the 5 G line is wholly contained in zone IV and there is no zone III. Courtesy of Allen D. Elster, MRIquestions.com.

1.4 Medical Devices

The standard published by the International Organization for Standardization, ISO 13485 is in regard to medical devices and quality management systems. It is an internationally agreed standard for quality management in the medical device industry [31]. To paraphrase the ISO document, the following is a definition of a medical device [26].

Medical Device – any instrument apparatus, machine, implant, material, or other similar or related article, intended by the manufacturer to be used, alone or in combination, for human beings for one or more of the specific purpose or purposes of diagnosis, prevention, monitoring, treatment, or alleviation of disease or injury, supporting or sustaining life.

ISO 13485 definition is also used by ASTM International in the test standards for magnetically induced displacement force and torque as well as for medical device marking [14,15,26]. The ASTM standard for RF induced heating from passive implants uses a definition for an implant in medicine [13]. It stipulates that an implant is an object, structure, or device intended to reside within the body for diagnostic, prosthetic, or other therapeutic purposes. The Medical Devices Bureau of Health Canada states that a medical device could be any product used in the treatment, mitigation, diagnosis or prevention of a disease or abnormal physical condition [24]. Health Canada uses the ISO 13485 when it comes to quality system certificates.

Medical devices vary greatly in complexity, from pacemakers and defibrillators to bedpans and gloves [60]. When a device is readily removable, there is little to no concern for when the patient enters an MR scanner. This thesis was written in regard to the concerns with permanent or semi-permanent implantable medical devices. Systematically testing for the safety of medical implants during MR scans began in the 1990s as a response to the rapid growth of MRI as a diagnostic method. The U.S. Center for Devices and Radiological Health (CDRH), a branch of the Food and Drug Administration (FDA), requested ASTM International (then named the American Society for Testing and Materials) to develop test standards for various device interactions [25]. This resulted in the development of the ASTM standards regarding magnetically induced force and torque, RF induced heating, and medical device marking amongst others. The ASTM task group requested by the

CDRH proposed the following set of terminology for classifying medical devices by safety in an MR scanner [25].

MR Safe - An item that poses no known hazards in all MR environments. MR Safe items are composed of materials that are electrically non-conductive, non-metallic, and non-magnetic [25,26].

MR Conditional - An item that has been demonstrated to pose no known hazards in a specified MR environment with specified conditions of use. To be present within an MR scanner, the field conditions that need to be known include, but are not limited to, the field strength, spatial gradient, dB/dt, RF fields, and SAR [25,26].

MR Unsafe - An item that is known to pose hazards in all MR environments [25]. An item which poses unacceptable risks to the patient, medical staff or persons within the MR environment [26].



Figure 1.4-1: Symbols proposed by ASTM International in ASTM F2503-13 for MR Safe, MR Conditional and MR Unsafe [26]. Reprinted with permission from ASTM International, reference 26.

1.4.1 Electromagnetic Material Properties

Some material properties that can result in interactions with the EM environment from the MR scanner include conductivity and resistivity, permittivity, and permeability. Electrical conductivity represents a material's ability to conduct an electric current while conversely, resistivity is how strongly a material resists the flow of an electric current and can be found by taking the reciprocal of the conductivity. An excellent conductor such as copper, the material commonly used in coil windings, has a conductivity of 6×10^7 S/m and resistivity of 1.68×10^{-8} Ωm at 20°C. Air on the other hand, a poor conductor, has a resistivity on the order of 10^{16} Ωm and a conductivity on the order of 10^{-15} S/m at 20°C. The permittivity of a material describes the amount of charge needed to generate electric flux in that material and is denoted by ϵ_m . The permittivity of vacuum is constant and denoted by ϵ_0 . The relative permittivity is the ratio of ϵ_m to ϵ_0 and is denoted by ϵ_r .

The permeability of a material is the measure of a material's ability to allow an external magnetic field to pass through it. It can be described as the degree of magnetization that a material obtains when placed in an external magnetic field. The permeability of a material is denoted by μ_m while the permeability of vacuum is μ_0 . The relative permeability of a material is the ratio of μ_m to μ_0 and is denoted by μ_r . A related concept is the magnetic susceptibility of a material, χ_m , which is a measure of how much a material will become magnetized when exposed to an external magnetic field. Mathematically, χ_m is a dimensionless quantity that is the proportionality constant found by the ratio of the net magnetization, \mathbf{M} , and the magnetic field strength, \mathbf{H} [56].

The magnetic susceptibility of materials can be used to broadly categorize materials into one of three groups since magnetism is an intrinsic property of matter and all substances possess in some form [16]. Materials are categorized as diamagnetic, paramagnetic, or ferromagnetic. As mentioned previously, this thesis focuses on materials in the paramagnetic range with the reason being that some of the most common metals to be used in medical implants such as stainless steel, titanium, and cobalt chrome, are all within the paramagnetic range [27,28].

Diamagnetism – Materials of this kind exhibit no net magnetic dipole moment until they are exposed to an external magnetic field. When an external field is applied, these materials show a magnetic moment that opposes the applied field. Diamagnetic materials repel the external magnetic field and have a negative magnetic susceptibility. Diamagnetism is an effect that occurs in all materials however, the effect is overcome in paramagnetic and ferromagnetic material that possess stronger attraction to the external field. Diamagnetic substances include inert gases, copper, and silver [16].

Paramagnetism – Without an external magnetic field present, the magnetic moments in a paramagnetic material exist in random orientations that cancel each other out and thus have no net magnetic moment. When an external field is applied however, the magnetic moments of paramagnetic substances align in the direction of the field and are denoted by a positive magnetic susceptibility. Paramagnetic materials affect the magnetic field in a positive way and are attracted by the applied field [16].

Ferromagnetism – When ferromagnetic material, come into contact with an external magnetic field, there is strong attraction and alignment. Even when taken out of the field, ferromagnetic materials retain their magnetization, are permanently magnetized and become permanent magnets [16].

A common source of confusion regarding the magnetic susceptibility of a material is the usage of the term itself. There are three concepts to recognize, volume, mass, and molar susceptibilities. What is typically referred to as magnetic susceptibility is the volume susceptibility, a dimensionless quantity. Mass and molar susceptibilities are defined in terms of the magnetization per unit mass or mole of material [56]. When referring to the magnetic susceptibility of a material in this thesis, it is the volume susceptibility, the dimensionless proportionality constant between \mathbf{M} and \mathbf{H} , that is being described.

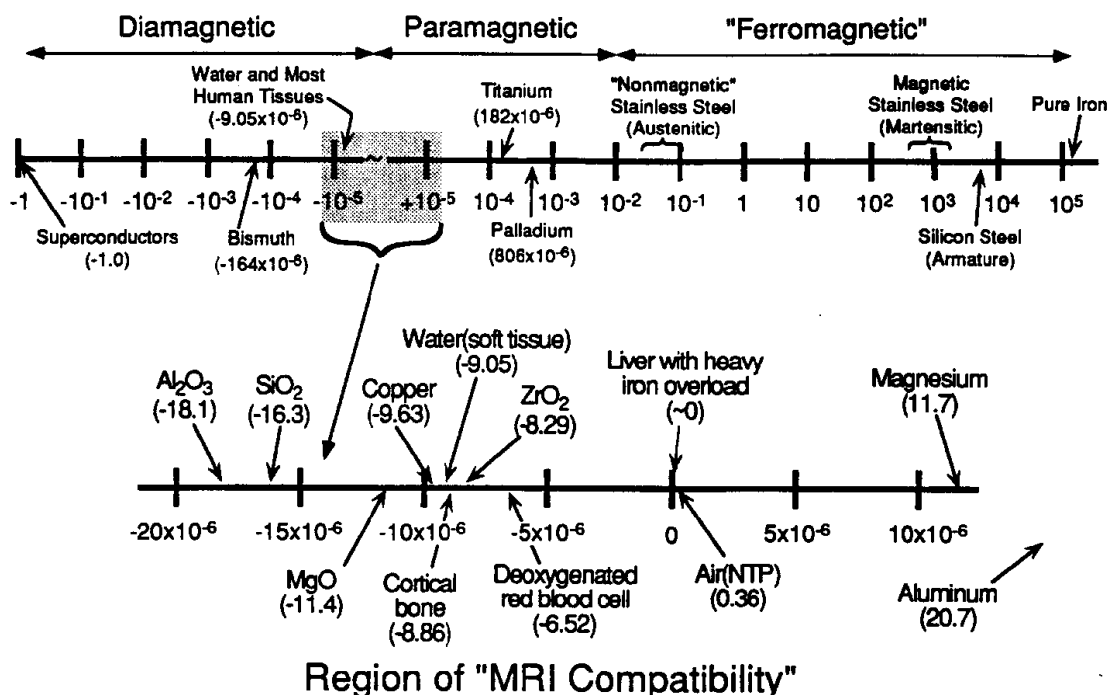


Figure 1.4-2: The spectrum of magnetic susceptibility divided into diamagnetic, paramagnetic, and ferromagnetic regions with well-known materials labelled [7]. The ferromagnetic region of the section begins at $\chi_m > 10^{-2}$. Medical implant grade metals such as commercially pure titanium and stainless steel are shown in the paramagnetic region [7,27,28]. Although these materials are not ferromagnetic, they are outside of the region of MRI compatibility. Reprinted with permission from John Wiley and Sons, reference 56.

1.4.2 Interactions with an MR Scanner

The different possible device interactions, and some biological interactions, were mentioned previously in section 1.3.4. This subsection will discuss the possible interactions in more detail. Interactions of magnetic materials in the MR environment include, heating from RF and gradient fields, vibrations from the gradients, and force and torque from the static field. Figure 1.4-3 is from ISO/TS 10974, a document outlining a variety of test methods for assessing the safety of medical implants in MRI.

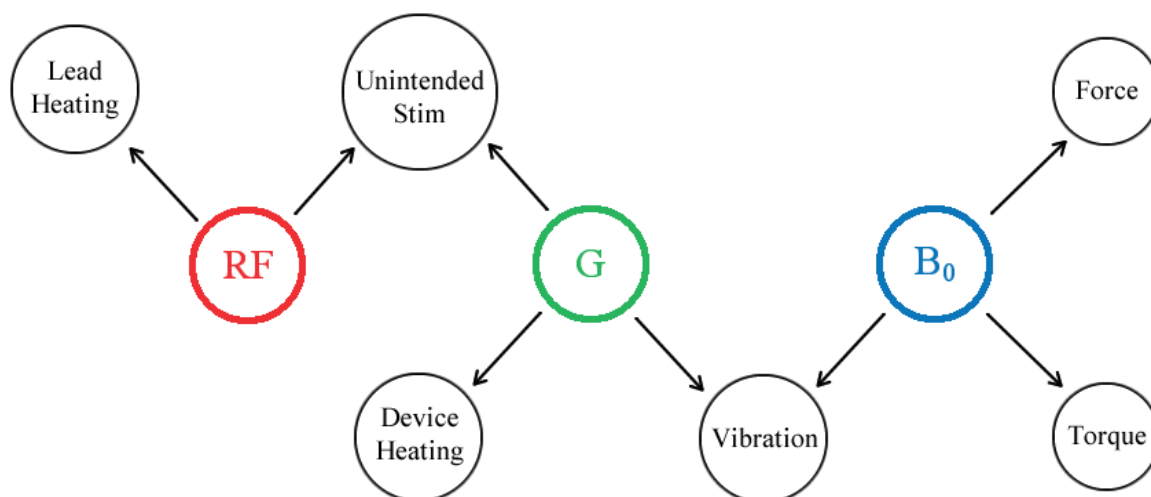


Figure 1.4-3: Possible device interactions with the static magnetic field, B_0 , pulsed gradient and radiofrequency fields. This diagram was retrieved from the standard, ISO/TS 10974, which offers methods for evaluating all of the interactions shown as well as device malfunction from output fields individually and in tandem [11]. ASTM International has also published test standards for magnetically induced force and torque, and RF induced heating in passive implants [13-15]. The International Electrotechnical Commission has published test standards on the safety and performance of medical electric equipment in MRI [34]. Copied by Xiao Fan Ding with the permission of the Standards Council of Canada (SCC) on behalf of ISO.

1.4.2.1 Radiofrequency Interactions

The primary concern from exposure to the RF fields is heating, which can occur in human tissue as well as in the tissue regions surrounded by passive medical implants and the leads of active implanted medical devices (AIMDs) [11,15,17]. Passive implants do not require a supply of electricity while active implants do.

The phenomenon of tissue heating in MRI is due to the exposure of tissues to RF pulses. Recall that RF pulses are named so because they are millisecond applications of electromagnetic waves in the radiofrequency range of the spectrum. Therefore, RF pulses are a form of electromagnetic radiation that carry some energy [23]. It is that energy being

deposited into the body after an applied RF pulse in MR imaging. The energy deposited manifests as joule heating owing to the small electrical conductivity of biological tissue [57].

The characteristics of tissues in relation to the incident RF wavelength are important factors in determining power deposited into tissue by and RF pulse. If the tissue is large, in surface area, in relation to the incident wavelength, RF energy is predominantly absorbed on the surface. Conversely, if the tissue is small compared to the wavelength, there is little absorption at all [58].

RF induced temperature rise in tissue is related to the SAR, a measure of power deposited into tissue by RF exposure. SAR is not a measure of heating, though it is directly proportional to the rate of change of temperature. SAR is the RF power absorbed per unit mass of an object. The expression for SAR is given in equation 1.4-1 where σ is the conductivity of the material, E is the electric field amplitude, and ρ is the density of tissue [9].

$$\text{SAR} = \frac{\sigma E^2}{2\rho} \quad (1.4-1)$$

The rate of the change of temperature in tissue as a response to SAR is given by equation 1.4-2 where T is the temperature, t is time, and C is the specific heat capacity and $C_{\text{water}} \cong 4186 \text{ J}/(\text{kg} \cdot ^\circ\text{C})$ [9].

$$\frac{dT}{dt} = \frac{\text{SAR}}{C} \quad (1.4-2)$$

The International Electrotechnical Commission (IEC) defines four measures of SAR [9],

Whole-body – SAR averaged over the total mass of the patients' body over a specified time. The limit is $2 \text{ W} \cdot \text{kg}^{-1}$ in normal operation.

Partial-body – SAR averaged over the mass of the patients' body that is exposed by the volume RF transmit coil and over a specified time. The limit is $2\text{-}10 \text{ W} \cdot \text{kg}^{-1}$ in normal operation, depending on the amount of exposed patient mass.

Head – SAR averaged over the mass of the patients' head and over a specific time. The limit is $3.2 \text{ W} \cdot \text{kg}^{-1}$ in normal operation.

Local – SAR averaged over any 10 g of patient body and over a specific time. The limit is 10-20 $\text{W} \cdot \text{kg}^{-1}$, depending on the part of the body.

The IEC SAR limits are for an averaging time of 6 min, under normal operating mode, and SAR values over any 10 s period cannot exceed three times the stated values [9]. Normal operating mode is the mode of operation of MR equipment in which none of the outputs have a value that can cause physiological stress to patients [11,34]. Normal operating mode is in the absence of additional sources that can cause stress/harm to patients such as medical implants. With the presence of medical implants, passive or active, RF induced heating in tissue can be enhanced. As opposed to normal operating mode, first level controlled operating mode is the operation of MR equipment under medical supervision appropriate to the patient's condition. Second level operating mode requires ethics approval from an institutional review board and is typically for human research [34]. It should be noted that a single RF pulse can produce a large enough instantaneous SAR that exceeds SAR limits. A single pulse however, is unlikely to provide sufficient energy to result in significant temperature rise [9].

1.4.2.2 Gradient Interactions

Foreign material interacting with the pulsed gradients during MRI may experience heating, vibrations, and voltages. Biological tissue interacting with the pulsed gradients may experience PNS. Due to the temporally changing gradient magnetic field, dB/dt , eddy currents may form on conductive material. Not only conductive components that make up an implant in a patient, but also the conductive tissue, nerves, of the patient [9,11]. Device interactions may lead to harm, discomfort, or malfunction [11]. PNS causes discomfort and becomes hazardous when occurring near cardiac tissue [17].

Gradient induced heating can occur on medical devices that have electrically conducting components (i.e. device enclosure, internal circuitry, and battery components).

Heating occurs due to the induced eddy currents from the temporally changing magnetic field [11]. An alternative name for this effect may be eddy current induced heating [10]. Following Faraday's law of induction, the change of the magnetic field through the suitable devices induces eddy currents and the material subsequently converts electric energy into thermal energy [17,59]. The effect of heating increase with distance from the magnetic isocentre [10].

Gradient induced vibrations are most common on conductive planar surfaces and are caused by the time varying magnetic moments produced from the aforementioned induced eddy currents. Vibrations are a potential for patient harm as they may cause devices to malfunction. In the absence of conductive surfaces, there is little likelihood of induced vibrations [11]. Apart from vibrations, when the induced magnetic moments interact with the static field, there is the potential for induced torque apart from the induced static torque from device interaction with static field [9].

Gradient induced electric potentials, or gradient induced voltages, can occur within a single AIMD lead, between AIMD leads, or between electrodes and a conductive AIMD enclosure. These voltages, when in contact with adjacent tissue, can cause harm to the patient. As with all the aforementioned device interactions, device malfunction is also a possibility [11,33].

Apart from foreign objects interacting with the switched gradients, biological tissue can also interact leading to the safety concern of PNS [9]. The effect of PNS has previously been mentioned in section 1.3.4 and will be discussed in greater detail here. Take for example, in single shot echo-planar imaging (EPI), a rapidly oscillating gradient is used to collect all the signal from a sample. As mentioned previously, the gradients are used to spatially encode the positions of the nuclei of the sample in the scanner [36]. The method by which this is done is by making the magnetic field inside the bore vary linearly with position. In single shot EPI, all of the data is acquired after one RF excitation pulse. The high dB/dt from this process raises concerns of induced eddy currents on the peripheral nerves. It has been shown that PNS affects a substantial percentage of the general population [32]. The IEC limit on dB/dt in regard to PNS is given in equation 1.4-3. The

limit is on a 20-cm-radius cylinder surrounding the patient where $t_{\text{rectangle}}$ is the duration of a rectangular dB/dt pulse [9].

$$\left. \frac{dB}{dt} \right|_{\text{max}} = \left(16 \frac{\text{T}}{\text{s}} \right) \left(1 + \frac{0.36 \times 10^{-3} \text{ s}}{t_{\text{rectangle}}} \right) \quad (1.4-3)$$

1.4.2.3 Magnetically Induced Displacement Force

The static field gradient, the difference in static field strength around the scanner, can induce a displacement force on an object [9,13]. Ferromagnetic objects can experience an induced force strong enough such that they become airborne as projectiles [16]. Assume that a device has an overall magnetic dipole moment of \mathbf{m} is placed in a spatially varying magnetic flux density, \mathbf{B} , the magnetic force, \mathbf{F}_m , induced can be described by equation 1.4-4 [9].

$$\mathbf{F}_m = (\mathbf{m} \cdot \nabla) \mathbf{B} \quad (1.4-4)$$

$$\mathbf{F}_m = \begin{pmatrix} \left(m_x \frac{\partial B_x}{\partial x} + m_y \frac{\partial B_x}{\partial y} + m_z \frac{\partial B_x}{\partial z} \right) \hat{\mathbf{x}} \\ \left(m_x \frac{\partial B_y}{\partial x} + m_y \frac{\partial B_y}{\partial y} + m_z \frac{\partial B_y}{\partial z} \right) \hat{\mathbf{y}} \\ \left(m_x \frac{\partial B_z}{\partial x} + m_y \frac{\partial B_z}{\partial y} + m_z \frac{\partial B_z}{\partial z} \right) \hat{\mathbf{z}} \end{pmatrix} \quad (1.4-5)$$

When the magnetic field is varying only in the z-direction and that m_z is the only component of the magnetic moment, the magnetic force expression becomes equation 1.4-6.

$$\mathbf{F}_m = m_z \frac{\partial B_z}{\partial z} \hat{\mathbf{z}} \quad (1.4-6)$$

Further considering that a device of volume, V , and saturation magnetization of, M_s , the magnitude of magnetic force becomes equation 1.4-7.

$$F_m = \frac{M_s V}{\mu_0} \frac{\partial B_z}{\partial z} \quad (1.4-7)$$

In equation 1.4-7, μ_0 is the permeability of vacuum. This force is proportional to the static field of the MR scanner [16].

The standard test for magnetically induced displacement force is performed by measuring the deflection angle of a device under testing (DUT). The DUT is attached by a thread of negligible mass to a fixture. The primary measurement tool is a protractor. All material used, other than the DUT, should not interact with the MR environment [9,13]. Figure 1.4-4 shows the schematic of a deflection test for magnetically induced displacement force. If the deflection angle, θ , is less than 45 deg, then the induced force from the scanner poses no more risk than the force experienced everyday from the Earth's gravity. It should be noted that 45 deg is not an acceptance criterion but rather, a conservative reference point [13]. For each DUT, an acceptance criterion unique to that device needs to be determined.

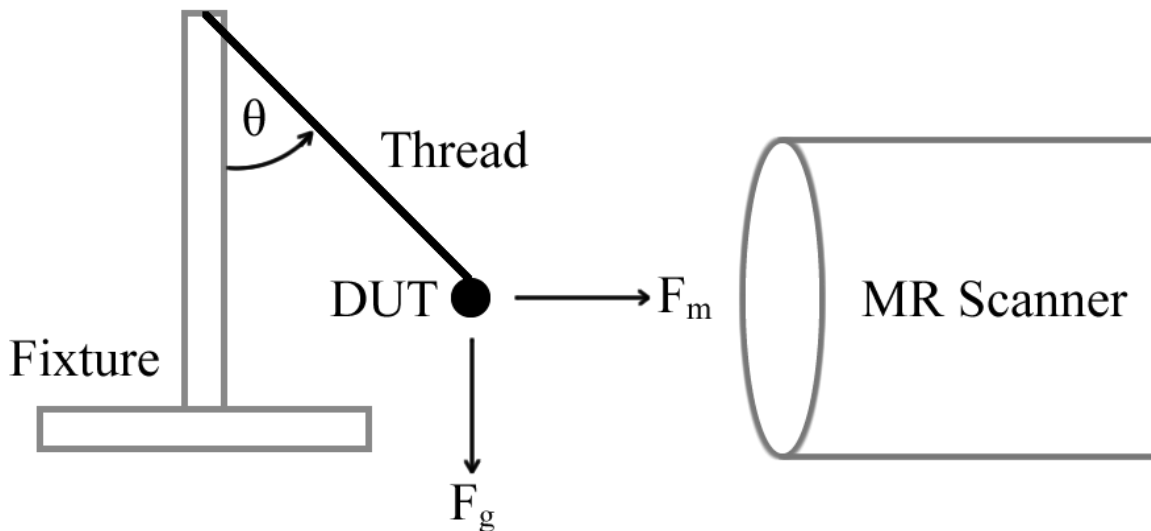


Figure 1.4-4: The basic schematic of the deflection test method used measure magnetically induced displacement force [9]. The DUT, the black circle, experiences a magnetically induced force, F_m , as well as its own weight, F_g . θ is the deflection angle.

The weight of a device, the force due to gravity, can be found simply as the product between the density, ρ , volume, V , and acceleration due to gravity, g . The force ratio then, can be found between the magnetically induced force, F_m , and the weight of the object, F_g .

The force ratio is shown in equation 1.4-9 where F_m was retrieved from equation 1.4-7 and the weight of an object can be calculated from 1.4-8.

$$F_g = \rho g V \quad (1.4-8)$$

$$\text{Force Ratio} = \frac{F_m}{F_g} = \frac{M_s}{\mu_0 \rho g} \frac{\partial B_z}{\partial z} \quad (1.4-9)$$

1.4.2.4 Magnetically Induced Torque

Apart from a magnetically induced force, the other major interaction between material and the static field is a magnetically induced torque. The possibility of torque induced on foreign material entering the static field environment of the scanner is the only concern of this thesis.

Like the displacement force, torque induced on a device is due to interactions with the static field of the MR scanner. A magnetic torque is induced on non-spherical magnetic objects that have magnetizations not precisely distributed along the axis of the magnetic field [9]. A sphere of linear magnetic material will have an induced torque of zero and is shown in appendix A.4.

The torque on non-spherical objects will be in the direction such that the longest dimensions of the object will try to align with the static field [9]. For example, a cylinder placed in a uniform magnetic field, \mathbf{H}_0 , will experience an induced torque. The cylinder is considered an idealized device given its simple geometry. The field is assumed to be along the direction of the MR bore, the z-direction, and the cylinder is assumed to be uniformly magnetized with a saturation magnetization, M_s , in the xz-plane. The device has rotated θ degrees away from the x-axis and M_s is α degrees away from the normal. The relevant magnetic energies are those due to external and normal, N_n , and transverse, N_t , demagnetizing fields. The total magnet static energy per volume, W_T , is therefore given by equation 1.4-10.

$$W_T = -\frac{M_s^2}{2\mu_0}(N_n - N_t) \sin^2 \alpha - M_s H_0 \sin(\theta + \alpha) \quad (1.4-10)$$

At equilibrium, it is required that the angular of change of W_T with respect to α is zero. Equation 1.4-10 then becomes,

$$W_T = -\frac{M_s^2}{2\mu_0}(N_n - N_t) \sin(2\alpha) - M_s H_0 \cos(\theta + \alpha) = 0 \quad (1.4-11)$$

By making the definition 1.4-12, equation 1.4-11, the energy minimization, can be rewritten as 1.4-13.

$$\beta = \frac{M_s}{2\mu_0 H_0} (N_n - N_t) \quad (1.4-12)$$

$$\beta \sin(2\alpha) + \cos(\theta + \alpha) = 0 \quad (1.4-13)$$

The torque about the y-axis is given by 1.4-14.

$$\tau_y = M_s H_0 \cos(\theta + \alpha) \times V \quad (1.4-14)$$

The maximal amplitude of the torque is 1.4-15.

$$\tau_{max} = \frac{M_s^2}{2\mu_0} (N_n - N_t) \times V \quad (1.4-15)$$

In equations 1.4-14 and 1.4-15, V is the volume of the device.

One method of measuring the static field induced torque is to place a device on a platform suspended by torsional springs [9,14]. This method was outlined in a previous version of the ASTM standard for measuring torque which, as of 2017, has been updated to include alternative methods. The torque measured using torsional springs is proportional to the deflection angle of spring from the equilibrium position. The angular dependence of the torque is determined by measurement of the deflection angle as a function of the device position [9]. The acceptance criterion for the torsional spring torque tests is determined by the product of the longest dimension of the device and its weight. Should the magnetically induced torque be less than this criterion, then the induced torque poses no greater threat

than the torque induced everyday from the Earth's gravity. Similar to induced force, this criterion is a conservative reference point [9,14].

Apart from the focus of this thesis, the induced eddy currents on conductive material is another source of torque [9]. This effect can be observed by measuring the time required for a sheet made out of a good conductor to fall flat in the static field. Eddy current torque is not believed to pose a safety issue in MRI but has been reported for certain devices such as metallic heart valves [59]. Eddy current torque was not considered in the studies presented in this thesis.

1.5 Electromagnetic Interactions Relevant to Torque

Electromagnetism is the branch of physics that studies the relationship between electricity and magnetism (EM). The fundamental concepts of EM used throughout this thesis are discussed in this subchapter. Section 1.5 relies heavily on *Electricity & Magnetism* by Munir H. Nayfeh and Morton K. Brussel and *Introduction to Electrodynamics* by David J. Griffiths [22,23].

Relationships Between Electromagnetic Quantities

The terms magnetic field is often used to describe different but closely related quantities, \mathbf{B} and \mathbf{H} . The magnetic field, \mathbf{B} , is also called the magnetic flux density and is given in units of tesla, T. The magnetic field, \mathbf{H} , is also called the magnetic field strength is given in units of amperes per meter, $\frac{\text{A}}{\text{m}}$. The relationship between \mathbf{B} and \mathbf{H} is given by equation 1.5-1.

$$\mathbf{B} = \mu_0(\mathbf{H} + \mathbf{M}) \quad (1.5-1)$$

In the above equation, μ_0 is the magnetic permeability in a vacuum and is constant at $4\pi \times 10^{-7} \frac{\text{H}}{\text{m}}$. \mathbf{M} is the magnetization in units of $\frac{\text{A}}{\text{m}}$. By definition, the magnetization is the density of magnetic dipole moments in magnetic material, shown in equation 1.5-2.

$$\mathbf{M} = \frac{\sum \mathbf{m}}{V} \quad (1.5-2)$$

This thesis primarily examines materials in the paramagnetic range. Materials of this variety have a magnetization, \mathbf{M} , sustained by the field that it is in. When the external field, \mathbf{H} , is removed, \mathbf{M} disappears as well. The magnetization, being proportional to the field, can be expressed in terms of \mathbf{H} using the magnetic susceptibility, χ , as a proportionality constant.

$$\mathbf{M} = \chi \mathbf{H} \quad (1.5-3)$$

Materials that obey equation 1.5-3 are known as linear magnetic material. Substituting equation 1.5-3 into equation 1.5-1 it can be shown that in linear material, \mathbf{B} is proportional to \mathbf{H} by the magnetic permeability of the material.

$$\mathbf{B} = \mu_m \mathbf{H} \quad (1.5-4)$$

The ratio of μ_m to μ_0 is the relative permeability, μ_r . The relative permeability itself is can be written in terms of the relative susceptibility.

$$\mu_r = \frac{\mu_m}{\mu_0} = 1 + \chi \quad (1.5-5)$$

1.5.1 A Sphere of Linear Magnetic Material

A classic EM problem involves finding the magnetic flux density, \mathbf{B} , inside and outside of a sphere of linear magnetic material embedded a uniform external magnetic field, \mathbf{H}_0 . The sphere has a magnetic permeability of μ_1 and the medium that it has been placed in has a magnetic permeability of μ_2 . The sphere is placed at the origin with \mathbf{H}_0 pointing along the z direction. Appendix A.2 details the solution for \mathbf{B} inside and outside of the sphere.

$$\mathbf{B}_{\text{in}} = \frac{3\mu_r}{\mu_r + 2} B_0 \hat{\mathbf{z}} \quad (1.5-6)$$

$$\mathbf{B}_{\text{out}} = \begin{pmatrix} B_0 R^3 \frac{\mu_r - 1}{\mu_r + 2} \frac{3xz}{(x^2 + y^2 + z^2)^{\frac{5}{2}}} \hat{\mathbf{x}} \\ B_0 R^3 \frac{\mu_r - 1}{\mu_r + 2} \frac{3yz}{(x^2 + y^2 + z^2)^{\frac{5}{2}}} \hat{\mathbf{y}} \\ B_0 \left(1 + R^3 \frac{\mu_r - 1}{\mu_r + 2} \frac{x^2 + y^2 - 2z^2}{(x^2 + y^2 + z^2)^{\frac{5}{2}}} \right) \hat{\mathbf{z}} \end{pmatrix} \quad (1.5-7)$$

Equations 1.5-6 and 1.5-7 are true for when \mathbf{H}_0 is along the z direction. For a more general solution when \mathbf{H}_0 and also \mathbf{B}_0 is in an arbitrary direction,

$$\mathbf{B}_0 = \langle B_{0x} \hat{\mathbf{x}} \quad B_{0y} \hat{\mathbf{y}} \quad B_{0z} \hat{\mathbf{z}} \rangle$$

the magnetic flux density inside and outside of the sphere would be given by the following,

$$\mathbf{B}_{\text{in}} = \frac{3\mu_r}{\mu_r + 2} \begin{pmatrix} B_{0x} \hat{\mathbf{x}} \\ B_{0y} \hat{\mathbf{y}} \\ B_{0z} \hat{\mathbf{z}} \end{pmatrix} \quad (1.5-8)$$

In equation 1.5-8, the magnetic flux density inside of the sphere is equal in magnitude to equation 1.5-6. Though the direction of \mathbf{B} inside the sphere changes as \mathbf{B}_0 changes, the magnitude remains the same regardless of direction.

$$\begin{aligned} & \mathbf{B}_{\text{out}} \\ & = \begin{pmatrix} \left(B_{0x} + R^3 \frac{\mu_r - 1}{\mu_r + 2} \left(\frac{3x(yB_{0y} + zB_{0z}) - B_{0x}(y^2 + z^2 - 2x^2)}{(x^2 + y^2 + z^2)^{\frac{5}{2}}} \right) \right) \hat{\mathbf{x}} \\ \left(B_{0y} + R^3 \frac{\mu_r - 1}{\mu_r + 2} \left(\frac{3y(xB_{0x} + zB_{0z}) - B_{0y}(x^2 + z^2 - 2y^2)}{(x^2 + y^2 + z^2)^{\frac{5}{2}}} \right) \right) \hat{\mathbf{y}} \\ \left(B_{0z} + R^3 \frac{\mu_r - 1}{\mu_r + 2} \left(\frac{3z(xB_{0x} + yB_{0y}) - B_{0z}(x^2 + y^2 - 2z^2)}{(x^2 + y^2 + z^2)^{\frac{5}{2}}} \right) \right) \hat{\mathbf{z}} \end{pmatrix} \end{aligned} \quad (1.5-9)$$

1.5.2 An Infinitely Long Cylinder of Linear Magnetic Material

Another classic EM problem is finding \mathbf{B} inside and outside of an infinitely long cylinder of linear magnetic material embedded in an arbitrary \mathbf{H}_0 . The magnetic permeability of the cylinder and surrounding are μ_1 and μ_2 . Appendix A.3 details the solution for \mathbf{B} inside and outside of the cylinder when the direction of \mathbf{H}_0 is perpendicular to the longitudinal axis.

$$\mathbf{B}_{\text{in}} = \frac{2\mu_r}{\mu_r + 1} B_0 \hat{\mathbf{x}} \quad (1.5-10)$$

$$\mathbf{B}_{\text{out}} = \begin{pmatrix} B_0 \left(1 + R^2 \frac{\mu_r - 1}{\mu_r + 1} \frac{x^2 - y^2}{(x^2 + y^2)^2} \right) \hat{\mathbf{x}} \\ B_0 R^2 \frac{\mu_r - 1}{\mu_r + 1} \frac{2xy}{(x^2 + y^2)^2} \hat{\mathbf{y}} \\ 0 \end{pmatrix} \quad (1.5-11)$$

The solution for \mathbf{B} when \mathbf{H}_0 is parallel to the cylinder is the following,

$$\mathbf{B}_{\text{in}} = \mu_r B_{0z} \hat{\mathbf{z}} \quad (1.5-12)$$

$$\mathbf{B}_{\text{out}} = B_{0z} \hat{\mathbf{z}} \quad (1.5-13)$$

Equations 1.5-10 and 1.5-11 are true for when \mathbf{H}_0 is perpendicular to the cylinder and equations 1.5-12 and 1.5-13 are true when \mathbf{H}_0 is parallel. As was with the case of a sphere, when \mathbf{H}_0 and also \mathbf{B}_0 is in an arbitrary direction, the magnetic flux density inside and outside of the cylinder would be given by the following,

$$\mathbf{B}_{\text{in}} = \begin{pmatrix} \frac{2\mu_r}{\mu_r + 1} B_{0x} \hat{\mathbf{x}} \\ \frac{2\mu_r}{\mu_r + 1} B_{0y} \hat{\mathbf{y}} \\ \mu_r B_{0z} \hat{\mathbf{z}} \end{pmatrix} \quad (1.5-14)$$

$$\mathbf{B}_{\text{out}} = \begin{pmatrix} \left(B_{0x} + R^2 \frac{\mu_r - 1}{\mu_r + 1} \frac{2xyB_{0y} + B_{0x}(x^2 - y^2)}{(x^2 + y^2)^2} \right) \hat{\mathbf{x}} \\ \left(B_{0y} + R^2 \frac{\mu_r - 1}{\mu_r + 1} \frac{2xyB_{0x} + B_{0y}(y^2 - x^2)}{(x^2 + y^2)^2} \right) \hat{\mathbf{y}} \\ B_{0z} \hat{\mathbf{z}} \end{pmatrix} \quad (1.5-15)$$

1.5.3 Force and Torque on a Magnetic Dipole Moment

The force on a magnetic dipole moment was previously described in section 1.4.2.3 through equation 1.4-4. The use of equation 1.4-4 has previously been shown to be effective in finding the force induced on an object that has been discretized into smaller components

In a similar vein to force, it is known that the torque on an object with a magnetic dipole moment placed in a uniform field is represented by the following,

$$\boldsymbol{\tau} = \mathbf{m} \times \mathbf{B} \quad (1.5-16)$$

Where $\boldsymbol{\tau}$ is the torque induced, \mathbf{m} is the magnetic dipole moment, and \mathbf{B} is the uniform field that it is placed in.

$$\boldsymbol{\tau} = \begin{pmatrix} (m_y B_{0z} - m_z B_{0y}) \hat{\mathbf{x}} \\ (m_z B_{0x} - m_x B_{0z}) \hat{\mathbf{y}} \\ (m_x B_{0y} - m_y B_{0x}) \hat{\mathbf{z}} \end{pmatrix} \quad (1.5-17)$$

When applied to a sphere, the torque reduces to zero and is shown in greater detail in Appendix A.4.

1.6 Regulatory Environment

In the United States, the Food and Drug Administration (FDA) is charged with ensuring the safety and effectiveness of medical devices. More than 1700 types of devices, 500 000 medical device models, and 23 000 manufacturers are regulated by this agency [60]. The global medical device industry totals in the billions of US dollars with almost half the production and consumption occurring in the United States [60,61]. This has given the United States an effective regulatory environment in regard to medical devices.

The FDA's risk assessment of medical devices is performed through the processes of premarket and postmarket evaluations. The FDA premarket evaluation and approval is conducted by the CDRH, the same agency that requested ASTM international to produce

test standards for evaluating device safety in MR. Medical devices are placed into three classes (I, II, and III) corresponding to low, moderate, or high risk respectively in terms of how well their safety and effectiveness can be assured [60]. Class I devices include, gloves, stethoscopes and tongue blades. The safety and effectiveness of class I devices can be assured through good manufacturing practices, the ethics of producing commercial goods. Class II devices include medical equipment such as gastroenterology endoscopes and MRI scanners. In addition to good manufacturing practices, class II need to meet or exceed predefined industry and performance standards specific to the device. Class III devices include medical implants such as pacemakers and joint replacements. Devices of this class have the same requirements as the previous two but can only be truly assured with clinical trials.

For a new emerging device, there are several ways of receiving market clearance from the FDA. If it's a low risk device, it may be exempt from intense scrutiny and need only registration and listing with the FDA. Moderate and high risk devices however, have two ways of receiving market clearance. The first is demonstrating that there is a case of 'sufficient equivalence', meaning the device has the same intended use and technological characteristics as a previously approved device. The second is demonstrating its safety and effectiveness through premarket approval (PMA), a scientific document submitted to the FDA. The PMA includes studies on the device looking into its biocompatibility, toxicology, stress wear, shelf life, and since the 1990s, compatibility in MRI. Once a device becomes commercially available, the FDA has the authority to surveil and require tracking for any device as postmarket evaluation. This is to combat inadequate reporting of approved devices.

There are several agencies that publish standards in regard to medical device safety or patient safety during MRI. The definitions and standards published by the International Organization for Standardization (ISO), ASTM International (ASTM), the International Electrotechnical Commission (IEC), and the National Electrical Manufacturers Association (NEMA) are often cited. Two important documents considering static field induced torque on medical implants are ISO test standard 10974 and ASTM F2213-17 [11,14]. ISO 10974 is the broader of the two and is primarily concerning AIMDs [11].

ASTM F2213-17 takes a more general approach and is applicable to any device [14]. Since the ASTM standard is applicable to a greater test population, the ISO standard section for torque is brief and directly cites the former. This thesis applies the ASTM method for measuring torque.

1.6.1 How Large Families of Implants Are Assessed

In 2011, the FDA approved for the first time, an MR conditional pacemaker [62]. The device, the Revo MRI SureScan Pacing System (Medtronic Inc., Mounds View, USA), was designed with the intention of being functional during MRI. Testing on the device was modified the system to use as little ferromagnetic material as possible, modified leads and internal circuitry to limit interaction with electromagnetic fields. The device was conditional to a static field strength of 1.5 T, maximum SAR of 2 W/kg for each sequence, and a maximum slew rate of 200 T/m/s [63]. Furthermore, with this device, imaging is limited to certain parts of the body. The isocenter of the body RF transmitter coil must be positioned such that it is above the superior surface of the C1 vertebra or below the inferior surface of the T12 vertebra [62, 63].

The FDA approval of the Revo system was based on the results from a population of 464 patients; 258 individuals receiving an MR exam and 206 individuals in the control group. Regulations required the study to have at least 200 scanned patients [64]. The FDA required that no patient participating had an existing or abandoned active medical devices or leads of any kind. The device being tested must have been implanted at least six weeks prior in the left or right pectoral region [62]. Pacemaker performance was assessed by the pacing capture threshold at a pulse duration of 0.5 ms. Of the individuals who received an MR exam, none had shown MR related complications during or after the scan [62].

The postmarket evaluation for this device required the company to conduct a study of chronic lead performance and the device's function following multiple MRI scans. In regard to lead performance, the FDA requested a study enrolling 1810 individuals within thirty months, with follow up studies conducted for at least five years. What the FDA expects is a complication-free rate of greater than 92.5% over the five years of the

postmarket study. For multiple MR scans, the FDA requested to see the cumulative change in pacing capture thresholds [63].

The Revo MRI SureScan Pacing System is one device that is almost entirely enclosed with extended leads. This device was also designed with minimal MR interactions in mind. For a product line of similar devices, or a device family, the same scrutiny would need to be placed for every individual product. For a device with many components that are applied differently depending on the patient condition, each configuration needs to be considered.

1.6.2 ASTM Methods for Device Interactions in MR

ASTM International has published four documents regarding medical device interactions in the MR environment and one for standard marking practices of medical devices in terms of their safety in the MR environment.

ASTM F2052-15 covers the measurement of magnetically induced displacement force from the static magnetic field gradients [13]. The test method described in ASTM F2052-15 has previously been discussed in section 1.4.2.3 and shown in figure 1.4-4. In short, the DUT is attached by a thread and allowed to hang freely. The DUT is positioned near the scanner bore, where the static field gradient is strongest, and as it experiences a magnetically induced force, it is pulled towards the scanner and the deflection angle is measured. The induced force is proportional to the weight of the object and the tangent of the deflection angle [9,13].

ASTM F2119-07 covers the test method for characterizing distortion and signal loss artifacts produced by passive implants during MRI. In this method, pairs of images are generated with and without the implant in the field of view. Image artifacts are assessed by computing differences outside the region corresponding to the implant between reference and implant images. This is performed for spin echo images and gradient echo images [64].

ASTM F2182-11a covers the measurement method for RF induced heating on or near passive medical implants. The implant is placed within a gelled saline phantom that mimics the electrical and thermal properties of the human body. The local SAR is assessed to characterize the exposure conditions at that location. Temperature probes are placed at locations where the induced implant heating is expected to be the greatest. The phantom is placed in a clinical scanner or an apparatus capable of reproducing the RF field. The specification of the RF field is such that it is capable of producing a sufficient whole-body SAR of about 2 W/kg averaged over the phantom volume for 15 min. This procedure is performed twice, first with the implant in place, and again with the implant removed [15].

ASTM F2503-13 is an international standard on marking medical devices and other items that might be used in the MR environment [26]. This standard defines the terms MR Safe, MR Conditional, and MR Unsafe which has been previously discussed in section 1.4. The standard symbols that are used are shown in figure 1.4-1.

1.6.3 ASTM Methods for Torque Assessment

ASTM F2213-17 is the most recent document published by ASTM International detailing test methods for assessing static field induced torque on medical implants. This document lists five methods; ‘torsional spring’, ‘pulley’, ‘low friction surface’, ‘suspension’, and ‘calculation based on magnetically induced force’. The calculation based on induced force, suspension, and low friction surface methods require further testing from the remaining two methods should some torque be observed. The torsional spring and pulley methods are the definitive methods for measuring a quantitative torque value. The acceptance criterion stated in this document is the torque due to gravity during everyday use, the product of the weight of the device and its longest dimension.

Calculation Based on Magnetically Induced Force Method

The calculation based on magnetically induced force method is meant to be performed in conjunction with measurements from F2052 and provides an upper bound for the magnetically induced torque. This method is most appropriate for devices composed of a single material and not appropriate for devices containing magnets or ferromagnetic material and relies on the following equation,

$$\tau_{\max} = \frac{M_s F_m}{4(\nabla B)} \quad (1.6-1)$$

In equation 1.6-1, F_m is the induced displacement force, ∇B is the spatial gradient of the magnetic field at the position where F_m was measured, and M_s is the saturation magnetization. Both F_m and ∇B are quantities that are carried over from F2052. This method assumes M_s is unknown. Conservative estimates of 2.2 T, M_s of iron, and greatest M_s value of materials within the implant are used with equation 1.6-1 to generate two upper bounds. Should the upper bounds exceed the acceptance criterion, then further testing is required from the remaining four methods.

Suspension Method

The suspension method is useful for devices that are difficult to place on the low friction surface and align the principal axes with the z-axis of the MR system. The device is suspended by a thread that is less than 1% of the mass of the device. It is preferable that the device be suspended from a single point but if required, the thread should be twisted such that it hangs from the fixture at a single point but is attached to the device in two or more points. The device is positioned such that its centre of mass is as close to the magnetic isocentre as possible and allowed to rotate to equilibrium. The suspended device is now rotated slowly in 45 degree increments until a full 360-degree rotation is completed. After each rotation, the device is observed for realignment with the static field. If not observed, then the induced torque is not substantial, and no further testing is required. Otherwise, the low friction surface, torsional spring, or pulley methods should be performed.

Low Friction Surface Method

The low friction surface method uses a low friction, non-metallic, and non-conductive surface. Outside of the MR environment, the device, using the side with the lowest friction, is placed on such a surface with one end fixed and slowly raised until the angle of repose is reached. That is the angle at which the device is on the verge of sliding. It is important that the device should slide and not roll. The coefficient of friction can be found from the following equation where μ is the coefficient of friction and θ_{repose} is the angle of repose.

$$\mu = \tan \theta_{\text{repose}} \quad (1.6-2)$$

Once the coefficient of friction is known, the device is once again placed on the low friction surface as near the magnetic isocentre of the MR scanner as possible. The device and surface are in the xz-plane and the device is oriented such that one principal axis is aligned in the z-direction. The device is rotated in 45 degree increments until a full 360-degree rotation is completed and observed for alignment with the static field after each rotation. This process is repeated for each principal axis. If device remained motionless, then the induced torque is less than the product between the longest dimension, L , and frictional force, F_f .

$$F_f = \mu mg \quad (1.6-3)$$

$$\tau < LF_f \quad (1.6-4)$$

In equation 1.6-3, m is the mass of the device and g is the acceleration of gravity. If the device did align with the static field, then further testing from the torsional spring or pulley methods are required.

Torsional Spring Method

The torsional spring method is the most familiar as it has been discussed briefly in section 1.4.2.4. This method has a device fixed to a holding platform, with a fixed angular measurement tool, which is suspended above and below by torsional springs. The device is allowed to rotate to equilibrium outside of the MR environment. All parts of the apparatus should be non-ferromagnetic. The apparatus is placed into the scanner such that the device is as close to the magnetic isocentre as possible with one principal axis of the device in the vertical direction. The holding platform is then allowed to rotate in 10 degree increments until a full 360-degree rotation is completed. With each rotation, the deflection angle is measured. This process is repeated for each principal axis. The induced torque, τ , is proportional to the torsional spring constant, k , and deflection angle, $\Delta\theta$.

$$\tau = k\Delta\theta \quad (1.6-5)$$

Pulley Method

The pulley method is used in this thesis. In this method, the device is fixed to a rotating platform that is connected to a low-friction pulley. The apparatus and device are placed into the MR scanner such that the device is as close to the magnetic isocentre as possible with one principal axis of the device oriented vertically. A thread is extended from the pulley to a force gauge that is positioned far enough that the device still operates properly. The device is allowed to rotate to equilibrium and the thread is pulled slowly rotating the platform for 360 degrees. As the platform rotates the device away from equilibrium, there is some tension in the thread measured by the force gauge as the device tries to realign with the static field. During the rotation, the peak force measurement, F , is recorded. The device is then taken away and an empty platform is rotated with the peak force measurement being the friction between the platform and pulley, F_f . This process is repeated for each principal axis and the induced torque, τ , can be calculated from the radius of the pulley, R , and force measurements.

$$\tau = R(F - F_f) \quad (1.6-6)$$

1.7 Thesis Overview

This thesis is organized into four chapters. Chapter 1 provided the background information and motivation behind the studies conducted. Chapter 4 concludes this thesis with summaries of the studies conducted in Chapters 2 and 3. It continues to discuss the future research directions as well as the limitations of each work.

Chapter 2 presents the computational method for assessing the torque induced on several sets of stainless-steel 316 and stainless-steel 304 cylinders. This chapter outlines the simulation setup in the finite element method software, COMSOL Multiphysics (COMSOL Inc., Stockholm, Sweden) and subsequent analysis in MATLAB (MathWorks Inc., Natick, USA). This chapter begins by verifying that the parameters going into the COMSOL model yields a result that agrees with theory. Starting with objects with simple geometries, i.e. a sphere and a long cylinder, it was verified that the when such objects were placed into a static field, the results from COMSOL agree with what the theoretical values would be for such objects. This chapter continues to demonstrate how to calculate the induced torque on a discretized cylinder of finite length.

Chapter 3 presents a comparison of measurement uncertainties between measurement methods published in ASTM F2213-17 with a focus on the ‘pulley method’. The ASTM standard includes five methods, but only two aim to measure a value for magnetically induced torque. Those two methods were put through error propagation based on instrument uncertainties. The study then continues to examine the systematic uncertainty of static friction in the apparatus designed for the pulley method.

1.8 References

- [1] Canadian Agency for Drugs and Technologies in Health (CADTH), “The Canadian Medical Imaging Inventory, 2017,” 2018
- [2] Canadian Agency for Drugs and Technologies in Health (CADTH), “The Canadian Medical Imaging Inventory, 2015,” 2016
- [3] OECD (2017), *Health at a Glance 2017: OECD Indicators*, OECD Publishing, Paris. http://dx.doi.org/10.1787/health_glance-2017-en
- [4] OECD (2019), Magnetic resonance imaging (MRI) exams (indicator). doi: 10.1787/1d89353f-en (Accessed on 15 January 2019)
- [5] Kalin, R., & Stanton, M. S. (2005). Current clinical issues for MRI scanning of pacemaker and defibrillator patients. *PACE - Pacing and Clinical Electrophysiology*, 28(4), 326–328.
- [6] Simpson, C. S., & Gillis, A. M. (2006). The pacemaker and implantable cardioverter defibrillator recall issue – a Canadian perspective. *Canadian Journal of Cardiology*, 22(6), 467–471.
- [7] Schenck, J. F. (2000). Safety of Strong, Static Magnetic Fields. *Journal of Magnetic Resonance Imaging*, 12, 2–19.
- [8] Kanakaraj, J., & Kathiravan, S. (2013). A Review on Potential Issues and Challenges in MR Imaging. *The Scientific World Journal*, 2013(5096), 1–10.
- [9] Nyenhuis, J. A., Park, S.-M., Kamondetdacha, R., Amjad, A., Shellock, F. G., & Rezai, A. R. (2005). MRI and Implanted Medical Devices: Basic Interactions With an Emphasis on Heating. *IEEE Transactions on Device and Materials Reliability*, 5(3), 467–480.
- [10] Graf, H., Steidle, G., & Schick, F. (2007). Heating of metallic implants and instruments induced by gradient switching in a 1.5-Tesla whole-body unit. *Journal of Magnetic Resonance Imaging*, 26(5), 1328–1333.
- [11] International Organization for Standardization (ISO). (2018). *Assessment of the safety of magnetic resonance imaging for patients with an active implantable medical device*.

- [12] Bungartz, H.-J., Mehl, M., & Zenger, C. (2009). Computer Science and Numerical Fluid Mechanics – An Essential Cooperation. In *100 Volumes of “Notes on Numerical Fluid Mechanics”* (pp. 437–450).
- [13] ASTM International. (2015). *Standard Test Method for Measurement of Magnetically Induced Displacement Force on Medical Devices in the Magnetic Resonance Environment*.
- [14] ASTM International. (2017). *Standard Test Method for Measurement of Magnetically Induced Torque on Medical Devices in the Magnetic Resonance Environment*.
- [15] ASTM International. (2011). *Standard Test method for Measurement of Radio Frequency Induced Heating On or Near Passive Implants During Magnetic Resonance Imaging*.
- [16] Westbrook, C., & Kaut, C. (1998). *MRI in Practice* (2nd ed.). Cambridge: Blackwell Science.
- [17] McRobbie, D. W., Moore, E. A., Graves, M. J., & Prince, M. R. (2006). *MRI From Picture to Proton* (2nd ed.). New York: Cambridge University Press.
- [18] Iwasa, Y. (2009). *Case Studies in Superconducting Magnets: Design and Operational Issues* (2nd ed.). Cambridge: Springer Publishing.
- [19] Furlani, E. P. (2001). Permanent Magnet Applications. In *Permanent Magnet and Electromechanical Devices* (pp. 207–333). Elsevier.
- [20] FONAR. (n.d.). FONAR MRI. Retrieved January 24, 2019, from <http://www.fonar.com/index-no-flash.htm>
- [21] Philips. (n.d.). Panorama HFO 1.0T - DS. Retrieved January 24, 2019, from <http://www.healthcare.philips.com/main/products/mri/systems/panorama/>
- [22] Nayfeh, M. H., & Brussel, M. K. (1989). *Electricity and Magnetism* (1st ed.). John Wiley & Sons, Inc.
- [23] Griffiths, D. J. (2013). *Intorduction to Electrodynamics* (4th ed.). Pearson.
- [24] Health Canada. (2017). *Safe Medical Devices in Canada*. Ottawa.
- [25] Woods, T. O. (2007). Standards for Medical Devices in MRI : Present and Future. *Journal of Magnetic Resonance Imaging*, 26, 1186–1189.

- [26] ASTM International. (2013). *Standard Practice for Marking Medical Devices and Other Items for Safety in the Magnetic Resonance Environment*.
- [27] Bannan, K. El, Handler, W. B., Wyenberg, C., Chronik, B. A., & Salisbury, S. P. (2013). Prediction of Force and Image Artifacts Under MRI for Metals Used in Medical Devices. *IEEE/ASME Transactions on Mechatronics*, 18(3), 954–962.
- [28] Zhou, D. B., Wang, S. P., Wang, S. G., Ai, H. J., & Xu, J. (2016). Bulk Metallic Glasses: MRI Compatibility and Its Correlation with Magnetic Susceptibility. *Journal of Materials Science and Technology*, 32(6), 496–504.
- [29] Caciagli, A., Baars, R. J., Philipse, A. P., & Kuipers, B. W. M. (2018). Exact expression for the magnetic field of a finite cylinder with arbitrary uniform magnetization. *Journal of Magnetism and Magnetic Materials*, 456, 423–432.
- [30] Jin, J. (2010). Practical Electromagnetic Modeling Methods. *Encyclopedia of Magnetic Resonance*. <https://doi.org/10.1002/9780470034590.emrstm1113>
- [31] International Organization for Standardization (ISO). (2016). *Medical devices — Quality management systems — Requirements for regulatory purposes*.
- [32] Ehrhardt, J. C., Lin, C. S., Magnotta, V. A., Fisher, D. J., & Yuh, W. T. C. (1997). Peripheral nerve stimulation in a whole-body echo-planar imaging system. *Journal of Magnetic Resonance Imaging*, 7(2), 405–409.
- [33] Zhang, S. H., Tse, Z. T. H., Dumoulin, C. L., Kwong, R. Y., Stevenson, W. G., Watkins, R., Ward, J., Wang, W., & Schmidt, E. J. (2016). Gradient-induced voltages on 12-lead ECGs during high duty-cycle MRI sequences and a method for their removal considering linear and concomitant gradient terms. *Magnetic Resonance in Medicine*, 75(5), 2204–2216. <https://doi.org/10.1002/mrm.25810>
- [34] International Electrotechnical Commission (IEC). (2015). *Medical electrical equipment – Part 2-33: Particular requirements for the basic safety and essential performance of magnetic resonance equipment for medical diagnosis*.
- [35] Lvovsky, Y., Stautner, E. W., & Zhang, T. (2013). Novel technologies and configurations of superconducting magnets for MRI. *Superconductor Science and Technology*, 26, 1–71.

- [36] Hidalgo-Tobon, S. S. (2003). Theory of Gradient Coil Design Methods for Magnetic Resonance Imaging. *Concepts in Magnetic Resonance Part A*, 36A(4), 223–242.
- [37] Ham, C. L. G., Engels, J. M. L., van de Wiel, G. T., & Machielsen, A. (1997). Peripheral Nerve Stimulation during MRI: Effects of High Gradient Amplitudes and Switching Rates. *Journal of Magnetic Resonance Imaging*, 7(5), 933–937.
- [38] Mansfield, P., & Chapman, B. (1986). Active magnetic screening of coils for static and time-dependent magnetic field generation in NMR imaging. *Journal of Physics E: Scientific Instruments*, 19, 540–545.
- [39] Charifoulline, Z. (2006). Residual Resistivity Ratio (RRR) Measurements of LHC Superconducting NbTi Cable Strands. *IEEE Transactions on Applied Superconductivity*, 16(2), 1188–1191.
- [40] Helthuis, J. H. G., Zwan, A. Van Der, Doormaal, T. P. C. Van, Bleys, R. L. A. W., Harteveld, A. A., Toorn, A. Van Der, ... Zwanenburg, J. J. M. (2018). High resolution 7T and 9.4T-MRI of human cerebral arterial casts enables accurate estimations of the cerebrovascular morphometry. *Scientific Reports*, 8, 1–8.
- [41] Cosmus, T. C., & Parizh, M. (2011). Advances in Whole-Body MRI Magnets. *IEEE Transactions on Applied Superconductivity*, 21(3), 2104–2109.
- [42] Marrow, G. (2000). Progress In MRI Magnets. *IEEE Transactions on Applied Superconductivity*, 10(1), 744–751.
- [43] Morrow, G. R., & Rosner, C. H. (1987). Superconducting magnets for magnetic resonance imaging applications. *IEEE Transactions on Magnetics*, 23(2), 1294–1298.
- [44] Pennsylvania Patient Safety Advisory. (2009). *Safety in the MR Environment : MR Safety Screening Practices*.
- [45] Kanal, E., Barkovich, A. J., Bell, C., Borgstede, J. P., Bradley Jr, W. G., Froelich, J. W., ... Hernandez, D. (2013). ACR Guidance Document on MR Safe Practices : 2013. *Journal of Magnetic Resonance Imaging*, 37, 501–530.

- [46] Gourzoulidis, G., Karabetsos, E., Skamnakis, N., Kappas, C., Theodorou, K., Tsougos, I., & Maris, T. G. (2015). The electromagnetic environment of Magnetic Resonance Imaging systems. Occupational exposure assessment reveals RF harmonics. *Journal of Physics: Conference Series*, 6–10.
- [47] Pauly, J., Le Roux, P., Nishimura, D., & Macovski, A. (1991). Parameter Relations for the Shinnar-Le Roux Selective Excitation Pulse Design Algorithm. *IEEE Transactions on Medical Imaging*, 10(1), 53–65.
- [48] Gonano, C. A., Zich, R. E., & Mussetta, M. (2015). Definition for Polarization P and Magnetization M Fully Consistent with Maxwell ' s Equations. *Progress In Electromagnetics Research B*, 64, 83–101.
- [49] Haacke, E. M., Brown, R. W., Thompson, M. R., & Venkatesan, R. (1999). *Magnetic Resonance Imaging: Physical Principles and Sequence Design*.
- [50] Edelman, R. R. (2014). The History of MR Imaging as Seen through the Pages of Radiology. *Radiology*, 273(2 (Suppl)), 181–200.
- [51] Queen's Univeristy. (2015). Emergency Shutdown and Quench Procedures. Retrieved from <http://neuroscience.queensu.ca/MRI-facility/operation-procedures/shutdown>
- [52] Turner, B. D. (2007). Design Fundamentals: Shielding Issues for Medical Products: Basic Magnetic Shielding Issues for MRI Systems. *Conformity*, (May), 48–53.
- [53] Hoult, D. I., & Bhakar, B. (1997). NMR Signal Reception : Virtual Photons and Coherent Spontaneous Emission. *Concepts in Magnetic Resonance*, 9(5), 277–297.
- [54] Hodgkin, A. L., & Huxley, A. F. (1952). A Quantitative Description of Membrane Current and Its Application to Conduction and Excitation in Nerve. *Journal of Physiology*, 117, 500–544.
- [55] Stephanie, C. (2017). FDA clears first 7T magnetic resonance imaging device.
- [56] Schenck, J. F. (1996). The role of magnetic susceptibility in magnetic resonance imaging: MRI magnetic compatibility of the first and second kinds. *Medical Physics*, 23(6), 815–850.
- [57] Bottomley, P. A., Redington, R. W., Edelstein, W. A., & Schenck, J. F. (1985). Estimating Radiofrequency Power Deposition in Body NMR Imaging *. *Magnetic Resonance in Medicine*, 2, 336–349.

- [58] Shellock, F. G. (2000). Radiofrequency Energy-Induced Heating During MR Procedures: A Review. *Journal of Magnetic Resonance Imaging*, 12, 30–36.
- [59] Condon, B., & Hadley, D. M. (2000). Potential MR Hazard to Patients With Metallic Heart Valves : The Lenz Effect. *Journal of Magnetic Resonance Imaging*, 12, 171–176.
- [60] Maisel, W. H. (2004). Medical Device Regulation: An Introduction for the Practicing Physician. *Annals of Internal Medicine*, 140, 294–302.
- [61] Monsein, L. H. (1997). Primer on Medical Device Regulation Part I. History and Background. *Radiology*, 205, 1–9.
- [62] Mitka, M. (2011). First MRI-Safe Pacemaker Receives Conditional Approval From FDA. *Journal of the American Medical Association*, 305(10), 985–986.
- [63] Wilkoff, B. L., Bello, D., Taborsky, M., Vymazal, J., Kanal, E., Heuer, H., ... Sommer, T. (2011). Magnetic resonance imaging in patients with a pacemaker system designed for the magnetic resonance environment. *Heart Rhythm*, 8(1), 65–73.
- [64] ASTM International. (2013). *Standard Test Method for Evaluation of MR Image Artifacts from Passive Implants*.

Chapter 2

Computational Evaluation of Stainless-Steel Cylinders for Static Field Induced Torque

This chapter discusses the methods and tools used for the computational evaluation, simulation, and subsequent verification of static field induced torque on a set of stainless-steel cylinders. This study was conducted to obtain preliminary results for the development of a fast, accurate, and systematic method of evaluating the torque induced on medical devices from the static field of an MR scanner. This chapter begins with a brief background and motivation for the study. It goes on to discuss in detail the computational methods used and the verification of those methods. Internationally recognized standard test methods for measuring the torque induced on objects were used for experimental verification. For an object of simple geometry, a cylinder, there is good correlation between simulated and experimentally obtained torque values.

2.1 Introduction

The use of MRI as a diagnostic modality has seen tremendous growth in the past decade. In Canada, between 2012 and 2016, three times as many MRI units were installed than decommissioned with the trend of net growth continuing into 2018 [1,2]. In parallel, the use of implantable medical devices has also seen widespread usage [3]. The presence such devices presents a risk to patients who are referred to an MR exam due to the interactions between the implant and electromagnetic environment of the MR scanner. These safety concerns are an issue that device manufacturers need to address. The various interactions that may cause harm to patients in MR include, heating, vibrations, forces, and the focus of this study, torques [4]. It is the responsibility of the manufactures to know the limitations of the electromagnetic fields produced by an MR scanner such that their product does not pose as a hazard.

Commercial implants can be placed into one of three categories; MR safe, MR conditional, or MR unsafe, depending on how hazardous the implant is in the MR environment. The MR environment is the volume of space that surrounds the scanner within a magnetic field of five gauss. During a scan, the MR environment can change from having a static and uniform field to a spatially and temporally varying one with field strengths varying from the milliteslas to teslas. An implant that is MR safe poses no known hazards in all MR environments and conversely, MR unsafe implants is known to pose hazards in all MR environments. MR conditional implants have demonstrated to not pose as a hazard in a specified MR environment with specified conditions of use [5]. MR conditional devices are restricted to certain imaging regions of the body and under specific field strengths for specific durations of time. It is the purpose of device testing is to identify the conditions that make an implantable device MR conditional, compile the results and have the device be properly labeled as such.

For an implant that exists in a single form, the task of testing for its safety in MR may not be so daunting. The challenge arises when medical device is a family of similar devices or a device made up of many components. Joint replacements may be an example of the former. There is tremendous variability in the anatomical proportions of individuals

and joint replacements are often designed as a product line of similar devices that vary predominantly by size. An example of the former may be a cervical spine fixation system. Depending on the severity of the user's condition, a fixation system may be implemented in numerous orientations. In either case, there may be thousands of configurations to take into consideration. It becomes impractical to rely on experimental testing alone for every conceivable scenario. There is a need for fast, accurate, and systematic testing of medical implants.

The objective of this study is therefore, to develop and verify a computer simulation that solves for the static field-induced torque based on the static field strength, geometry, material and orientation of an idealized device, a cylinder. The simulation should have the capacity to solve for all configurations and identify the worst configuration, the one that suffers from the greatest induced torque. Experimental measurements using standard test methods can then be taken on the identified worst configuration. Those results can be referred to as conservative limitations for the entire device family.

2.2 Theory

The numerical method used to find the magnetic field inside and outside of the test cylinders is the finite element method (FEM). It has been shown for objects whose geometries are more complicated than a sphere or an infinitely long cylinder, FEM is a valid method for solving the associated magnetic fields [8]. This study uses FEM to solve for the magnetic fields of a set of cylinders of finite lengths placed in a static field environment and from that, solve for the torque induced on each object.

There are two parts to this study. The first is a verification of parameters chosen to be used in the FEM simulations. Since it is known that FEM is a valid method, it needs to be shown that the implementation of chosen parameters produces a result that can be verified. FEM is used to find the magnetic field inside and outside of a sphere and an infinitely long cylinder, two objects for which the analytical solutions are known. Verification can be done by finding how well the FEM results agree with analytical

solutions. The second part of this study is the simulation of stainless-steel rods exposed to a static and uniform magnetic field. Rods of finite lengths serve as idealized devices with simple geometries. The results from using FEM to solve for the magnetic field inside these rods can be used to solve for the induced torque and subsequently verified with results from experimental measurements. It is expected that the longest rods will be the ‘worst cases’ that experience the greatest torque.

Part 1 of this study concerns linear media, which obey the following,

$$\mathbf{H} = \frac{\mathbf{M}}{\chi} \quad (2-1)$$

In equation 2-1, \mathbf{H} is the magnetic field strength and is proportional to \mathbf{M} , the magnetization, which is the density of magnetic dipole moments, \mathbf{m} , per volume, V .

$$\mathbf{M} = \frac{\sum \mathbf{m}}{V} \quad (2-2)$$

Thus, from equation 2-1, \mathbf{B} is also proportion to \mathbf{H} by the following,

$$\mathbf{B} = \mu_0(\mathbf{H} + \mathbf{M}) = \mu\mathbf{H} \quad (2-3)$$

Where,

$$\mu \equiv \mu_0(1 + \chi) = \mu_0\mu_r \quad (2-4)$$

Throughout this study, the static field is implemented into the simulation software according to the following definitions. Consider that the static field of the MR scanner is denoted by \mathbf{B}_0 such that,

$$\mathbf{B}_0 = \langle B_{0x}\hat{\mathbf{x}} \quad B_{0y}\hat{\mathbf{y}} \quad B_{0z}\hat{\mathbf{z}} \rangle \quad (2-5)$$

Equation 2-5 can be represented as a vector pointing in any arbitrary direction by,

$$\mathbf{B}_0 = B_0(\cos(\alpha)\sin(\beta)\hat{\mathbf{x}} \quad \cos(\alpha)\cos(\beta)\hat{\mathbf{y}} \quad \sin(\alpha)\hat{\mathbf{z}}) \quad (2-6)$$

In equation 2-6, the static field is pointing in an arbitrary direction defined by α , the angle between the vector and the xy-plane, and β , the angle between the projection of the vector and the y-axis. This is shown in figure 2-1.

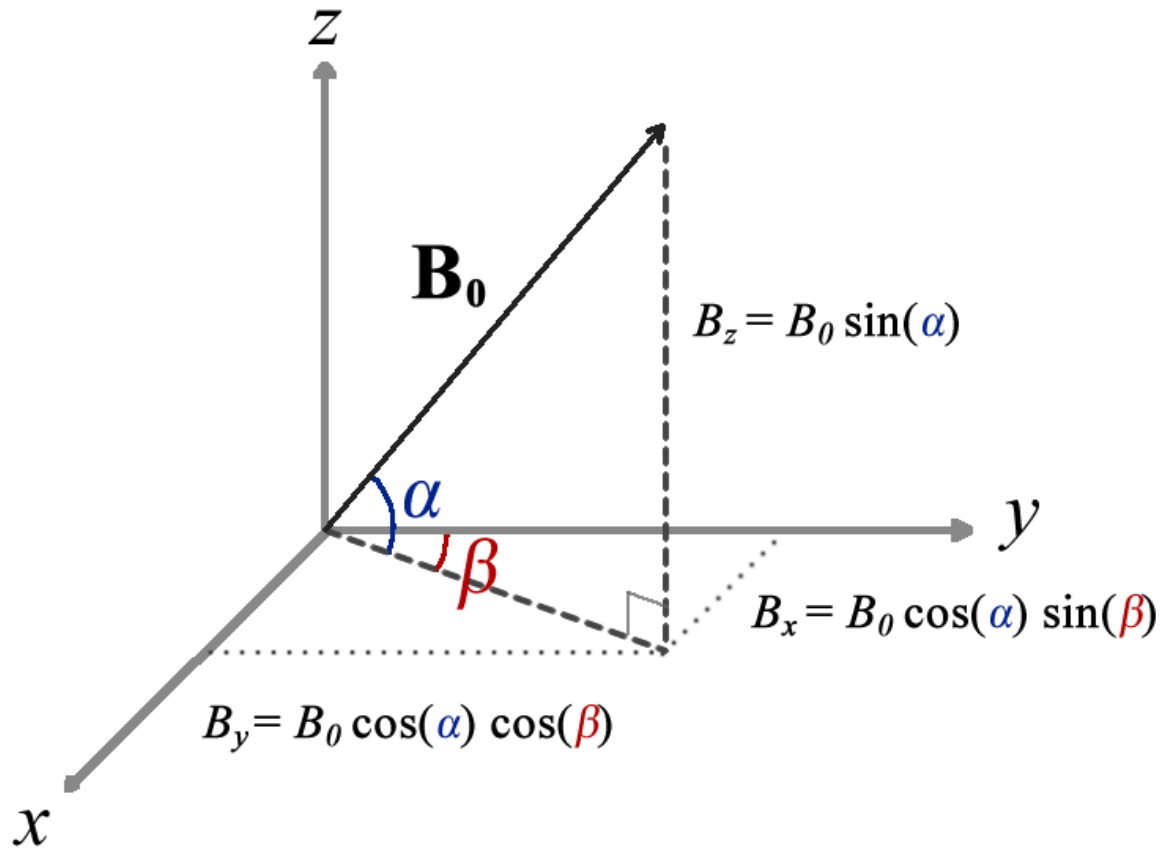


Figure 2-1: The method of defining the direction of the static field in cartesian coordinates that was implemented in COMSOL and MATLAB. The \mathbf{B}_0 vector was separated into its x , y , and z components. The angle α forms between the vector and the xy -plane. The angle β forms between the projection of \mathbf{B}_0 onto the xy -plane and the y -axis. When α is 90 degrees, regardless of what β is, the direction of the field is along the z -axis. When β is 90 degrees, changing α will rotate the field about the y -axis.

2.2.1 Magnetic Field Inside and Outside of a Sphere

It is known that for a sphere of linear magnetic material, the magnetic flux density inside and outside of the sphere is given by the following,

$$\mathbf{B}_{\text{in}} = \frac{3\mu_r}{\mu_r + 2} \begin{pmatrix} B_{0x}\hat{\mathbf{x}} \\ B_{0y}\hat{\mathbf{y}} \\ B_{0z}\hat{\mathbf{z}} \end{pmatrix} \quad (2-7)$$

$$\mathbf{B}_{\text{out}} = \begin{pmatrix} \left(B_{0x} + R^3 \frac{\mu_r - 1}{\mu_r + 2} \left(\frac{3x(yB_{0y} + zB_{0z}) - B_{0x}(y^2 + z^2 - 2x^2)}{(x^2 + y^2 + z^2)^{\frac{5}{2}}} \right) \right) \hat{\mathbf{x}} \\ \left(B_{0y} + R^3 \frac{\mu_r - 1}{\mu_r + 2} \left(\frac{3y(xB_{0x} + zB_{0z}) - B_{0y}(x^2 + z^2 - 2y^2)}{(x^2 + y^2 + z^2)^{\frac{5}{2}}} \right) \right) \hat{\mathbf{y}} \\ \left(B_{0z} + R^3 \frac{\mu_r - 1}{\mu_r + 2} \left(\frac{3z(xB_{0x} + yB_{0y}) - B_{0z}(x^2 + y^2 - 2z^2)}{(x^2 + y^2 + z^2)^{\frac{5}{2}}} \right) \right) \hat{\mathbf{z}} \end{pmatrix} \quad (2-8)$$

2.2.2 Magnetic Field Inside and Outside of an Infinitely Long Cylinder

It is known that for an infinitely long cylinder of linear magnetic material, the magnetic flux density inside and outside of the cylinder is given by the following,

$$\mathbf{B}_{\text{in}} = \begin{pmatrix} \frac{2\mu_r}{\mu_r + 1} B_{0x}\hat{\mathbf{x}} \\ \frac{2\mu_r}{\mu_r + 1} B_{0y}\hat{\mathbf{y}} \\ \mu_r B_{0z}\hat{\mathbf{z}} \end{pmatrix} \quad (2-9)$$

$$\mathbf{B}_{\text{out}} = \begin{pmatrix} \left(B_{0x} + R^2 \frac{\mu_r - 1}{\mu_r + 1} \left(\frac{2xyB_{0y} + B_{0x}(x^2 - y^2)}{(x^2 + y^2)^2} \right) \right) \hat{\mathbf{x}} \\ \left(B_{0y} + R^2 \frac{\mu_r - 1}{\mu_r + 1} \left(\frac{2xyB_{0x} + B_{0y}(y^2 - x^2)}{(x^2 + y^2)^2} \right) \right) \hat{\mathbf{y}} \\ B_{0z} \hat{\mathbf{z}} \end{pmatrix} \quad (2-10)$$

2.2.3 The Force on a Magnetic Dipole Moment

It is known that the force, \mathbf{F} , on a magnetic dipole moment is given by the following [7],

$$\mathbf{F} = (\mathbf{m} \cdot \nabla) \mathbf{B} \quad (2-11)$$

From equations 2-1 through 2-4 and expanding, the force on a magnetic moment can be written as the following [20],

$$\mathbf{F} = \frac{\chi V}{\mu_0(1 + \chi)} \begin{pmatrix} \left(B_x \frac{\partial B_x}{\partial x} + B_y \frac{\partial B_x}{\partial y} + B_z \frac{\partial B_x}{\partial z} \right) \hat{\mathbf{x}} \\ \left(B_x \frac{\partial B_y}{\partial x} + B_y \frac{\partial B_y}{\partial y} + B_z \frac{\partial B_y}{\partial z} \right) \hat{\mathbf{y}} \\ \left(B_x \frac{\partial B_z}{\partial x} + B_y \frac{\partial B_z}{\partial y} + B_z \frac{\partial B_z}{\partial z} \right) \hat{\mathbf{z}} \end{pmatrix} \quad (2-12)$$

2.2.4 The Volume Magnetic Susceptibility of Stainless-Steel Alloys

In the second part of this study, the static field induced torque on stainless-steel rods is experimentally measured to verify simulations on the same material. The two grades of stainless-steel (SS) used are 316 and 304. Both these grades belong to the greater category of austenitic stainless-steel and is considered to be weakly magnetic [12]. In the simulation software used, the material of the device simulated is defined solely by the relative permeability, μ_r , which by equation 2-4, is related to magnetic susceptibility, χ , a measure of how much a material will become magnetized when placed in an external

magnetic field. As shown in equation 2-1, magnetic susceptibility is a dimensionless proportionality constant between the magnetization, \mathbf{M} , and magnetic field strength, \mathbf{H} [7]. The *magnetic susceptibility* in equation 2-1 is also known as the *volume susceptibility*, both terms are often used interchangeably with *susceptibility*. The mass susceptibility, χ_m , is the ratio of the volume susceptibility with the density of the material. The molar susceptibility, χ_M , is the product of the mass susceptibility with the molecular weight of the material [12]. Throughout this study, only the volume susceptibility will be used. Table 2-1 shows some values for the susceptibility of SS316 and SS304 in literature.

Material	Susceptibility [ppm]	Source
SS 304	3520	[10]
SS (MR Safe Type)	3000 to 5000	[11]
SS (nonmagnetic, austenitic)	3520 to 6700	
Austenitic steels at Room Temp	1000 to 20 000	[12]
SS 316	30 000 to 9×10^6	
SS 304	864	[13]
SS 316	2496	
SS 304	20 000	[14]
SS 316	20 000	
SS 304	4000 to 4400	[15]
SS 316	2800 to 2600	

Table 2-1: Approximate magnetic susceptibility values collected from literature for SS 304, SS 316, and relevant alloys.

From table 2-1, it is clear that there is significant inconsistency within the literature for what the susceptibilities of SS304 and SS316 are. This was not unexpected for a number of reasons. To begin with, there is not an exact composition for either material. Table 2-2 lists the relevant chemical composition requirements. It has been shown that changes on a chemical composition level can affect magnetic susceptibility [17]. In addition, the susceptibilities of stainless steel, in particular grades 303 and 304, depend on their thermal

history [13]. When heavily cold worked, the susceptibility of SS316 can increase by a factor 3000 due to its internal structure changing from austenitic (paramagnetic and MR conditional) to martensitic (ferromagnetic and MR unsafe) [12]. It has also been shown that differently cut stainless-steel samples exhibit different magnetic properties when in the vicinity of a magnetron magnet [13]. The only definitive way of finding the susceptibility is to measure each individual lot.

		C	Mn	P	S	Si	Cr	Ni	Mo	N
SS304	Min	-	-	-	-	-	17.5%	8.0%	-	-
	Max	0.07%	2.00%	0.045%	0.030%	0.75%	19.5%	10.5%	-	0.10%
SS316	Min	-	-	-	-	-	16.0%	10.0%	2.00%	-
	Max	0.08%	2.00%	0.045%	0.030%	0.75%	18.0%	14.0%	3.00%	0.10%

Table 2-2: ASTM A240/A240M-18 standard chemical composition requirements, as percentages of total mass, for SS304 and SS316. It should be noted that iron, Fe, is the predominant ingredient for both grades of stainless-steel [16].

One method of measuring susceptibility is by using the deflection test from ASTM F2052-15 [18]. In equation 2-13, α is the deflection angle, ρ is the density of the material, g is the acceleration due to gravity, μ_0 is the permeability of free space, $|\mathbf{B}_0|$ is the magnitude of the static field, and $|\nabla|\mathbf{B}_0||$ is the magnitude of the static field gradient.

$$\chi = \frac{\rho\mu_0g \tan(\alpha)}{|\mathbf{B}_0||\nabla|\mathbf{B}_0||} \quad (2-13)$$

In this study, a parameter sweep of the magnetic susceptibility from 1000 ppm to 15000 ppm was performed in COMSOL Multiphysics for cylinders that vary from 3, 5, 7, and 9 cm in length and diameters of 0.5 in and 0.25 in, same as the machined cylinders that will be used for experimental measurements. The magnetic susceptibility was assumed to be the same although as mentioned previously, how a piece of stainless-steel is cut can alter its magnetic properties. The anticipated magnetically induced torque was plotted against

the magnetic susceptibility to generate a curve that will be used to approximate for the magnetic susceptibility of the machined cylinders.

2.3 Methods

The computational software used was COMSOL Multiphysics 5.3a (COMSOL Inc., Stockholm, Sweden). The AC/DC module within COMSOL was used for all simulations. Subsequent analysis was performed in MATLAB (Mathworks Inc., Natick, USA). Experimental measurements were performed on a Discovery MR 750 3.0T clinical magnetic resonance imaging scanner (GE Healthcare, Chicago, USA).

2.3.1 Part 1: Verification of Parameters for Simulating Linear Magnetic Material in a Static Magnetic Field

The setup in COMSOL for the verification of parameters was heavily based on COMSOL tutorial 12735, *Magnetically Permeable Sphere in a Static Magnetic Field*, where a sphere of some relative permeability, μ_r , was placed in a uniform and static magnetic field, B_0 [9]. Since the analytical solutions for the magnetic fields inside and outside are known for a sphere and an infinitely long cylinder, the results from COMSOL can be verified.

Setup of Parameters in COMSOL Multiphysics

Two separate models were created for this portion of the study; a long cylinder where the radius is at most one tenth that of the length, and a sphere defined solely by the radius. These objects were placed within a two layered block as shown in figure 2-2. The outer layer of the block is the *Infinite Element Domain (IED)*, an exterior shell volume that was assumed to extend to infinity. All domains with the exception of the device, the cylinder and sphere, were made out of air. The material properties of the device were

defined solely an arbitrarily chosen μ_r such that it remained a linear magnetic material. The field, \mathbf{B}_0 , was arbitrarily chosen as well.

The physics used in COMSOL was *Magnetic Fields, No Currents (mfnc)* for which all domains were selected for. In the settings for this physics, under *Background Magnetic Field*, a *Reduced Field* was selected. This allowed for the x, y, and z components of the static field to be defined. Equation 2-4 was implemented into COMSOL as the reduced field in terms of the magnetic field strength, \mathbf{H} , rather than \mathbf{B} . The orientation of the static field relative to the objects, defined by α and β , were arbitrarily chosen since the resulting fields in any arbitrary direction are known from equation 2-7 through 2-10.

All domains were discretized and meshed with free tetrahedrals. The size of tetrahedrals for the domains that made up the objects used the predefined *Extremely Fine* setting while the remaining domains were meshed with the *Finer* setting. The meshed diagrams for both models are shown in figure 2-3.

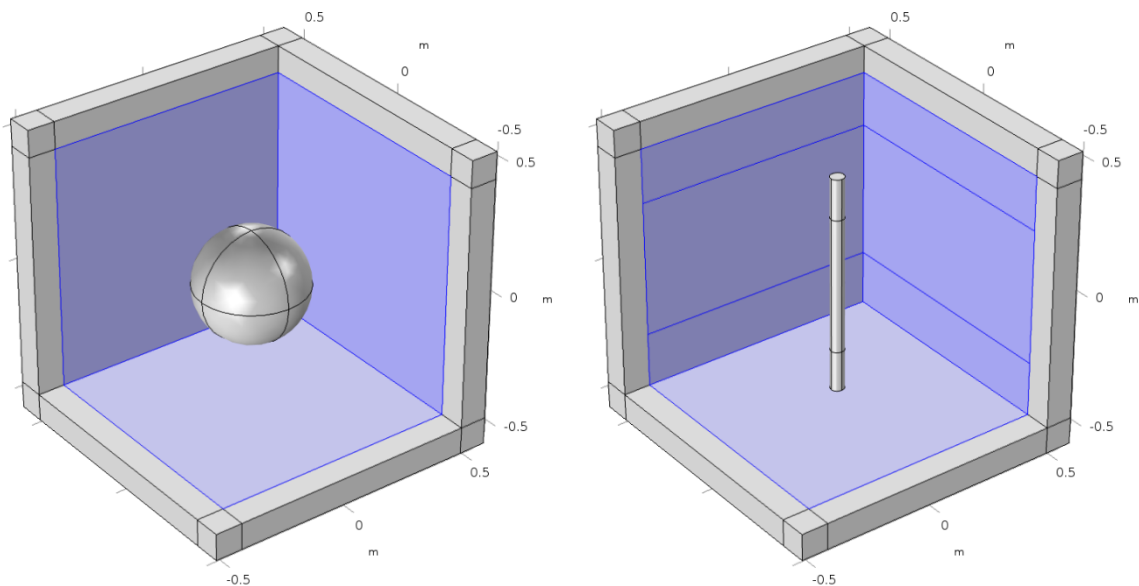


Figure 2-2: On the right is a long cylinder defined in a two-layered block. On the right is a sphere defined in a two-layered block. In both models, some domains have been hidden from view so that the cylinder and spheres are visible. The outer layer of the block is the IED. The objects, cylinder and sphere, and the blue portion of the block are what COMSOL

solves the B field for, the IED is not solved for. The objects are defined by an arbitrarily chosen relative permeability and all surrounding domains were defined by air.

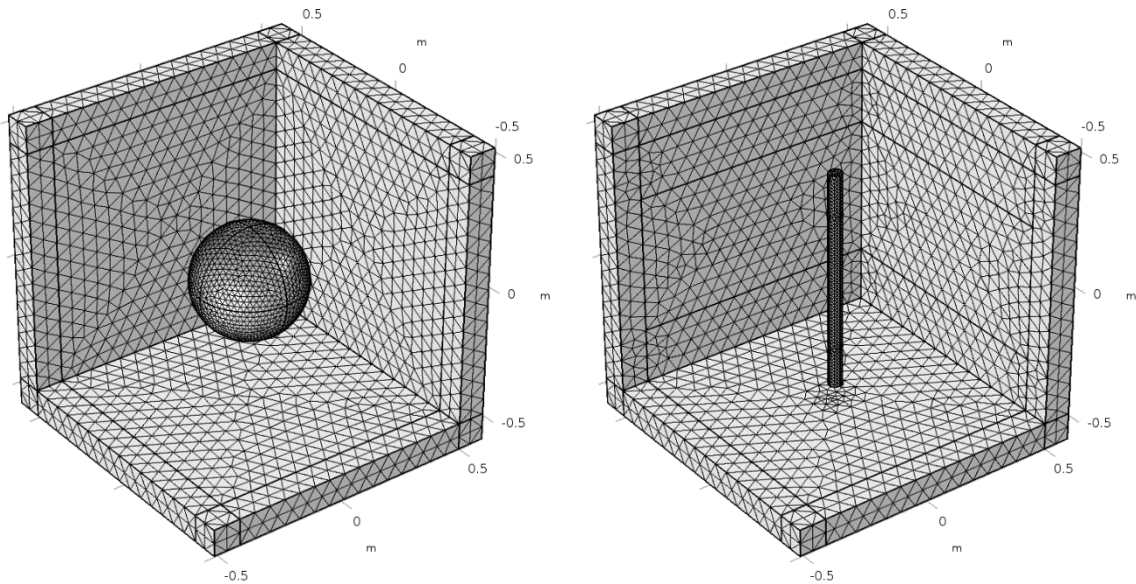


Figure 2-3: The objects from figure 2-3 discretized with free tetrahedrals. The objects, the cylinder and sphere, were discretized with a finer setting than the surrounding environment.

Setup of Study, Results, and Data Export in COMSOL Multiphysics

To find the magnetic fields inside and outside of the objects from these two models, a stationary study can be computed. Without specifying any parametric sweeps, COMSOL solves for what the magnetic fields are inside and outside of the cylinder and sphere, defined in *Geometry*, placed in the magnetic field, defined in *Magnetic Fields, No Currents (mfnc)*. In each step of the study, the physics and parameter sweep to solve for were identified. For this portion of the study, the only physics solved for was *Magnetic Fields, No Currents (mfnc)*. Parameter sweeps that do not involve changing the geometry setup can be defined as an *Auxiliary Sweep* in whichever step of the study. Auxiliary sweeps can be performed on the material properties, field strength, or α and β , changing the direction of the field, amongst other parameters. A *Parametric Sweep* needs to be selected under the study if the parameter changes the geometry such as the length or orientation of the device.

A 3D slice plot of the magnitude of the resulting B field in the XY, XZ, and YZ planes was automatically generated. The data plotted was specified in *Study 1/Solution 1* where a selection was made so that the infinite element domain was excluded from the plots. In the case of cylinder, it was also useful to exclude the ends of the cylinder as they would not exist in an infinitely long cylinder. Data was exported from COMSOL as a text file formatted into a spreadsheet. The B_x , B_y , and B_z data at each discretized tetrahedral shown in figure 2-3 was exported.

Importing Data into MATLAB and Verification of Results

Using the *load* function in MATLAB, the text file exported from COMSOL was imported as a $6 \times N$ matrix where N is the number of elements exported. The first three columns contain the x , y , and z coordinates while the following three are the B_x , B_y , and B_z at each position. From equations 2-7 through 2-10, the field at each exported position can be calculated. The regression between the two series, B field from COMSOL and the analytical B field, was plotted for the field outside of the objects. With FEM being a numerical method, the values from COMSOL are approximations and so for the field inside of the objects, the mean and standard deviation of the distribution of approximated values was found. The percent difference of the mean from the analytical value was then found.

2.3.2 Part 2: Simulation of Stainless-Steel Rods in a Static and Uniform Magnetic Field

Part 2, similar to Part 1, sets up in COMSOL an object placed within a static magnetic field. COMSOL calculates the magnetic field as well as the gradient of the magnetic field, which is then exported to MATLAB where the torque induced on the object is calculated. A total of 16 objects were used from a set of stainless-steel 316 and 304 cylinders that were 0.25 in (0.635 cm) and 0.5 in (1.27 cm) in diameter with lengths of 3, 5, 7, and 9 cm. The certificates of test for these cylinders are in appendix B. Throughout this study, to maintain a consistent use of metric units, the 0.25 in and 0.5 in diameters are referred to as thinner and thicker cylinders respectively. The cylinders acted as idealized

devices and were placed in the MR environment of a 3 T scanner. The simulated results for induced torque were verified with measured values by performing the ‘Pulley Method’ from the test standard ASTM F2213-17 [5].

2.3.2.1 Computational Setup

Setup of Parameters in COMSOL Multiphysics

The setup in COMSOL Multiphysics is similar to what was previously done for a cylinder placed in a static magnetic field in Part 1. A cylinder was defined inside a two layered block with the outer layer serving as the infinite element domain. The length and diameter of the cylinder changed with each iteration of the simulation to match the physical cylinders that were experimentally tested. All domains other than the cylinder were made out of air. The cylinder material was defined by the magnetic permeability of stainless-steel 304 or 316.

Two physics simulations were implemented for this study, *Magnetic Fields, No Currents (mfnc)* to setup the static field environment and field interactions with the cylinders and *PDE Coefficient* to calculate the spatial gradients of the magnetic fields from the first physics. In *Magnetic Fields, No Currents*, for which all domains were selected, a static field of 3 T was defined according to equation 2-6. The angles α and β were chosen such that, as shown in figure 2-1, the direction of the static field was along the long axis of the cylinder. During the study, α and β were chosen such that with each iteration, the direction of the static field rotates about the y-axis. In *PDE Coefficient*, all domains were selected again, the *Dependent variable quantity* and *Source term quantity* were selected to be the *Magnetic flux density*. Three dependent variables were chosen and were arbitrarily named, they represent B_x , B_y , and B_z calculated in *Magnetic Fields, No Currents*. The

Absorption Coefficient was set to $\begin{pmatrix} 1 & 0 & 0 \\ 0 & 1 & 0 \\ 0 & 0 & 1 \end{pmatrix}$ while all other coefficients were set to zero.

The source term was set to $\begin{pmatrix} \text{mfnc. } B_x \\ \text{mfnc. } B_y \\ \text{mfnc. } B_z \end{pmatrix}$.

As was with the setup in Part 1, all domains were discretized with free tetrahedrals. The device, the cylinder, was discretized with the *Extremely Fine* setting while the remaining domains used the *Finer* setting.

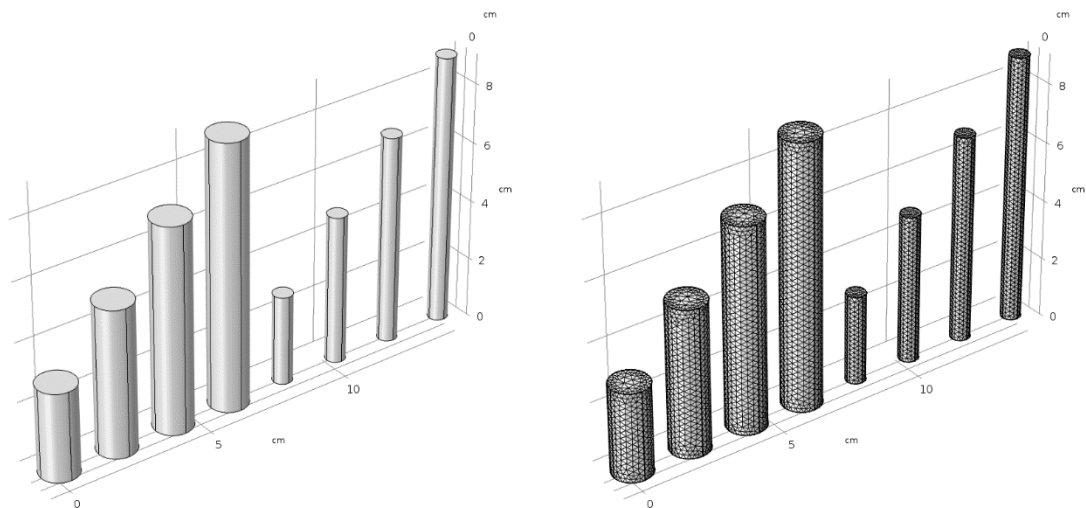


Figure 2-4: The left shows two sets of cylinders, thicker and thinner, with lengths of 3, 5, 7, and 9 cm. On the right is the same set of cylinders discretized with free tetrahedrals. These cylinders have the same dimensions as the physically engineered cylinders that will be experimentally measured for induced torque. In COMSOL, these cylinder models were placed in a two-layered block of air, similar to what is shown in figure 2-3.

Setup of Study, Results, and Data Export in COMSOL Multiphysics

The study consisted of two stationary steps. Step 1 was used to solve for *Magnetic Fields, No Currents*, while step 2 was used to solve for *Coefficient Form PDE*. In both steps, an *Auxiliary sweep* was setup with α and β such that the direction of the static field rotated for 360 degrees in steps of 15 degrees about the y-axis. Step 1 relied on *Physics controlled* settings while step 2 used *User controlled* settings that built upon the results from step 1.

Two datasets were formed from this study. *Study 1/Solution 1(sol 1)* held the solution to step 2 while *Study 1/Solution Store 1(sol 2)* held the results from step 1. From both datasets, the only domain selected was the device. The datasets were exported as three spreadsheets that held the magnetic flux components, the spatial gradients of the magnetic flux components, and the volumes of each discretized element.

Importing Data into MATLAB and Solving for Torque

Using the *load* function in MATLAB, the datasets were imported and used to calculate the induced force at each element. The induced torque was calculated by finding the induced force on each element from a single point, the centre of the cylinder then summed up. This is repeated for each iteration of the static field.

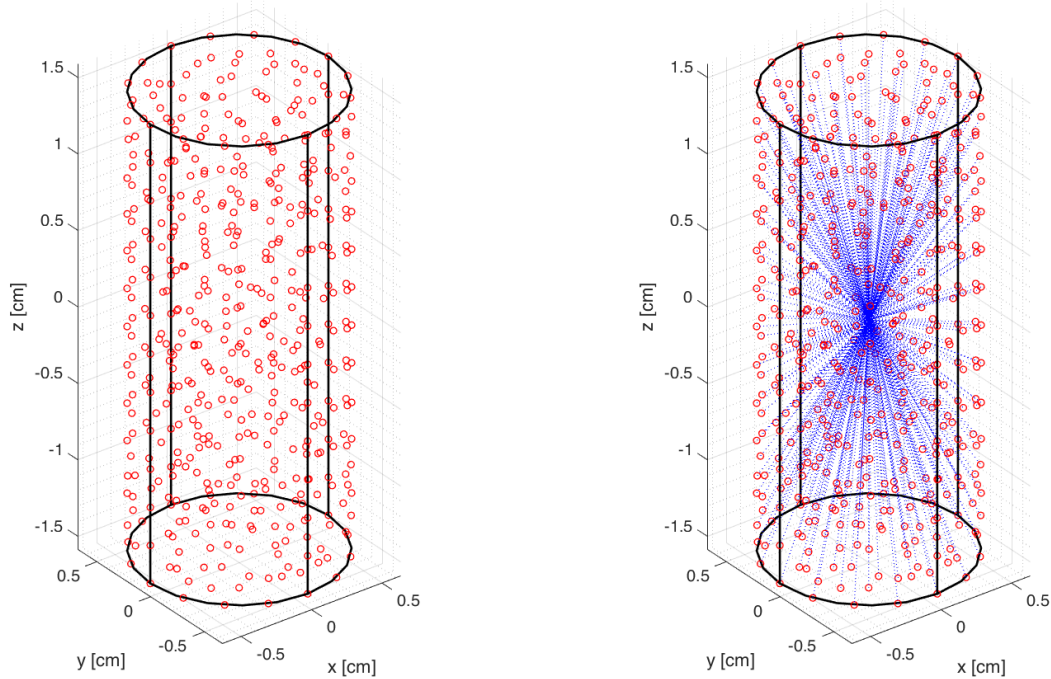


Figure 2-5: Using the thicker 3 cm long cylinder from figure 2-4 as an example. On the left is a plot of the positions of each element exported from COMSOL (red circles). On the right is the same plot of positions (red circles) with lines drawn from each position to the centre of the cylinder (blue dotted). At each position (red circles), the force induced is calculated and the torque from each element at a distance (length of blue dotted lines) from the origin is found.

2.3.3 Experimental Setup

To verify the simulated results, experimental measurements were taken on the physically machined cylinders. The certificates of test for the cylinders are in appendix B. The experiment performed was the ‘Pulley Method’ from the test standard, ASTM F2213-17 [19]. The measurements were carried out in the static environment of a 3 T MR, figure 2-9.

All parts of the apparatus used, figure 2-8, were non-magnetic and non-metallic as required in the ASTM standard. The cylinders, figure 2-7, were placed onto a 3D printed holder that could freely rotate with minimal friction. The platform was positioned such that the cylinder was at the magnetic isocentre of the MR scanner. From the platform, a thread was extended to a force sensor, which in turn was mounted to a linear displacement mechanism operated by a crank, figure 2-6. The force sensor was positioned such that it was as close to apparatus as the displacement mechanism would allow. As the crank was rotated, the force sensor would move away from the apparatus and by the thread, the platform would rotate.

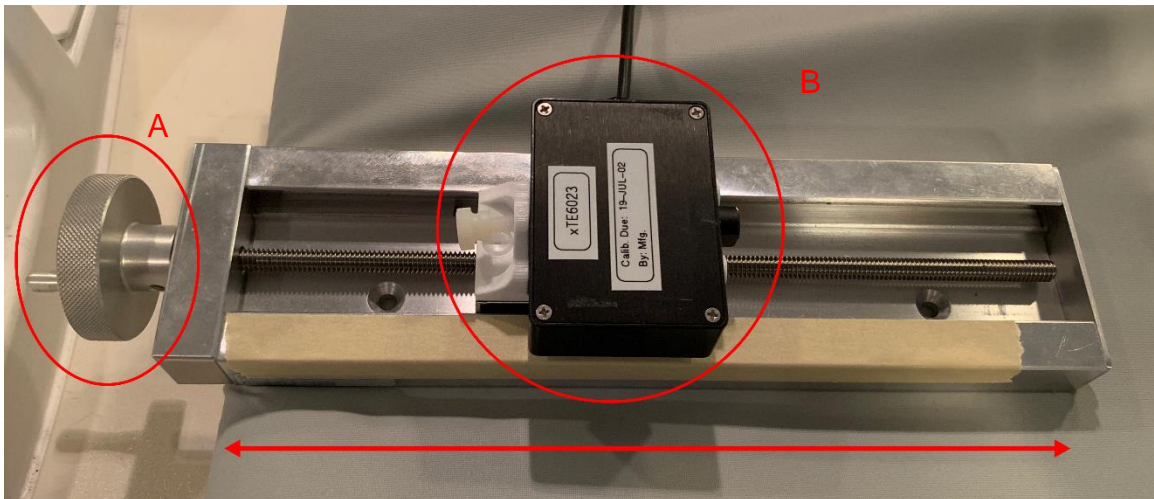


Figure 2-6: The linear displacement mechanism that holds the force sensor (B). While taking measurements, this apparatus was positioned such that the crank (A) faced away from the scanner and the force sensor was positioned at the greatest distance away from the crank. A thread was extended from the force sensor to the rotatable platform which held the test cylinders. By turning the crank clockwise, the force sensor was gradually moved to the left, pulling on the thread and setting the rotatable platform into motion. This apparatus was made from weakly magnetic material. The forces and torques induced on it are negligible.

Due to a torque induced on the cylinder, its longest dimension, the length of the cylinder, will try to align with the static field, the direction of the bore. As the force sensor was moved away, rotating the platform, due to the alignment with the static field, the tension in the thread was recorded. The peak tensions occur when the cylinder is perpendicular to the field. The linear mechanism allowed two 360-degree rotations producing four peaks and four troughs. The peaks occur approximately when the cylinder is perpendicular to the direction of the external field.

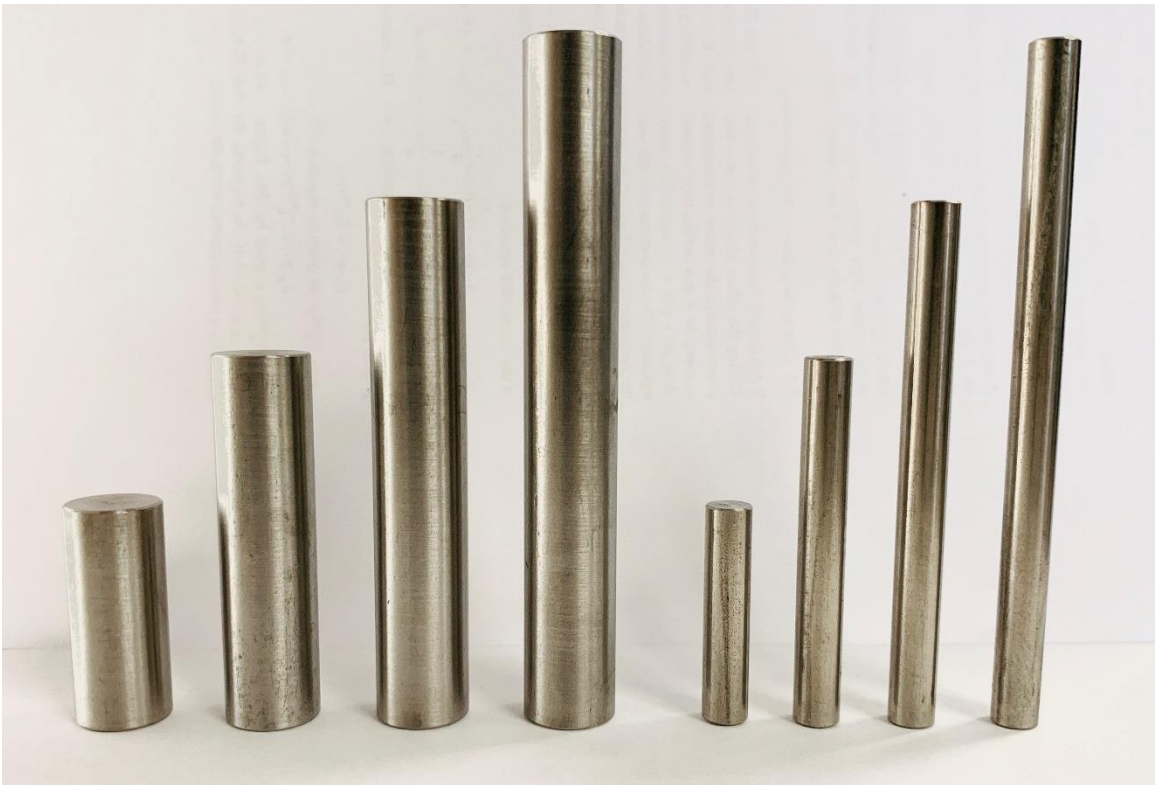


Figure 2-7: Two sets, thick and thin diameters (1.27 and 0.635 cm), of cylinders each cut from a single rod into four lengths (3, 5, 7, and 9 cm). The image shows the stainless-steel 316 set, there is an identical set for stainless-steel 304, a total of 16 cylinders were used for experimental measurements.

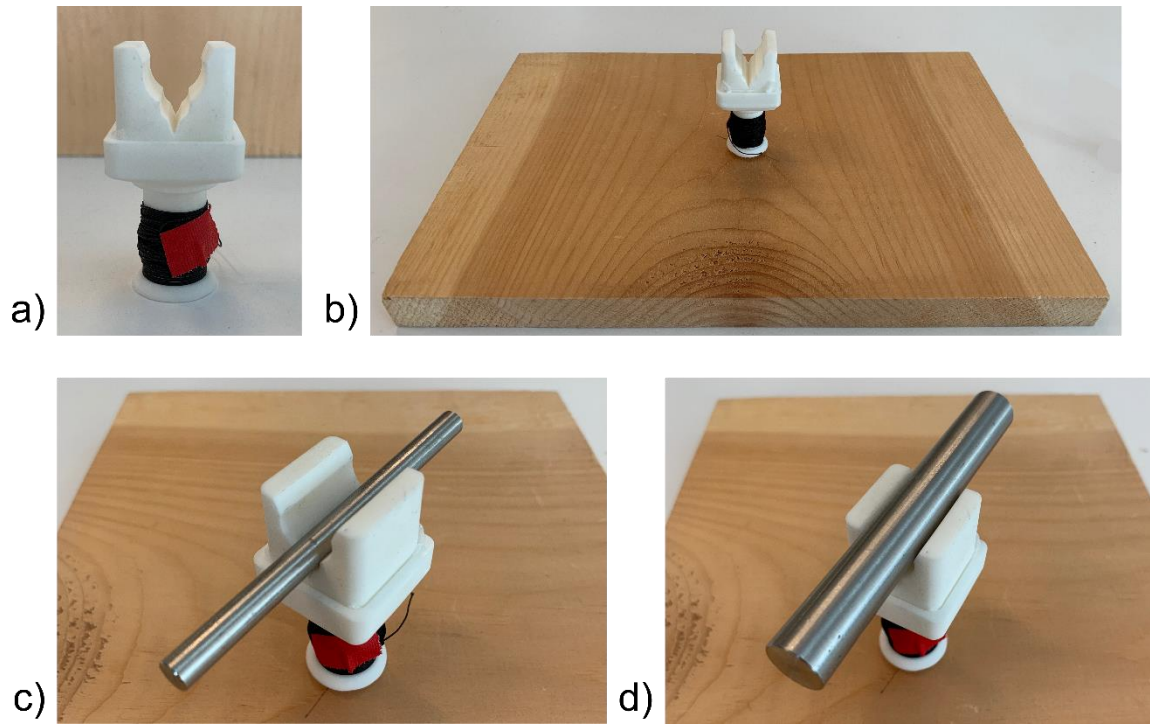


Figure 2-8: The apparatus that holds the test cylinders and placed at the magnetic isocentre of the MR scanner. The rotatable platform (a) sits on top of a wooden peg (b). The rotatable platform was designed specifically for the circumferences of the test cylinders: thinner (c) and thicker (d). When positioned into the MR scanner, the cylinders are positioned such that the axis of rotation is at the centre of mass of each cylinder.



Figure 2-9: The apparatus holding the test cylinders (A) from figure 2-8 is fixed to the patient table of an MR scanner with tape. The linear displacement mechanism holding the force sensor (B) from figure 2-6 is positioned at a distance such that all equipment still functions accurately. The patient table is moved into the MR scanner to position apparatus (A). There is a thread extended from (B) to (A). As the force sensor moves away from the scanner, the device is rotated and the tension in the string is recorded with device (C). Device (C) is the digital meter displaying the force reading and zeros the force sensor.

2.4 Results

2.4.1 Part 1: 3D Slice Plots from COMSOL and Analytical Plots MATLAB

Figure 2-10 shows 3D slice plots generated in COMSOL of the magnetic flux inside and outside of an infinitely long cylinder and sphere. Similarly, figure 2-11 shows the same kind of plot except it was made in MATLAB using equations 2-7 through 2-10. In both figures, three planes intersecting at the origin were plotted together. In all models, COMSOL and MATLAB, sphere and cylinder, the relative permeability of the object and surrounding was 2 and 1 respectively. The external field strength was 1 T in the x-direction and implanted according to equation 2-6.

An effective method of visualizing the simulated dataset from COMSOL and the analytically found dataset from MATLAB would be to plot the percent differences between the two using the analytical as truth. If COMSOL were capable of approximating for the B field perfectly, then there would be a percent difference of 0. This was done separately for the data inside and outside of the sphere and cylinder models. Considering that the mean percent difference in each distribution is less than 1%, COMSOL can be considered a suitable tool for modeling linear magnetic material in a uniform magnetic field.

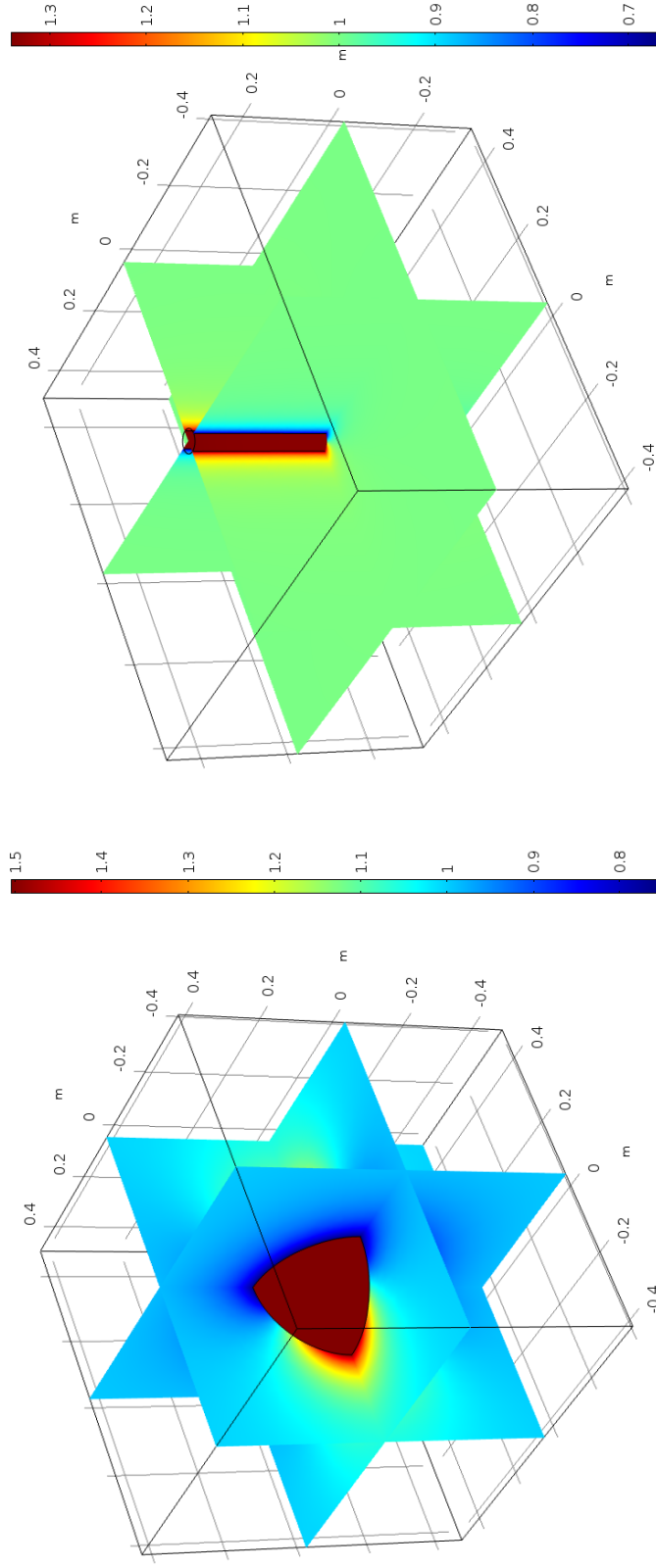


Figure 2-10: 3D Slice plots generated in COMSOL after solving for the B field inside and outside of a sphere (left) and cylinder (right) of linear material placed in a static and uniform external magnetic field. The colorbar is in Teslas and correspond to the resulting B field. In the model of the cylinder, only the middle section where the field is uniform is shown. It is the middle region that will be verified with the analytical solution later on. In both plots, the xy , xz , and yz -planes intersect at the origin.

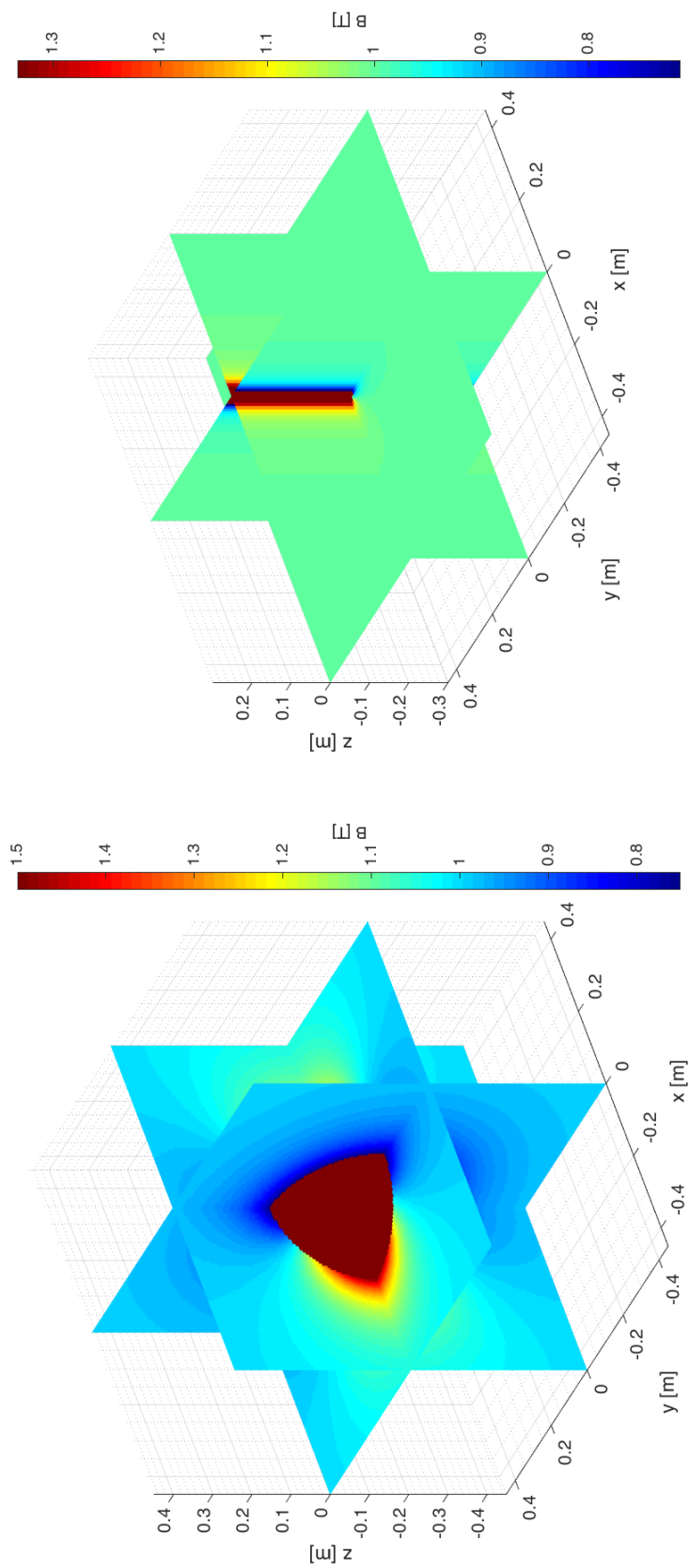


Figure 2-11: Similar to figure 2-11, this figure shows 3D slice plots of the B field inside and outside of a sphere (left) and cylinder (right) of linear material placed in a static and uniform external magnetic field. These plots however, were made by creating a 3D meshgrid of cartesian coordinates for which each position, the B field was calculated according to equations 2-7 through 2-10. Through initial inspection, these plots look very similar to those generated in COMSOL.

2.4.2 Part 1: Verification with Analytical Solution

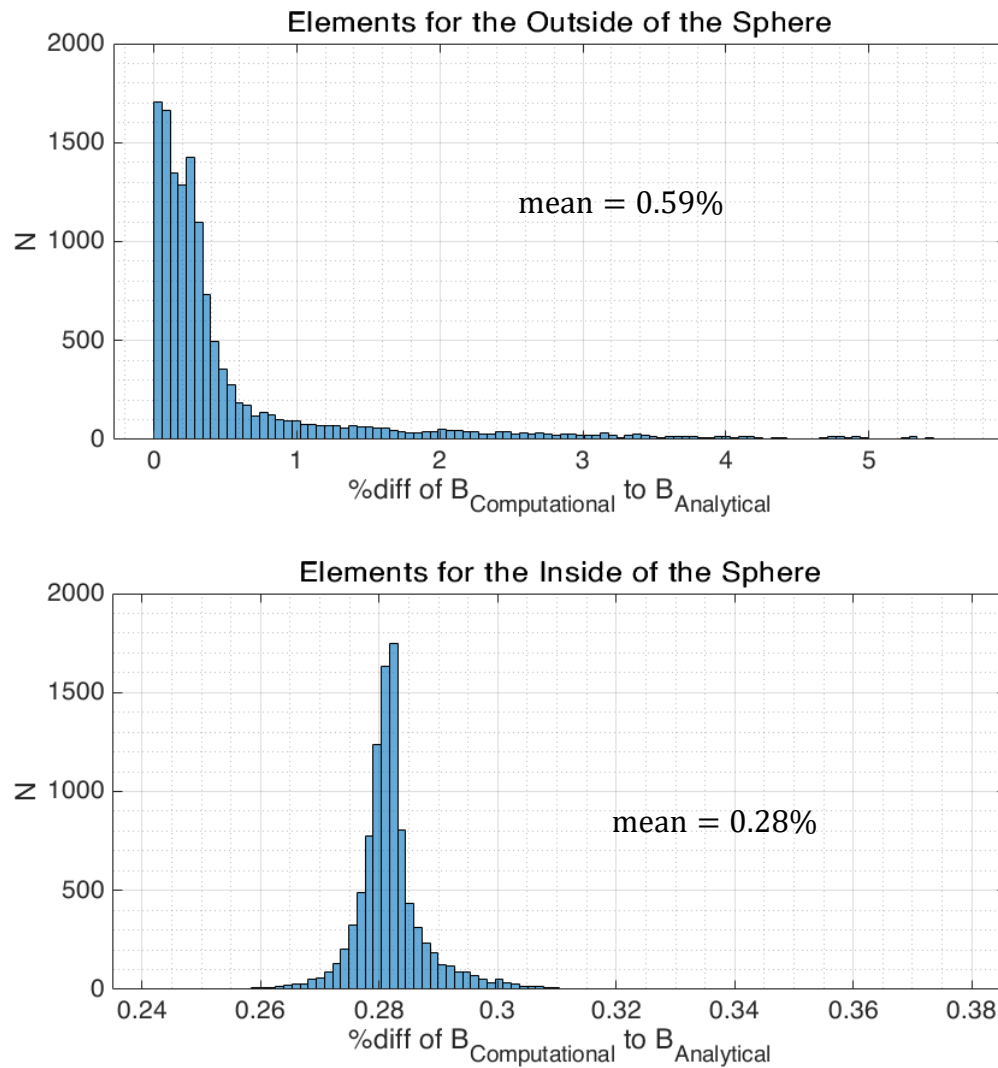


Figure 2-12: Analysis of COMSOL results for the sphere model. In the top image, the mean of the distribution of percent differences inside was 0.59%. The bottom image was the percent difference distribution inside of the object, the mean was 0.28%.

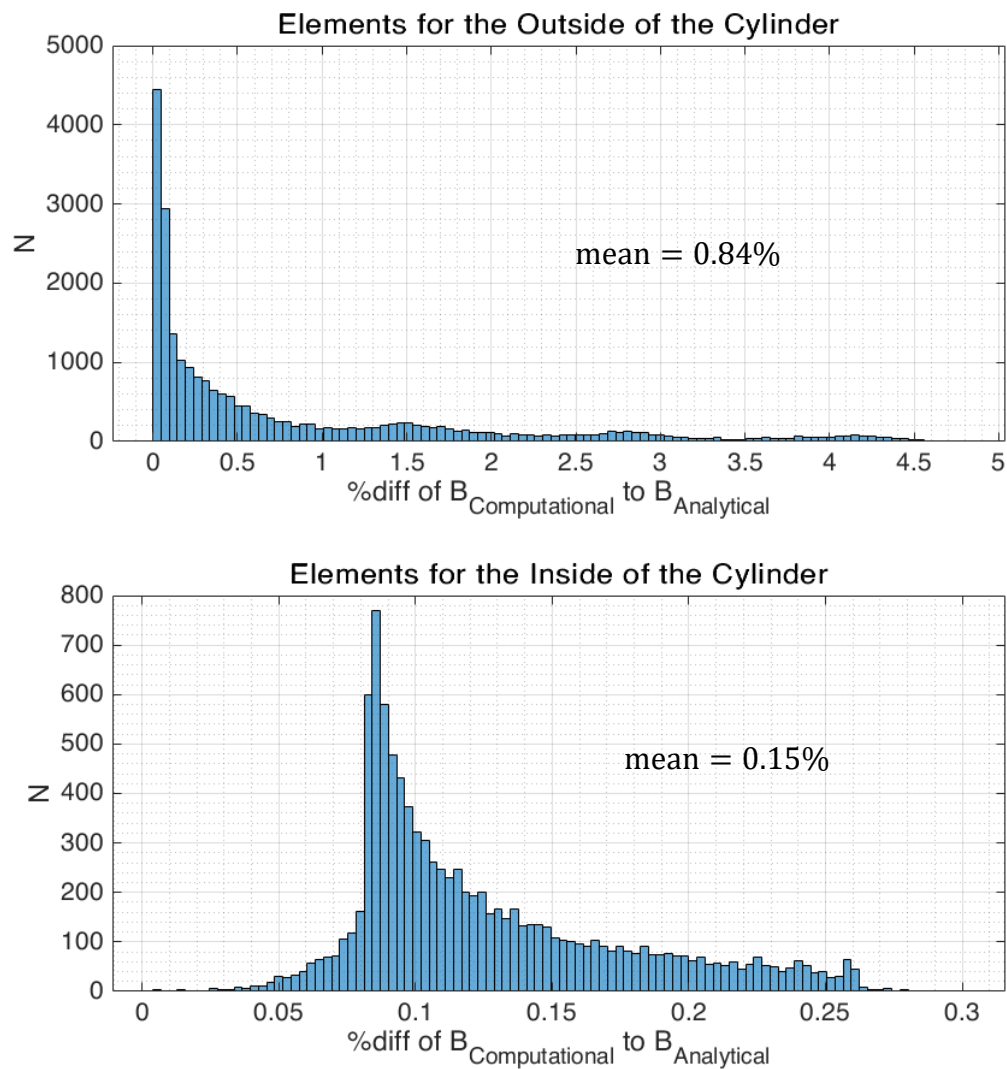


Figure 2-13: Analysis of COMSOL results for the cylinder model. In the top image, the mean of the distribution of percent differences inside was 0.84%. The bottom image was the percent difference distribution inside of the object, the mean was 0.15%.

2.4.3 Part 2: Finding the Magnetic Susceptibilities of the Stainless-Steel Cylinders

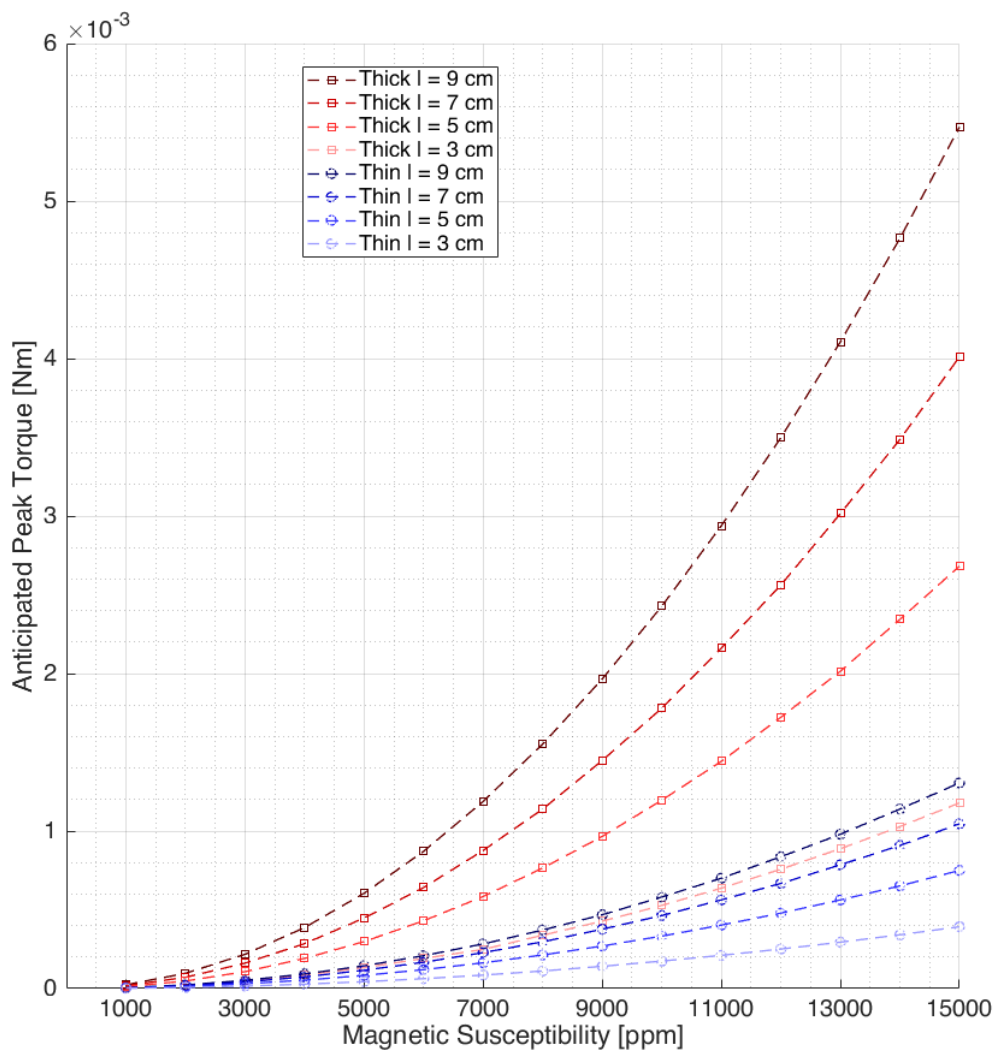


Figure 2-14: The relationship between magnetic susceptibility and induced torque for each geometry shown in figure 2-4. Since the precise magnetic susceptibility of the material used was not known, a parameter sweep of the magnetic susceptibility was performed from 1000 to 15000 ppm in steps of 1000 ppm. The data was fitted to obtain a mathematical relation between the anticipated peak torque and magnetic susceptibility which is shown in table 2-3.

Thick Rods ($d = 1.27$ cm)			
Length	Equation	95% Confidence Bounds ($y = ax^b$)	
		a	b
3 cm	$y = 5.590 \times 10^{-12}x^{1.993}$	4.833×10^{-12}	1.979
		6.346×10^{-12}	2.008
5 cm	$y = 1.188 \times 10^{-11}x^{2.001}$	1.132×10^{-11}	1.996
		1.243×10^{-11}	2.005
7 cm	$y = 1.833 \times 10^{-11}x^{1.997}$	1.753×10^{-11}	1.992
		1.913×10^{-11}	2.002
9 cm	$y = 2.414 \times 10^{-11}x^{2.001}$	2.373×10^{-11}	1.999
		2.455×10^{-11}	2.002
Thin Rods ($d = 0.635$ cm)			
3 cm	$y = 1.743 \times 10^{-12}x^{2.000}$	1.721×10^{-12}	1.999
		1.765×10^{-12}	2.001
5 cm	$y = 3.409 \times 10^{-12}x^{1.998}$	3.304×10^{-12}	1.994
		3.513×10^{-12}	2.001
7 cm	$y = 4.708 \times 10^{-12}x^{1.999}$	4.492×10^{-12}	1.994
		4.925×10^{-12}	2.003
9 cm	$y = 5.646 \times 10^{-12}x^{2.003}$	5.420×10^{-12}	1.999
		5.871×10^{-12}	2.007

Table 2-3: The equations for each of the susceptibility curves shown in figure 2-14. In each equation, the peak torque, y , is approximately proportional to magnetic susceptibility, x^2 . 95% confidence interval for both variables are provided. Using the experimentally measured peak torque values, the approximate magnetic susceptibility for each rod can be found.

2.4.4 Part 2: Experimentally Measured Induced Torque

Measured Peaks [mNm]				
Length	Thick SS316	Thick SS304	Thin SS316	Thin SS304
3 cm	0.133 ± 0.018	0.772 ± 0.016	0.052 ± 0.002	0.272 ± 0.008
5 cm	0.307 ± 0.018	1.710 ± 0.027	0.105 ± 0.004	0.515 ± 0.012
7 cm	0.444 ± 0.019	2.787 ± 0.040	0.145 ± 0.005	0.739 ± 0.016
9 cm	0.614 ± 0.021	3.728 ± 0.052	0.168 ± 0.006	0.936 ± 0.018
Associated Magnetic Susceptibility [ppm]				
3 cm	5034	12148	5447	12490
5 cm	5061	11941	5600	12413
7 cm	4983	12507	5576	13007
9 cm	5021	12369	5393	12693
mean \pm std	5025 ± 32	12241 ± 249	5504 ± 100	12651 ± 265

Table 2-4: Using the measured peaks listed in table 2-5, the magnetic susceptibility of each rod was found using the computational methods outlined in this study. The mean and standard deviation of the susceptibilities were found and implemented in COMSOL again to produce simulated peak torque values.

Thick SS316 ($\chi = 5025 \pm 32$ ppm)			
Length	Tests [mNm]	Sims [mNm]	% diff
3 cm	0.133 ± 0.018	0.134	0.579
5 cm	0.307 ± 0.018	0.301	1.872
7 cm	0.444 ± 0.019	0.452	1.914
9 cm	0.614 ± 0.021	0.612	0.299
Thick SS304 ($\chi = 512241 \pm 249$ ppm)			
3 cm	0.772 ± 0.016	0.788	2.030
5 cm	1.710 ± 0.027	1.786	4.387
7 cm	2.787 ± 0.040	2.675	4.121
9 cm	3.728 ± 0.052	3.640	2.396
Thin SS316 ($\chi = 55504 \pm 100$)			
3 cm	0.052 ± 0.002	0.053	2.103
5 cm	0.105 ± 0.004	0.103	1.590
7 cm	0.145 ± 0.005	0.141	2.824
9 cm	0.168 ± 0.006	0.175	3.792
Thin SS304 ($\chi = 512651 \pm 265$ ppm)			
3 cm	0.272 ± 0.008	0.279	2.599
5 cm	0.515 ± 0.012	0.547	6.004
7 cm	0.739 ± 0.016	0.744	5.831
9 cm	0.936 ± 0.018	0.928	0.876

Table 2-5: The calculated peak torque values from the measured forces. For each cylinder (two types of stainless-steel, two diameters, and four lengths), two full rotations were performed in the 3 T environment.

2.5 Conclusion

2.5.1 Verification of Using FEM to Find the Field Inside and Outside of Objects of Linear Magnetic Material

The verification of the setup of parameters in COMSOL are best shown in figures 2-12 and 2-13. Each figure is a distribution of percent differences found at each element exported from the models. The mean percent difference of the inside and outside of the sphere were 0.59% and 0.28%. The mean percent difference of the inside and outside of the cylinder were 0.84% and 0.15%. These values provide enough evidence to show that COMSOL is an effective tool for modeling linear magnetic material placed in an external magnetic field.

2.5.2 Verification of Computational Method to Calculate the Torque Induced on Stainless-Steel Cylinders from the Static Field of an MR Scanner

In both simulated and experimentally measured results, summarized in table 2-6, the torque induced on the cylinder by the static field increased with the length of the cylinder. It was expected that the longest cylinder in each set would be the 'worst case'. These expectations were reaffirmed by measurements. For objects with simple geometries, such as the cylinders used, the computational method outlined in this study was able to correctly rank the cylinders from least to greatest risk. It was also shown that, while knowing the necessary susceptibility parameter of the object, it was possible to produce simulated torque peaks to within 10% difference from measured values. Therefore, provided the static field strength, device geometry, orientation, and material properties, this study has shown that the static field induced torque can be accurately and correctly calculated.

One of the greatest limitations of this study was that the magnetic susceptibilities of the rods purchased was not known. The exact composition for each rod is available in appendix B however the magnetic susceptibility is not amongst the listed properties. A future step should include testing done on material that have better defined magnetic properties such as those available in the CRC handbook or ASM handbook, one of the only published sources for magnetic susceptibility. Other common metals used in medical implants should also be investigated such as titanium alloys (χ under 200 ppm) and cobalt chrome alloys (χ from 700 to 1500 ppm) [21].

Another limitation of this study was in the method for performing the ASTM method to measure the torque induced on the cylinders. The linear displacement mechanism shown in figure 2-6 relied on human operation which was not consistent over the distance the force sensor needed to travel. The force measurements had some dependence on the speed at which the crank was being turned. An improvement would incorporate a method of moving the force sensor at a constant speed such as a motor and remove the human element all together.

Future steps should also include greater complexity in the sample devices such as a metal plate holding screws. Such an object more closely resembles the cervical spine fixation system mentioned in the introduction. Unlike the cylinders, which lack multiple components, that only become longer, it is more difficult to anticipate which configuration of a plate with screws would be the worst case.

2.6 References

- [1] Canadian Agency for Drugs and Technologies in Health (CADTH). (2016). *The Canadian Medical Imaging Inventory, 2015*.
- [2] Canadian Agency for Drugs and Technologies in Health (CADTH). (2018). *The Canadian Medical Imaging Inventory, 2017*.
- [3] Kalin, R., & Stanton, M. S. (2005). Current clinical issues for MRI scanning of pacemaker and defibrillator patients. *PACE - Pacing and Clinical Electrophysiology*, 28(4), 326–328.
- [4] International Organization for Standardization (ISO). (2018). *Assessment of the safety of magnetic resonance imaging for patients with an active implantable medical device*.
- [5] ASTM International. (2013). *Standard Practice for Marking Medical Devices and Other Items for Safety in the Magnetic Resonance Environment*.
- [6] Nayfeh, M. H., & Brussel, M. K. (1989). *Electricity and Magnetism* (1st ed.). John Wiley & Sons, Inc.
- [7] Griffiths, D. J. (2013). *Introduction to Electrodynamics* (4th ed.). Pearson.
- [8] Caciagli, A., Baars, R. J., Philipse, A. P., & Kuipers, B. W. M. (2018). Exact expression for the magnetic field of a finite cylinder with arbitrary uniform magnetization. *Journal of Magnetism and Magnetic Materials*, 456, 423–432.
- [9] COMSOL Inc. (2014). *Magnetically Permeable Sphere in a Static Magnetic Field v5.3a*.
- [10] Bannan, K. El, Handler, W. B., Wyenberg, C., Chronik, B. A., & Salisbury, S. P. (2013). Prediction of Force and Image Artifacts Under MRI for Metals Used in Medical Devices. *IEEE/ASME Transactions on Mechatronics*, 18(3), 954–962.
- [11] Koch, K. M., Hargreaves, B. A., Pauly, K. B., Chen, W., Gold, G. E., & King, K. F. (2010). Magnetic resonance imaging near metal implants. *Journal of Magnetic Resonance Imaging : JMRI*, 32(4), 773–787.
- [12] Schenck, J. F. (1996). The role of magnetic susceptibility in magnetic resonance imaging: MRI magnetic compatibility of the first and second kinds. *Medical Physics*, 23(6), 815–850.

- [13] Salinger, G. L., & Wheatley, J. C. (1961). Magnetic susceptibility of materials commonly used in the construction of cryogenic apparatus. *Review of Scientific Instruments*, 32(7), 872–874.
- [14] Washko, S. D., & Aggen, G. (1990). Wrought Stainless Steels. In *Properties and Selection: Irons, Steels, and High-Performance Alloys* (pp. 841–907). ASM International.
- [15] Parent, S. B. (2017). *Static Magnetic Field Interactions of Medical Devices in The MRI Environment*.
- [16] ASTM International. (2018). *Standard Specification for Chromium and Chromium-Nickel Stainless Steel Plate, Sheet, and Strip for Pressure Vessels and for*.
- [17] Viennois, R., Giannini, E., van der Marel, D., & Černý, R. (2010). Effect of Fe excess on structural, magnetic and superconducting properties of single-crystalline $\text{Fe}_{1+x}\text{Te}_{1-y}\text{Se}_y$. *Journal of Solid State Chemistry*, 183(4), 769–775.
- [18] ASTM International. (2015). *Standard Test Method for Measurement of Magnetically Induced Displacement Force on Medical Devices in the Magnetic Resonance Environment*.
- [19] ASTM International. (2017). *Standard Test Method for Measurement of Magnetically Induced Torque on Medical Devices in the Magnetic Resonance Environment*.
- [20] Nyenhuis, J. A., Park, S.-M., Kamondetdacha, R., Amjad, A., Shellock, F. G., & Rezai, A. R. (2005). MRI and Implanted Medical Devices: Basic Interactions With an Emphasis on Heating. *IEEE Transactions on Device and Materials Reliability*, 5(3), 467–480.
- [21] Starcukova, J., Starcuk, Z., Hubalkova, H., & Linetskiy, I. (2008). Magnetic susceptibility and electrical conductivity of metallic dental materials and their impact on MR imaging artifacts. *Dental Materials*, 24, 715–723.

Chapter 3

Uncertainty Analysis of Torque Measurement Methods Described in ASTM F2213-17

This chapter discusses a study done in determining the systematic error due to static friction in the apparatus design and the overall effect on measurement uncertainties associated with the Torsional Spring and Pulley methods from ASTM F2213-17. Although error propagation can be done on the equation provided by the standard, this study sought to take it one step further and investigate how limitations in the apparatus design can affect measurement precision, specifically, the static friction in the rotatable platform of the pulley method. This chapter heavily relies on the test standard and draws comparisons by applying the minimum requirements to perform each measurement method. This chapter closes with the identified dominant sources of error and provides recommendations on how to minimize measurement uncertainty.

3.1 Introduction

The number of people with permanent or semi-permanent medical implants has been increasing, a growth that is in parallel with the growth of MRI as a diagnostic tool not only in Canada, but also abroad [1-3]. For patients with medical implants that cannot be readily removed, there is a need to know whether they can receive a scan without complications, one of which is the possibility of an induced torque on the implant.

The current test standard for measuring magnetically induced torque on medical implants is the ASTM F2213-17 which lists five methods [4]. The acceptance criterion for this standard is the torque due to gravity, the product of the longest dimension of the device and the device weight. Three methods, ‘calculation based on induced force’, ‘low-friction surface’, and ‘suspension’ methods, do not measure the induced torque. Instead, these three determine whether a significant enough torque is present and further testing is warranted. The remaining two methods, ‘torsional spring’ and the ‘pulley’ methods, are the ones under consideration in this chapter as they aim to measure a quantitative torque value. The standard does not include the sources of measurement error associated with each method.

The objectives of this study are to identify the dominant sources of error in each method under consideration. This is accomplished through propagation of instrument errors and taking measurements based on the standard apparatus design to identify systematic sources of error. The key systematic error investigated in this study is the static friction in the rotatable platform described in the pulley method. Through the comparison of uncertainties, improvements can be made to the design and usage of each test apparatus.

3.2 Theory

It is known that for a function, x , such that,

$$x = f(u_1, u_2, \dots, u_n) \quad (3-1)$$

The uncertainty of function x , δ_x , based on known sources of error is propagated by the following.

$$\delta_x^2 = \delta_{u_1}^2 \left(\frac{\partial x}{\partial u_1} \right)^2 + \delta_{u_2}^2 \left(\frac{\partial x}{\partial u_2} \right)^2 + \dots + \delta_{u_n}^2 \left(\frac{\partial x}{\partial u_n} \right)^2 \quad (3-2)$$

Equation 3-2 is true when all independent variables are uncorrelated [2]. An expression for the measurement uncertainty of each method can be calculated and then propagated forward to see how uncertainty changes with torque.

3.2.1 Error Propagation in the Torsional Spring Method

In the torsional spring method, the device under test (DUT) is fixed, by non-magnetic and non-metallic means, to a platform suspended on top and bottom by torsion springs. Some angular measurement tool, a protractor for example, is also fixed to the apparatus. Outside the MR environment, the equilibrium angle of the torsion springs represents the zero-torque angle, θ_1 . The apparatus and device are placed inside the MR scanner such that the device is as close to the magnetic isocentre as possible. When there is a torque induced on the device, the platform rotates away from the zero-torque angle and a second angular measurement, θ_2 , is recorded. The deflection angle is therefore, the difference between θ_2 and θ_1 , $\Delta\theta$. This is repeated at 10° intervals until a full rotation is made. The torque measured using this method, τ_S , can be found from the following,

$$\tau_S = k\Delta\theta \quad (3-3)$$

By applying equation 3-2 to equation 3-3, the measurement error for this method can be found as the following,

$$\delta_{\tau_S} = \tau_S \sqrt{\left(\frac{\delta_k}{k}\right)^2 + 2\left(\frac{\delta_\theta}{\Delta\theta}\right)^2} \quad (3-4)$$

In equation 3-4, δ_{τ_S} is the uncertainty of equation 3-3, δ_k is the uncertainty in the torsional spring constant, and δ_θ is the uncertainty in angular measurement.

3.2.2 Error Propagation in the Pulley Method

In the pulley method the DUT is fixed, by non-magnetic and non-metallic means, to a rotating platform, shown in figure 3-1. The platform is connected to a low-friction, non-metallic pulley with some radius, R . The apparatus and device are positioned into the MR scanner such that the device is as near as practical to the isocentre. The platform is allowed to rest with the device aligned at its equilibrium position. A lightweight thread extends from the pulley to force sensor and as the sensor is slowly pulled away, the peak force measurement, F , during a full rotation is recorded. Another rotation is performed without the device and the peak force measurement is recorded as the friction in the pulley, F_f . The peak torque measured using this method, τ_P , can be found from the following,

$$\tau_P = R(F - F_f) \quad (3-5)$$

By applying equation 3-2 to equation 3-5, the measurement error for this method can be found as the following,

$$\delta_{\tau_P} = \tau_P \sqrt{\left(\frac{\delta_R}{R}\right)^2 + 2\left(\frac{\delta_F}{F - F_f}\right)^2} \quad (3-6)$$

In equation 3-6, δ_{τ_P} is the uncertainty of equation 3-5, δ_R is the uncertainty in radius of the pulley, and δ_F is the uncertainty in force measurement.

3.2.3 Sources of Measurement Uncertainty

The requirements for performing the torsional spring method include an angular measurement tool capable of measuring at least 1° increments. A chosen torsional spring diameter such that the maximal deflection angle is less than 25° . A torque measurement apparatus with a sensitivity greater than 0.1 of the acceptance criterion. The sources of error for the torsional spring method include the instrument error for measuring angular deflection and the error in the torsional spring constant. The standard recommends the use of a protractor. It is often quoted that the instrument uncertainty of a device that incorporates a graduated linear scale, such as a protractor or a ruler, is half of the smallest scale division [2]. Therefore, a protractor with the smallest scale division being 1° would have an uncertainty, δ_θ , of 0.5° [7]. The uncertainty in the torsional spring constant, δ_k , was given a conservative estimate of 0.1 mNm.

To perform the pulley method, the standard requires the force sensor to be positioned sufficiently away such that it is still functional. The sensitivity of the torque measurement apparatus should be no greater than 0.1 of the acceptance criterion. The standard does not mention requirements for static torque in the pulley. The sources of error for the pulley method are the measurement errors from a force sensor and measurement of the radius of the apparatus. The force sensor used in this study was MR03-025 Force Sensor (Mark-10 Co, Copiague, USA). The calibration for this device is in appendix C.1 for which the instrument uncertainty, δ_F , was reported to be 1.67 mN. The maximum force, F_{\max} , reading that this device can report is 1.11 N. The radius of the apparatus was measured with a ruler, the smallest division was 1 mm. The radius, R , was found to be 5.1 cm and the uncertainty, δ_R , was 1 mm [7]. The dominant source of error is likely a systematic source of error and not in the instrument error. The greatest contribution to measurement uncertainty is likely to be the ‘stickiness’ of the platform, the torque required to overcome static friction.

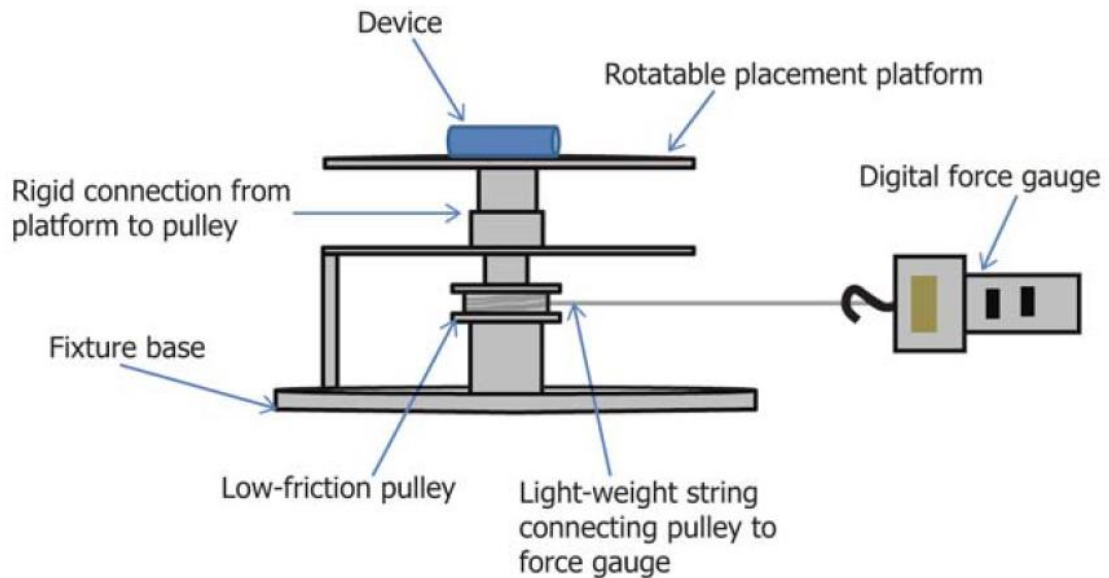
3.3 Methods

To find the error in static friction, measurements were made to determine the minimum amount of torque, ‘break torque’, required to set the apparatus into motion. The apparatus that was used was a modified design from what was shown in ASTM F2213-17. Figure 3-1 is the diagram described in the test standard. Figure 3-2 shows how the modified apparatus from figure 3-1. As was in the pulley method, a lightweight thread was extended from the cylindrical support, the low-friction pulley. Differing however, the thread was placed over yet another pulley that is attached to a mass. In this study, the torque that causes the platform to move is the weight of the mass attached to the thread rather than a torque induced by a magnetic field.

The rotatable platform was divided into twelve 30° sections. At the first section, the mass suspended from the pulley was incrementally increased until the weight was enough to allow the apparatus to make a full rotation. The mass was placed over the pulley slowly as to make sure that there was no unwanted impulse. Also, it was made sure that the mass was not swinging or spinning. The thread extending from the rotatable platform was made sure to not be in contact with the bottom of the platform causing unwanted friction.

The method chosen for incrementally increasing the mass was to place staples into a small basket. Staples were chosen since individually, the mass is insignificant, but multiple staples have a noticeable change in a tangible quantity. This process was repeated for each 30° section in order to have a static friction profile of the entire apparatus. For each mass used, there should be twelve measurements.

a)



b)

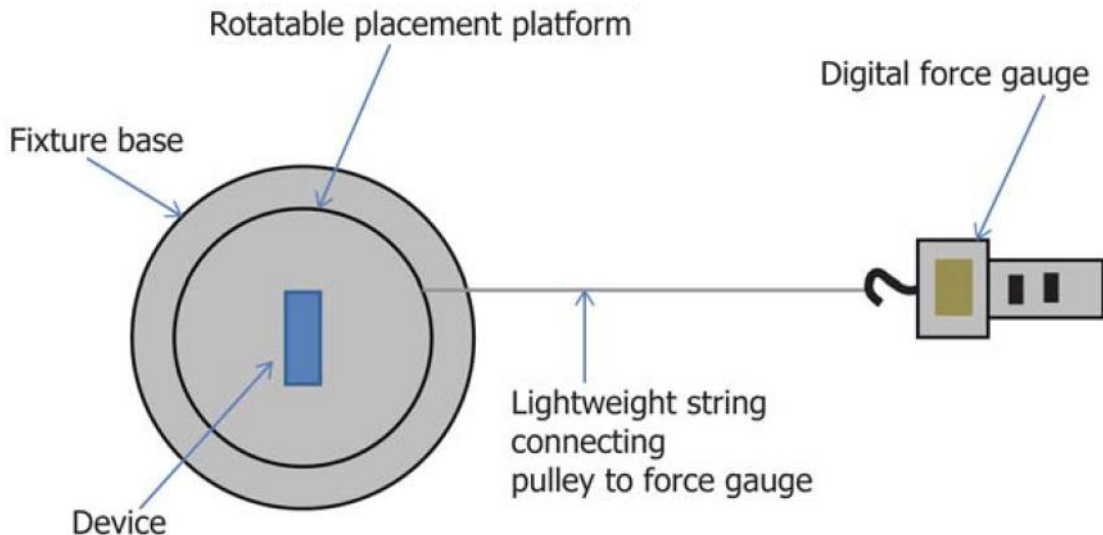


Figure 3-1: Schematic diagram for performing the pulley method from ASTM F2213-17. There is a thread extended from the low-friction pulley to the force gauge. The low friction pulley is fixed to the rotatable platform. As the force gauge is pulled away from the apparatus, the rotatable platform is set into motion [1]. Reprinted with permission from ASTM International, reference 4.

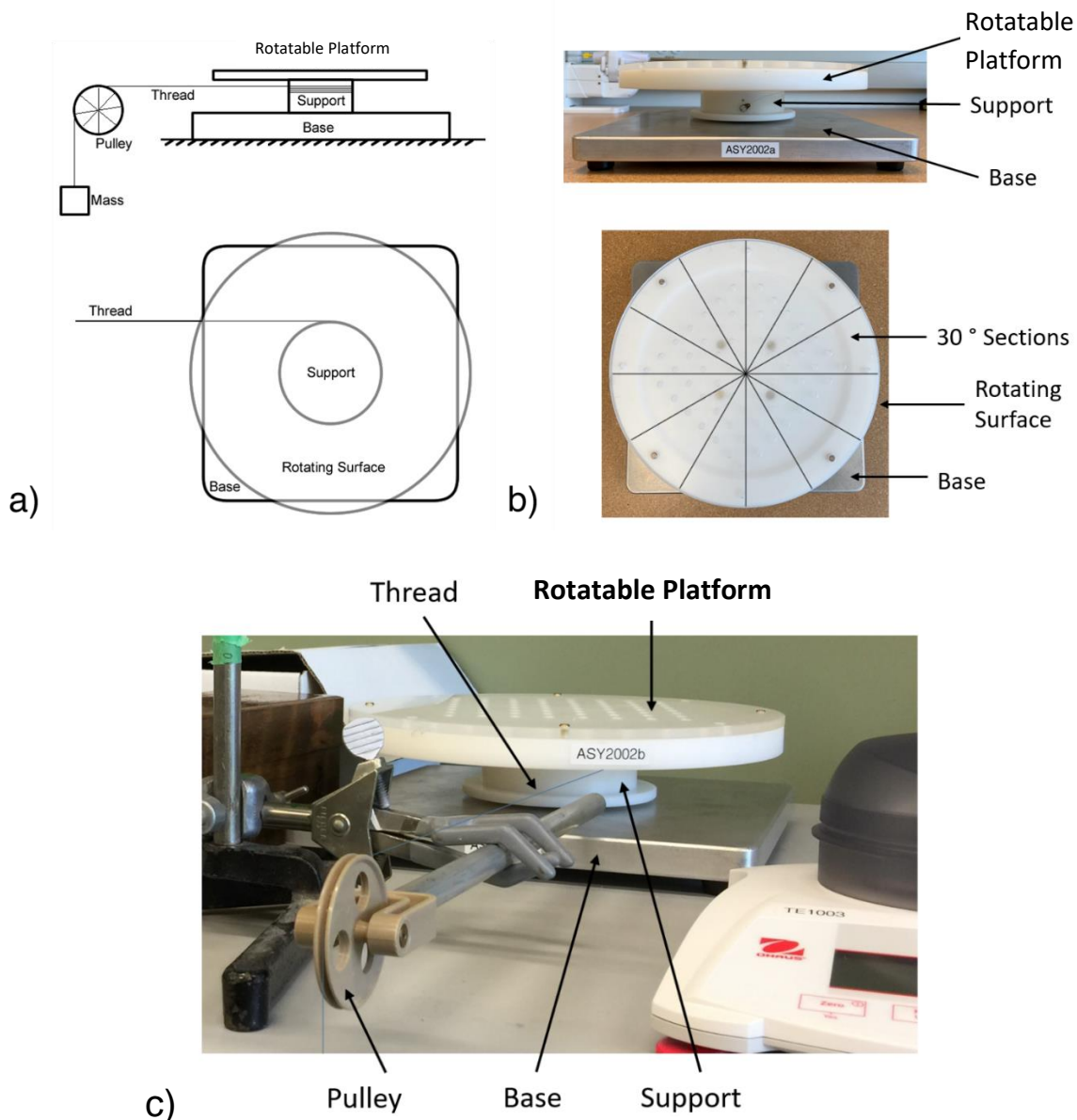


Figure 3-2: The rotating platform apparatus for measuring the minimum torque required to overcome static friction in the pulley method. a) Schematic of side and top views of the apparatus. b) Photographs of side and top views of the apparatus. c) The apparatus used with the thread extended to a second pulley which would be attached to a mass. This apparatus is a modified from what was described in ASTM F2213-17 and shown in figure 3-1. For this study, an empty apparatus was used, so no device was actually fixed to the platform. The mass attached to the pulley is a basket where small and measurable masses can be loaded into (shown only in schematic).

3.4 Results

Observations on what masses at which 30° section caused the rotatable platform to move is shown in table 3-1. The degree of movement at each section is labeled from 0 to 3. The static friction profile about the entire platform can be interpreted from table 3-1. It becomes clear that the sections around 300° to 90° exhibited the least friction since the smallest masses were able to set the platform into motion. The region around the 270° section had the greatest friction where it did not consistently move until 8.10 g mass was used.

A histogram of the number of instances of movement for each mass is shown in figure 3-3. The standard deviation of the data in figure 3-3 is 1.334 mNm. Within the first standard deviation, where the majority of observed rotations occurred, is the region of interest. $\delta_{F_s} = 0668$ mNm becomes the systematic source of error due to static friction in the error propagation. This leads to a new error propagation equation for the pulley method,

$$\delta_{\tau_P} = \tau_P \sqrt{\left(\frac{\delta_R}{R}\right)^2 + 2\left(\frac{\delta_F}{F - F_f}\right)^2 + \left(\frac{\delta_{F_s}}{\tau_P}\right)^2} \quad (3-7)$$

The smallest mass capable of setting the platform into motion was 2.62 ± 0.02 g. This was measured on an SPX123 laboratory balance (Ohaus Co., Parsippany, USA). The calibration report for this device is provided in appendix C.2. From the Earth Gravitational Model 2008, the acceleration due to gravity in London, Ontario at an elevation of 248 m is $9.8055 \pm 0.0001 \frac{\text{m}}{\text{s}^2}$ [8]. The radius of the apparatus pulley was previously measured to be 5.1 ± 0.1 cm. Therefore, the smallest mass corresponds to a weight of 25.7 ± 0.2 mN and a torque on the apparatus of 1.30 ± 0.03 mNm. This becomes the minimum that is used to generate figure 3-4. The smallest torque value is also used to calculate for an appropriate torsional spring constant so that comparable measurements of torque can be used. The spring constant of 1.30 mNm would be required to generate 1° deflection for comparable measures of torque.

	Total Mass (g)	Torque (mNm)	0°	30°	60°	90°	120°	150°	180°	210°	240°	270°	300°	330°
EMPTY	1.09	0.54	0	0	0	0	0	0	0	0	0	0	0	0
17 staples	1.60	0.79	0	0	0	0	0	0	0	0	0	0	0	0
34 staples	2.11	1.05	0	0	0	0	0	0	0	0	0	0	0	0
51 staples	2.62	1.30	0	0	0	1	0	0	0	0	0	0	0	0
2g mass	3.09	1.54	1	1	1	1	0	0	0	0	0	0	0	0
2g mass + 17 staples	3.60	1.79	1	1	1	1	0	1	0	0	0	0	1	1
2g mass + 34 staples	4.11	2.05	1	1	2	1	0	1	0	0	0	0	1	1
2g mass + 51 staples	4.62	2.30	1	1	2	1	0	1	0	0	0	0	0	1
2g mass + 67 staples	5.10	2.54	2	1	2	1	0	1	1	0	0	0	1	1
2g mass + 84 staples	5.61	2.80	2	2	2	1	0	1	0	1	1	1	1	2
5g mass	6.09	3.04	3	3	3	1	0	1	3	3	3	1	3	1
5g mass + 17 staples	6.60	3.29	1	3	3	3	1	3	3	3	3	1	3	3
5g mass + 34 staples	7.11	3.55	3	3	3	3	1	3	1	3	3	2	3	3
5g mass + 51 staples	7.62	3.80	3	3	3	3	3	3	3	3	3	2	3	3
5g mass + 67 staples	8.10	4.04	3	3	3	3	3	3	3	3	3	3	3	3

Table 3-1: The torque was calculated knowing the weight from the total mass used and the radius of the cylindrical support in figure 3-2. The observations are as follows: (0, white) the platform did not move, (1, green) the platform moved but not into subsequent 30° section, (2, yellow) the platform moved beyond subsequent 30° section but came to a rest due to friction, (3, orange) the platform moved and did not come to a rest. The empty measurements used the mass of the basket itself (1.09 g). The mean and standard deviation of the first instances where the weight of the load scored 3 at each section was found to be 3.249 ± 0.336 mNm.

The Torsional Spring Method		The Pulley Method	
$\delta_{\tau_S} = \tau_S \sqrt{\left(\frac{\delta_k}{k}\right)^2 + 2\left(\frac{\delta_\theta}{\Delta\theta}\right)^2}$		$\delta_{\tau_P} = \tau_P \sqrt{\left(\frac{\delta_R}{R}\right)^2 + 2\left(\frac{\delta_F}{F - F_f}\right)^2 + \left(\frac{\delta_{F_s}}{\tau_P}\right)^2}$	
Torsional Spring Constant	$k = 1.3$ mNm $\delta_k = 0.1$ mNm	Radius of Rotatable Platform	$R = 5.1$ cm $\delta_R = 1$ mm
Deflection Angle	$\theta_{min} = 1^\circ$ $\theta_{max} = 25^\circ$ $\delta_\theta = 0.5^\circ$	Force Sensor Measurements	$F_{min} = 0.03$ N $F_{max} = 1.11$ N $\delta_F = 1.67$ mN
		Uncertainty due to Static Friction	$\delta_{F_s} = 0.336$ mNm

Table 3-2: Summary of values going into error propagation that generates figure 3-4.

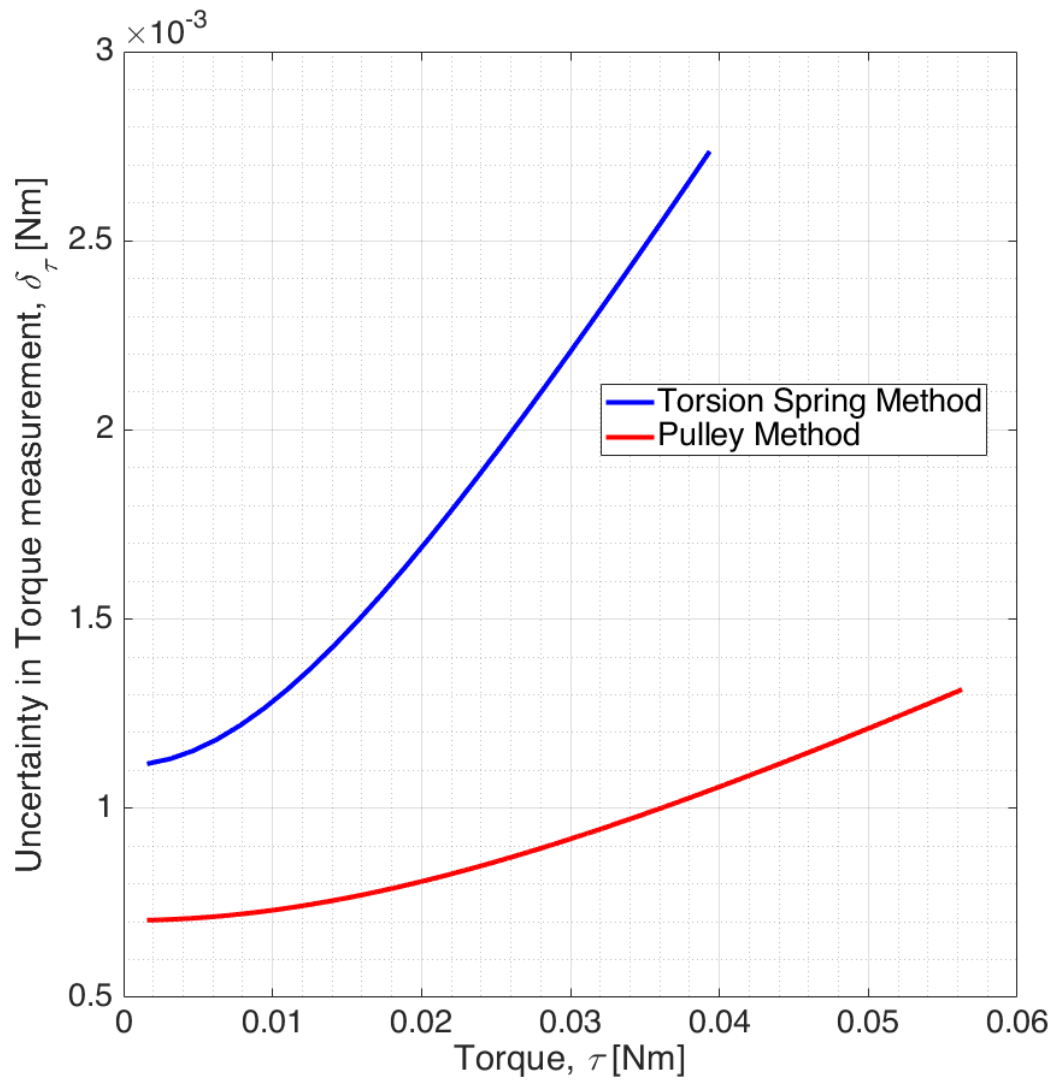


Figure 3-3: Graphical comparison between measurement methods. The data was propagated forward from the initial instance where a mass was capable of moving the apparatus from table 3-1. The pulley method offers a smaller measurement uncertainty than the torsional spring method for comparable measurements. The torsional spring method used equation 3-4. The pulley method used equation 3-7.

3.5 Conclusion

The dominant source of measurement uncertainty was identified for each method. In the torsional spring method, the angle measurement tool capable of measuring at least 1° increments. In the pulley method, the dominant source of error is the static friction, 'stickiness', in the rotating platform from the minimum amount of torque required to set the apparatus into motion. To minimize measurement uncertainty in the two methods, the following aspects of the two methods should be improved. In the torsional spring method, the deflection angle measurement tool should have greater precision than the 1° readings as described in test standard. In the pulley method, the break torque should be more consistent around the entire apparatus. One way of accomplishing this is to have a rotatable platform that is lighter in mass.

The goal of this study was to look into sources of measurement error associated with the two major test methods from ASTM F2213-17. It is easy to take an existing equation and put it through error propagation, but this study sought to take it one step further and experimentally measure the limitations of a particular apparatus design. The focus of this study was the static friction in the rotatable platform of the pulley method. Future steps may look into limitations in design not taken into consideration in this study. Those include the placement of the device relative to the platform, the friction between the thread and the platform, thickness of the thread used, the positioning of the force sensor, or the angle at which the thread contacts the platform. No limitations related to the torsional spring method were investigated at all.

3.6 References

- [1] Kalin, R., & Stanton, M. S. (2005). Current clinical issues for MRI scanning of pacemaker and defibrillator patients. *PACE - Pacing and Clinical Electrophysiology*, 28(4), 326–328.
- [2] Canadian Agency for Drugs and Technologies in Health (CADTH). (2018). *The Canadian Medical Imaging Inventory*, 2017.
- [3] Organisation for Economic Co-operation and Development (OECD). (2017). *Health at a Glance 2017*.
- [4] ASTM International. (2017). *Standard Test Method for Measurement of Magnetically Induced Torque on Medical Devices in the Magnetic Resonance Environment*.
- [5] Bevington, P. R., & Robinson, D. K. (2003). *Data Reduction and Error Analysis for the Physical Sciences* (3rd ed.).
- [6] Mark-10 Corporation, “MR03-025 Force Sensor”
- [7] Staedtler Mars, “Staedtler Mars 568”
- [8] Pavlis, N. K., Holmes, S. A., Kenyon, S. C., & Factor, J. K. (2013). Erratum: Correction to the development and evaluation of the earth gravitational model 2008 (EGM2008). *Journal of Geophysical Research: Solid Earth*, 118(5), 2633.

Chapter 4

Thesis Summary, Future Directions, and Conclusion

This chapter summarizes the findings of the two investigative chapters. It continues to offer future directions to take so that the greater goal of developing a computational system for finding the torque induced on any device can be accomplished. This chapter ends by highlighting the key investigation presented in this thesis and its importance in the further development of the greater goal.

4.1 Thesis Summary

4.1.1 Chapter 2 Summary

In Chapter 2, it was verified that COMSOL Multiphysics was able to accurately calculate the magnetic field inside and outside of objects with known analytical solutions, a sphere and cylinder of linear magnetic material, when placed in an external field. Taking advantage of this, COMSOL Multiphysics was used to further calculate the torque induced on stainless-steel cylinders. Verified with measured results, the computational results were within 10% difference. This method has shown to be fast and accurate as the data for one cylinder can be found within 10 minutes.

4.1.2 Chapter 3 Summary

In Chapter 3, an uncertainty analysis of the torque measurement apparatus described in ASTM F2213-17 was performed with an emphasis on the contribution of static friction. It was found that the apparatus described in the ‘Pulley Method’ offered a lower instrument uncertainty than the apparatus described in the ‘Torsional Spring Method’. This study was important should the apparatus be used in the future to verify computational results.

4.2 Future Directions

4.2.1 Investigate Torque Induced on Better Characterized Material

One of the greatest limitations of the study presented in Chapter 2 was that the volume magnetic susceptibility of the materials used was not known. For material such as stainless-steel 304 and 316, where the composition is not consistent, there is little to no literature available on the magnetic properties. The study performed in Chapter 2 should be repeated with better characterized material such as those presented in the CRC Handbook or pure metals. Not because such material may be used in medical implants, but they would serve as a good method for verifying that the computational method produces accurate information.

4.2.2 Extend Computational Torque and Force Models to More Complex Objects

The study in Chapter 2 was conducted on cylinders. Similarly, a previous study on magnetically induced force was also conducted on cylinders made from the same material, stainless-steel 304 and 316. Induced force and torque are the two major concerns when it comes to medical devices in the static field environment. Both studies should be extended to objects with more complex geometries for example, a metal plate holding screws. Such an object introduces an incredible amount of variability. The plates can vary in length and

capacity while the screws themselves can vary in length and the number placed onto the plate. Furthermore, unlike a cylinder, there is a lack of radial and bilateral symmetry with a plate and screws system which means the orientation within the field will play a greater role than it did in the cylinder studies. A study involving more complex devices will offer a more robust computational method for assessing static field interactions in general.

4.2.3 Investigate Eddy Current Torque

A phenomenon that was briefly discussed in Chapter 1 but was not explored in this thesis was the torque induced not from the static magnetic field, but from eddy currents induced on conductive material. The material does not necessarily need to be magnetic but electrically conducting. For example, aluminum and copper are good conductors and may experience eddy current torque but as diamagnetic material, they experience little to no static field induced torque. In short, conducting objects turning in the static magnetic field experience a torque due to the induced eddy currents. Eddy current torque will be an extension of the study conducted in Chapter 2 which used a computational method that ignored conductivity.

4.2.4 Automating Computational Processes

Currently, the method described to computationally find the torque induced on an object is only partially automated. COMSOL Multiphysics solves for the magnetic field inside and outside of the object described but it relies on human input to select for the necessary data to be exported and for the torque to be calculated in MATLAB. A fully automated method that begins with the defining parameters in COMSOL and ends with results from MATLAB would make the process more efficient. A possible method or automating tasks is using Python.

4.2.5 Investigate Very Long Objects Experiencing Interactions in Tandem

So far, the studies done in terms of torque and force look at the interactions separately. For example, a very long object that extends from inside the bore to the outside surrounding area, would experience static field induced torque and force in tandem. A study into how long objects behave in the static field would provide necessary information for a computational method that can completely assess static field interactions.

4.2.6 Extend Uncertainty Analysis of Rotating Test Platforms

Chapter 3 looked into the instrument uncertainty of an apparatus described in ASTM F2213-17 as the ‘Pulley Method’. In the study, the focus was the static friction in the rotating platform however, this is not the only limitation in apparatus design. In addition, the device placement relative to the platform, friction between thread and the platform, thickness of the thread used, positioning of the force sensor, and the angle at which the thread comes into contact with the platform should be looked into. Furthermore, an uncertainty analysis of the alternative measurement method, ‘Torsional Spring Method’, should be performed as well.

4.3 Conclusion

The key study within this thesis was the development and verification of the computational method for calculating the static field induced torque on idealized devices, stainless-steel 304 and 316 cylinders. By implementing the appropriate field and material conditions into COMSOL Multiphysics, it was possible to accurately calculate the torque induced to within 10% error from measured values. Furthermore, this method was capable of correctly ranking the cylinders in terms of risk and identify the ‘worst case’ out of each set.

It was also found that the peak torque induced increased linearly with the length of the cylinders. Considering the accuracy of the simulated results, the slopes of the linear plots between torque and length were also accurately found. The significance of this result is the capability of predicting the induced torque on cylinders that extend beyond the sets used.

A cylinder, however, is an incredibly simple object and does not properly characterize medical devices that are commercially available or seeking pre-market approval. Further investigations are necessary to accomplish the greater goal of developing a computational system that can accurately solve for the torque induced on a device of some arbitrary geometry and material placed within a clinical scanner. The preliminary results provided in this thesis is a necessary first step to accomplishing this goal.

Appendices

Here, some supplementary information directly related to the work presented in Chapters 2 and 3. In Appendix A, mathematical derivations for the magnetic flux equations are presented. These equations were used to verify the computational methods presented in Chapter 2. Appendix B includes the certificates of test for the stainless-steel rods used in Chapter 2. Appendix C includes the calibration certificates for the scientific equipment used in Chapters 2 and 3. Appendix D includes the copyright permissions for figures used throughout this thesis.

Appendix A: Derivation of Equations

A.1: Spherical and cylindrical coordinates

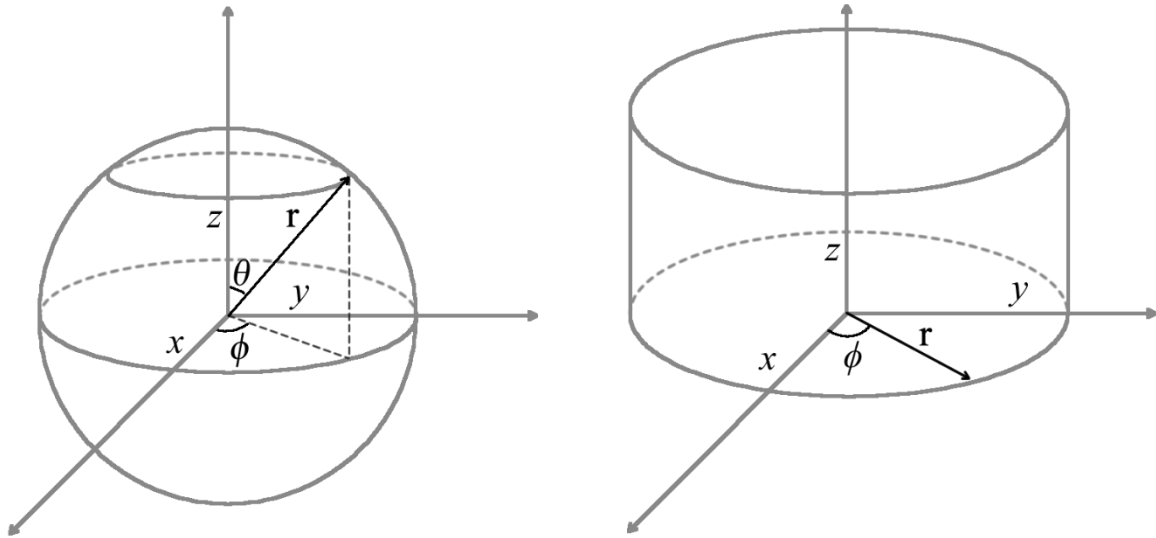


Figure A-1: Diagram of a sphere (left) and cylinder (right) drawn in euclidean space. In the sphere, the radius vector, \mathbf{r} , extends from the origin to the surface of the sphere whose magnitude, $|\mathbf{r}|$, is the radius, r . The zenith angle, θ , forms between the radius vector and the z axis. The azimuthal angle, ϕ , forms between the projection of the radius vector onto the xy plane and the x axis. In the cylinder, the radius vector, \mathbf{r} , extends from the z axis to the surface of the cylinder whose magnitude, $|\mathbf{r}|$, is the radius, r . The azimuthal angle, ϕ , forms between the projection of the radius vector onto the xy plane and the x axis.

The cartesian unit vectors in terms of spherical and cylindrical coordinates can be found by the following,

$$\begin{pmatrix} \hat{\mathbf{x}} \\ \hat{\mathbf{y}} \\ \hat{\mathbf{z}} \end{pmatrix} = \begin{pmatrix} \sin(\theta) \cos(\phi) & \cos(\theta) \cos(\phi) & -\sin(\phi) \\ \sin(\theta) \sin(\phi) & \cos(\theta) \sin(\phi) & \cos(\phi) \\ \cos(\phi) & -\sin(\phi) & 0 \end{pmatrix} \begin{pmatrix} \hat{\mathbf{r}} \\ \hat{\boldsymbol{\theta}} \\ \hat{\boldsymbol{\phi}} \end{pmatrix} \quad (\text{A.1-1})$$

$$\begin{pmatrix} \hat{\mathbf{x}} \\ \hat{\mathbf{y}} \\ \hat{\mathbf{z}} \end{pmatrix} = \begin{pmatrix} \cos(\phi) & -\sin(\phi) & 0 \\ \sin(\phi) & \cos(\phi) & 0 \\ 0 & 0 & 1 \end{pmatrix} \begin{pmatrix} \hat{\mathbf{r}} \\ \hat{\boldsymbol{\phi}} \\ \hat{\mathbf{z}} \end{pmatrix} \quad (\text{A.1-2})$$

A.2: Finding the magnetic flux density inside and outside of a sphere of linear material with the external field along z-direction

Given the magnetic scalar potentials Φ_1 and Φ_2 inside and outside of the sphere,

$$\Phi_1 = A_1 r \cos(\theta) + \frac{A_2}{r^2} \cos(\theta) \quad (\text{A.2-1})$$

$$\Phi_2 = C_1 r \cos(\theta) + \frac{C_2}{r^2} \cos(\theta) \quad (\text{A.2-2})$$

The constant A_2 is equal to zero because the potential inside the sphere should be finite at the origin. The constant C_1 is equal to $-H_0$ since $\Phi_2 = -H_0 r \cos(\theta)$ when r becomes very large. Equations A.2-1 and A.2-2 become,

$$\Phi_1 = A_1 r \cos(\theta) \quad (\text{A.2-3})$$

$$\Phi_2 = -H_0 r \cos(\theta) + \frac{C_2}{r^2} \cos(\theta) \quad (\text{A.2-4})$$

Two more equations relating A_1 and C_2 are required to determine the potentials. From the boundary condition of the sphere, $r = R$, it is known that Φ_1 is equal to Φ_2 .

$$A_1 R = -H_0 R + \frac{C_2}{R^2} \quad (\text{A.2-5})$$

The second equation used is determined from the continuity of the normal components of B since it is known that,

$$B_n = \mu H_n = -\mu \frac{\partial \Phi}{\partial r} \quad (\text{A.2-6})$$

In equation A.2-6, μ is the permeability of the material, μ_1 inside of the sphere and μ_2 outside. Applying equation A.2-6 to equations A.2-3 and A.2-4 and recalling that $r = R$, it can be found that,

$$-\mu_1 A_1 = \mu_2 H_0 + 2 \frac{\mu_2 C_2}{R^3} \quad (\text{A.2-7})$$

Using equations A.2-5 and A.2-7, it can be determined that A_1 and C_2 are,

$$A_1 = -\frac{3\mu_2 H_0}{\mu_1 + 2\mu_2} \quad (\text{A.2-8})$$

$$C_2 = \mu_2 H_0 R^3 \frac{\frac{\mu_1}{\mu_2} - 1}{\mu_1 + 2\mu_2} \quad (\text{A.2-9})$$

Substituting equations A.2-8 and A.2-9 into equations A3 and A4, the scalar potentials Φ_1 and Φ_2 can be determined to be,

$$\Phi_1 = -\frac{3\mu_2 H_0}{\mu_1 + 2\mu_2} r \cos(\theta) \quad (\text{A.2-10})$$

$$\Phi_2 = -H_0 r \cos(\theta) + H_0 \frac{R^3 \frac{\mu_1}{\mu_2} - 1}{r^2 \frac{\mu_1}{\mu_2} + 2} \cos(\theta) \quad (\text{A.2-11})$$

The magnetic flux density inside and outside of the sphere can now be found by applying the fact that $\mathbf{B} = \mu\mathbf{H}$ and $\mathbf{H} = -\nabla\Phi$. Applying the gradient in spherical coordinates reveals that,

$$\begin{aligned} \mathbf{B}_1 &= -\mu_1 \nabla\Phi_1 \\ &= \frac{3\mu_1}{\mu_1 + 2\mu_2} \mu_2 H_0 \begin{pmatrix} \cos(\theta) \hat{\mathbf{r}} \\ -\sin(\theta) \hat{\boldsymbol{\theta}} \\ 0 \end{pmatrix} \end{aligned} \quad (\text{A.2-12})$$

$$\begin{aligned} \mathbf{B}_2 &= -\mu_2 \nabla\Phi_2 \\ &= \mu_2 H_0 \begin{pmatrix} \cos(\theta) \hat{\mathbf{r}} \\ -\sin(\theta) \hat{\boldsymbol{\theta}} \\ 0 \end{pmatrix} + \mu_2 H_0 \frac{R^3 \frac{\mu_1}{\mu_2} - 1}{r^3 \frac{\mu_1}{\mu_2} + 2} \begin{pmatrix} 2 \cos(\theta) \hat{\mathbf{r}} \\ \sin(\theta) \hat{\boldsymbol{\theta}} \\ 0 \end{pmatrix} \end{aligned} \quad (\text{A.2-13})$$

Into cartesian coordinates, $\begin{pmatrix} \cos(\theta) \hat{\mathbf{r}} \\ -\sin(\theta) \hat{\boldsymbol{\theta}} \\ 0 \end{pmatrix}$ becomes $\hat{\mathbf{z}}$

Also, into cartesian coordinates, $\frac{1}{r^3} \begin{pmatrix} 2 \cos(\theta) \hat{\mathbf{r}} \\ \sin(\theta) \hat{\boldsymbol{\theta}} \\ 0 \end{pmatrix}$ becomes,

$$\frac{1}{r^3} \begin{pmatrix} 2 \cos(\theta) \hat{\mathbf{r}} \\ \sin(\theta) \hat{\boldsymbol{\theta}} \\ 0 \end{pmatrix} = \begin{pmatrix} \frac{3xz}{(x^2 + y^2 + z^2)^{\frac{5}{2}}} \hat{\mathbf{x}} \\ \frac{3yz}{(x^2 + y^2 + z^2)^{\frac{5}{2}}} \hat{\mathbf{y}} \\ \frac{x^2 + y^2 - 2z^2}{(x^2 + y^2 + z^2)^{\frac{5}{2}}} \hat{\mathbf{z}} \end{pmatrix} \quad (\text{A.2-14})$$

If the sphere was placed in air, then $\mu_2 = \mu_0$ and $\mu_1 = \mu_m$. Knowing that $\frac{\mu_m}{\mu_0} = \mu_r$, the field inside and outside of the sphere become,

$$\mathbf{B}_{\text{in}} = \frac{3\mu_r}{\mu_r + 2} B_0 \hat{\mathbf{z}} \quad (\text{A.2-15})$$

$$\mathbf{B}_{\text{out}} = \begin{pmatrix} B_0 R^3 \frac{\mu_r - 1}{\mu_r + 2} \frac{3xz}{(x^2 + y^2 + z^2)^{\frac{5}{2}}} \hat{\mathbf{x}} \\ B_0 R^3 \frac{\mu_r - 1}{\mu_r + 2} \frac{3yz}{(x^2 + y^2 + z^2)^{\frac{5}{2}}} \hat{\mathbf{y}} \\ B_0 \left(1 + R^3 \frac{\mu_r - 1}{\mu_r + 2} \frac{x^2 + y^2 - 2z^2}{(x^2 + y^2 + z^2)^{\frac{5}{2}}} \right) \hat{\mathbf{z}} \end{pmatrix} \quad (\text{A.2-16})$$

A.3: Finding the magnetic flux density inside and outside of an infinitely long cylinder of linear material with the external field perpendicular to the cylinder

Given the magnetic scalar potentials Φ_1 and Φ_2 inside and outside of the cylinder,

$$\Phi_1 = A_1 r \cos(\phi) \quad (\text{A.3-1})$$

$$\Phi_2 = -H_0 r \cos(\phi) + \frac{B_1}{r} \cos(\phi) \quad (\text{A.3-2})$$

The boundary conditions that occurs in this case is as it was with the sphere in section A.2.

At $r = R$, it is known that $\Phi_1 = \Phi_2$ and $-\mu_1 \frac{\partial \Phi_1}{\partial r} = -\mu_2 \frac{\partial \Phi_2}{\partial r}$. Therefore, the scalar potentials can be solved using the following,

$$A_1 R = -H_0 R + \frac{B_1}{R} \quad (\text{A.3-3})$$

$$-\mu_1 A_1 = \mu_2 H_0 + \mu_2 \frac{B_1}{R^2} \quad (\text{A.3-4})$$

Equations A.3-3 and A.3-4 can be used to solve for A_1 and B_1 ,

$$A_1 = -\frac{2\mu_2}{\mu_1 + \mu_2} H_0 \quad (\text{A.3-5})$$

$$B_1 = \frac{\mu_1 - \mu_2}{\mu_1 + \mu_2} H_0 R^2 \quad (\text{A.3-6})$$

Substituting equations A.3-5 and A.3-6 into A.3-1 and A.3-2 reveal that,

$$\Phi_1 = -\frac{2\mu_2}{\mu_1 + \mu_2} H_0 r \cos(\phi) \quad (\text{A.3-7})$$

$$\Phi_2 = -H_0 r \cos(\phi) + H_0 \frac{R^2}{r} \frac{\mu_1 - \mu_2}{\mu_1 + \mu_2} \cos(\phi) \quad (\text{A.3-8})$$

The magnetic flux density inside and outside of the sphere can now be found by applying the fact that $\mathbf{B} = -\mu\nabla\Phi$. Applying the gradient in cylindrical coordinates reveals that,

$$\begin{aligned}\mathbf{B}_1 &= -\mu_1\nabla\Phi_1 \\ &= \frac{2\mu_1}{\mu_1 + \mu_2}\mu_2H_0 \begin{pmatrix} \cos(\phi)\hat{\mathbf{r}} \\ -\sin(\phi)\hat{\boldsymbol{\phi}} \\ 0 \end{pmatrix}\end{aligned}\quad (\text{A.3-9})$$

$$\begin{aligned}\mathbf{B}_2 &= -\mu_2\nabla\Phi_2 \\ &= \mu_2H_0 \begin{pmatrix} \cos(\phi)\hat{\mathbf{r}} \\ -\sin(\phi)\hat{\boldsymbol{\phi}} \\ 0 \end{pmatrix} + \mu_2H_0\frac{R^2}{r^2}\frac{\mu_1 - \mu_2}{\mu_1 + \mu_2} \begin{pmatrix} \cos(\phi)\hat{\mathbf{r}} \\ \sin(\phi)\hat{\boldsymbol{\phi}} \\ 0 \end{pmatrix}\end{aligned}\quad (\text{A.3-10})$$

Into cartesian coordinates, $\begin{pmatrix} \cos(\theta)\hat{\mathbf{r}} \\ -\sin(\theta)\hat{\boldsymbol{\theta}} \\ 0 \end{pmatrix}$ becomes $\hat{\mathbf{x}}$.

Also, into cartesian coordinates, $\frac{1}{r^2} \begin{pmatrix} \cos(\phi)\hat{\mathbf{r}} \\ \sin(\phi)\hat{\boldsymbol{\phi}} \\ 0 \end{pmatrix}$ becomes,

$$\frac{1}{r^2} \begin{pmatrix} \cos(\phi)\hat{\mathbf{r}} \\ \sin(\phi)\hat{\boldsymbol{\phi}} \\ 0 \end{pmatrix} = \begin{pmatrix} \frac{x^2 - y^2}{(x^2 + y^2)^2}\hat{\mathbf{x}} \\ 2xy \\ \frac{(x^2 + y^2)^2}\hat{\mathbf{y}} \\ 0 \end{pmatrix}\quad (\text{A.3-11})$$

If the cylinder was embedded in air, then $\mu_2 = \mu_0$ and $\mu_1 = \mu_m$. Knowing that $\frac{\mu_m}{\mu_0} = \mu_r$, the field inside and outside of the sphere become,

$$\mathbf{B}_{\text{in}} = \frac{2\mu_r}{\mu_r + 1}B_0\hat{\mathbf{x}}\quad (\text{A.3-12})$$

$$\mathbf{B}_{\text{out}} = \begin{pmatrix} B_0 \left(1 + R^2 \frac{\mu_r - 1}{\mu_r + 1} \frac{x^2 - y^2}{(x^2 + y^2)^2} \right) \hat{\mathbf{x}} \\ B_0 R^2 \frac{\mu_r - 1}{\mu_r + 1} \frac{2xy}{(x^2 + y^2)^2} \hat{\mathbf{y}} \\ 0 \end{pmatrix}\quad (\text{A.3-13})$$

A.4: Finding the static field induced torque on a sphere

Given the torque induced on a magnetic dipole moment is,

$$\boldsymbol{\tau} = \mathbf{m} \times \mathbf{B}_0 \quad (\text{A.4-1})$$

Where $\boldsymbol{\tau}$ is the torque induced, \mathbf{m} is the magnetic dipole moment, and \mathbf{B}_0 is the field that it is placed in. \mathbf{m} can be written in terms of B field inside of the object by its relationship with magnetization, \mathbf{M} . By definition, $\mathbf{M} = \frac{\Sigma \mathbf{m}}{V}$, and $\mathbf{m} = \mathbf{M}dV$ where dV is the volume of a magnetic moment. Also knowing that $\mathbf{M} = \chi \mathbf{H}$ and $\mathbf{B} = \mu_m \mathbf{H}$, equation A.4-1 becomes the following,

$$\boldsymbol{\tau} = \left(\frac{\chi dV}{\mu_m} \mathbf{B} \times \mathbf{B}_0 \right) \quad (\text{A.4-2})$$

From equation A.4-2, when performed using the computational methods relevant to this thesis, dV is the volume of each element exported from the modeling software. Solving for the cross product in equation A.4-2 reveals that,

$$\boldsymbol{\tau} = \frac{\chi dV}{\mu_m} \begin{vmatrix} \hat{\mathbf{i}} & \hat{\mathbf{j}} & \hat{\mathbf{k}} \\ B_x & B_y & B_z \\ B_{0x} & B_{0y} & B_{0z} \end{vmatrix} \quad (\text{A.4-3})$$

It is important to note that $\hat{\mathbf{i}}$, $\hat{\mathbf{j}}$, and $\hat{\mathbf{k}}$ are the same unit vectors as $\hat{\mathbf{x}}$, $\hat{\mathbf{y}}$, and $\hat{\mathbf{z}}$. Simplifying equation A.4-3 reveals that,

$$\boldsymbol{\tau} = \frac{\chi dV}{\mu_m} \begin{pmatrix} (B_y B_{0z} - B_z B_{0y}) \hat{\mathbf{i}} \\ (B_z B_{0x} - B_x B_{0z}) \hat{\mathbf{j}} \\ (B_x B_{0y} - B_y B_{0x}) \hat{\mathbf{k}} \end{pmatrix} \quad (\text{A.4-4})$$

In the case of the sphere, a similar method can be used to find the torque. Again, using equations 2, 3, and 4, equation A.4-1 becomes A.4-2 for which a cross product needs to be solved for and A.4-2 becomes A.4-3. Recalling from equation 8 the field inside of a sphere, equation A.4-3 becomes

$$\boldsymbol{\tau}_{\text{sphere}} = \left(\frac{\chi dV}{\mu_m} \right) \left(\frac{3\mu_r}{\mu_r + 2} \right) \begin{vmatrix} \hat{\mathbf{i}} & \hat{\mathbf{j}} & \hat{\mathbf{k}} \\ B_{0x} & B_{0y} & B_{0z} \\ B_{0x} & B_{0y} & B_{0z} \end{vmatrix} \quad (\text{A.4-5})$$

Equation A.4-5 is a cross product of a vector with itself and reduces to zero.

$$\boldsymbol{\tau}_{\text{sphere}} = 0 \quad (\text{A.4-6})$$

Equation A.4-1 cannot however, be used to find the torque inside of a finite cylinder as the magnetic field inside of a cylinder of linear material placed in an external field \mathbf{B}_0 is not known. Instead, using the computational method outlined in Chapter 2 of this thesis, the elements of a discretized cylinder are exported. For each element, the induced force, \mathbf{F}_m , is found and the torque from each element at a distance, \mathbf{r} , from the centre of the cylinder.

$$\boldsymbol{\tau}_{\text{cylinder}} = \sum_{\text{Volume}} \mathbf{F}_m \times \mathbf{r} \quad (\text{A.4-6})$$

Equation A.4-6 was used to find the torque induced on a cylinder of finite length. The torque of each element was found and then summed up to find the net torque on the entire structure.

Appendix B: Certificate of Tests for Stainless Steel Rods

B.1: Stainless steel 316 rod, diameter of 0.5 in. and length of 1 ft.



Certificate of Test

PRODEC QUALITY Page: 1

HEAT E161781 ORDER 675604/ 01 BOL 0240047 * CERTIFICATION * 07/18/17

SHIP TO:


----- YOUR ORDER & DATE -----
 0151531-STR 7/14/17 CUST# 0773001 CUST TAG#0009253

----- ITEM DESCRIPTION -----
 GRADE 316L/316 PRODEC QUALITY Ship Condition CONDA
 Size 316L RND CDA CONDA .2500 x 144.000 RL
 Country of Melt: UNITED KINGDOM Country of Mfg.: UNITED KINGDOM
 NAFTA Country of Origin is Country of Melt

No weld repair
 Free of mercury contamination, Free of radiation contamination
 No WEEE relevant substances; Meets EU electrical ROHS

Total Bundles 1 Total Weight 1989 Approx. Hot Red. Ratio 540:1

WO 2072828 Bundles: 1B

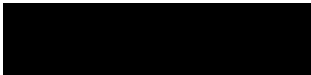
----- SPECIFICATIONS -----
 AMS 5648M, 5653H SAE AMS-00-S-763D
 ASME SA182 2007-2015 Ed ASME SA193 2015 Edition
 ASME SA479 2007-2015 Ed. ASME SA320 B8M CL1, 2015 Ed.
 ASTM A182/A182M 16a ASTM A262 15 Practice A/E
 ASTM A276-17 ASTM A314 15
 ASTM A479/A479M 17 ASTM A484 16
 ASTM A320 17a B8M Class 1 ASTM A193 16 B8M
 NACE MR0175-09, ISO 15156:09 DFARS 252.225.7009 10/4/11
 Federal Spec QQ-S-763F UNS S31600, AISI 316
 UNS S31603, AISI 316L Prodec Quality
 EN 10204 Type 3.1 Document RA-53 RAW 316L
 1.4401 K5CrNiMo17-12-2 316 Butech BU-36 Rev 2
 QTC is a prolongation of bar NACE MR0103-10
 Sol Ann 1900F min/WQ Bars are Eddy Current tested

----- MECHANICAL & OTHER TESTS -----
 Hardness as shipped (203 HB)
 Hardness as shipped 92 HRB
 Grain size 4.0 Tensile strength, KSI (MPa) 100.4 (692)
 Micro OK 0.2% Yield Strength, KSI (MPa) 81.2 (560)
 Intergranular corrosion OK 1% Yield Strength, KSI (MPa) 91.4 (630)
 Elongation 1/2 in 4D 44.0
 Elongation 1/2 in 5D 40.0
 Reduction of area % 67.9

-- Continued --

HEAT # E161781

 TRACER # 0511631US





Certificate of Test

PRODEC QUALITY

Page: 2

HEAT E161781 ORDER 675604/ 01 BOL 0240047 * CERTIFICATION * 07/18/17

SHIP TO:



CHEMICAL COMPOSITION				
Carbon (C)		.017	Manganese (Mn)	1.570
Phosphorus (P)		.032	Sulphur (S)	.025
Silicon (Si)		.540	Chromium (Cr)	16.890
Nickel (Ni)	10.090		Cobalt (Co)	.363
Copper (Cu)		.470	Moly (Mo)	2.040
Nitrogen (N)		.054		
Iron (Fe)	Balance			
Melt Practice		BAF		
Refining Practice		AOD		
De-long Ferrite		4.4		

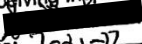
Knowingly & willfully falsifying or concealing a material act on this form, or making false, fictitious or fraudulent statements or representations herein could constitute a felony punishable under federal statutes. We hereby certify that the test results shown in this report are correct and accurate as contained in the records of the company and are in compliance with the specifications, codes, and standards listed above.

M.F. Marcanio, Quality Manager

HEAT # E161781

 TRACER # 0511631US

DO NOT WRITE IN THESE SPACES

Receiving Inspection
 By: 
 Date: 7-21-17

Outokumpu Stainless Bar, LLC



B.2: Stainless steel 316 rod, diameter of 0.25 in. and length of 1 ft.



Certificate of Test

PRODEC QUALITY

Page: 1

HEAT E161781 ORDER 675604/ 01 BOL 0240047 * CERTIFICATION * 07/18/17

SHIP TO:



----- YOUR ORDER & DATE -----
 0151531-STR 7/14/17 CUST# 0773001 CUST TAG#0009253

----- ITEM DESCRIPTION -----
 GRADE 316L/316 PRODEC QUALITY Ship Condition CONDA
 Size 316L RND CDA CONDA .2500 x 144.000 RL
 Country of Melt: UNITED KINGDOM Country of Mfg.: UNITED KINGDOM
 NAFTA Country of Origin is Country of Melt

No weld repair
 Free of mercury contamination, Free of radiation contamination
 No WEEE relevant substances; Meets EU electrical ROHS

Total Bundles 1 Total Weight 1989 Approx. Hot Red. Ratio 540:1

WO 2072828 Bundles: 1B

----- SPECIFICATIONS -----
 AMS 5648M, 5653H SAE AMS-00-S-763D
 ASME SA182 2007-2015 Ed ASME SA193 2015 Edition
 ASME SA479 2007-2015 Ed. ASME SA320 B8M CLL, 2015 Ed.
 ASTM A182/A182M 16a ASTM A262 15 Practice A/E
 ASTM A276-17 ASTM A314 15
 ASTM A479/A479M 17 ASTM A484 16
 ASTM A320 17a B8M Class 1 ASTM A193 16 B8M
 NACE MR0175-09, ISO 15156:09 DFARS 252.225.7009 10/4/11
 Federal Spec QQ-S-763F UNS S31600, AISI 316
 UNS S31603, AISI 316L Prodec Quality
 EN 10204 Type 3.1 Document RA-53 RAN 316L
 1.4401 X5CrNiMo17-12-2 316 Butech BU-36 Rev 2
 OTC is a prolongation of bar NACE MR0103-10
 Sol Ann 1900F min/WQ Bars are Eddy Current tested

----- MECHANICAL & OTHER TESTS -----
 Hardness as shipped (203 HB)
 Hardness as shipped 92 HRB
 Grain size 4.0
 Micro OK
 Intergranular corrosion OK
 Tensile strength, KSI (MPa) 100.4 (692)
 0.2% Yield Strength, KSI (MPa) 81.2 (560)
 1% Yield Strength, KSI (MPa) 91.4 (630)
 Elongation % in 4D 44.0
 Elongation % in 5D 40.0
 Reduction of area % 67.9

-- Continued --

HEAT # E161781



TRACER # 0511631US





Certificate of Test

PRODEC QUALITY

Page: 2


HEAT E161781 ORDER 675604/ 01 BOL 0240047 * CERTIFICATION * 07/18/17

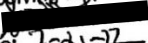
SHIP TO:

-----CHEMICAL COMPOSITION-----			
Carbon (C)	.017	Manganese (Mn)	1.570
Phosphorus (P)	.032	Sulphur (S)	.025
Silicon (Si)	.540	Chromium (Cr)	16.890
Nickel (Ni)	10.090	Cobalt (Co)	.363
Copper (Cu)	.470	Moly (Mo)	2.040
Nitrogen (N)	.054		
Iron (Fe)	Balance		
Melt Practice	EAF		
Refining Practice	AOD		
De-long Ferrite	4.4		

Knowingly & willfully falsifying or concealing a material act on this form, or making false, fictitious or fraudulent statements or representations herein could constitute a felony punishable under federal statutes. We hereby certify that the test results shown in this report are correct and accurate as contained in the records of the company and are in compliance with the specifications, codes, and standards listed above.

M.F. Marcanio, Quality Manager

HEAT # E161781

 TRACER # 0511631US

RECEIVED
 8/18/17
 Receiving Inspection
 By: 
 Date: 7-21-17

Outokumpu Stainless Bar, LLC




B.3: Stainless steel 304 rod, diameter of 0.5 in. and length of 1 ft.



Certificate of Test TR#0526972 US

HEAT E171238 ORDER 675603/ 01 BOL 0241966 * PRODEC QUALITY Page: 1
 * CERTIFICATION * 01/19/18

SHIP TO: [REDACTED]

HEAT # E171238



TRACER # 0526972US



Receiving Inspection

By: [REDACTED]

Date: 1/29/18

----- YOUR ORDER & DATE -----
 0151527-WIN 7/14/17 CUST# 0773001 CUST TAG#0009062

----- ITEM DESCRIPTION -----
 GRADE 304L/304 PRODEC QUALITY Ship Condition CONDA
 Size 304L RND CDA CONDA 2500 x 144.000 RL
 Country of Melt: UNITED KINGDOM Country of Mfg.: UNITED KINGDOM
 NAFTA Country of Origin is Country of Melt

No weld repair
 Free of mercury contamination, Free of radiation contamination
 No WEEE relevant substances; Meets EU electrical ROHS

Total Bundles 1 Total Weight 2041 Approx. Hot Red. Ratio 540:1

WO 2077180 Bundles: 1E

 AMS 5639J, 5647K
 ASME SA182 2007-2015 Ed
 ASME SA484 2015 Ed.
 ASME SA193 B8 2015 Edition
 ASTM A262 15 Practice A/E
 ASTM A314 15
 ASTM A484/A484M 16
 ASTM A193 16 B8
 NACE MR0175-09, ISO 15156:09
 Federal Spec QQ-S-763F
 UNS S30403, AISI 304L
 Prodec Quality
 EN 10204 Type 3.1 Document
 NACE MR0103-10
 QTC is a prolongation of bar
 No WEEE relevant substances
 Bars are Eddy Current tested

----- SPECIFICATIONS -----
 SAE AMS-00-S-763D
 ASME SA479 2007-2015 Ed.
 ASME SA320 B8 CLL, 2015 Ed.
 ASTM A182/A182M 17
 ASTM A276-17
 ASTM A479/A479M 17
 ASTM A320 17a B8 Class 1
 Solution Annealed Condition
 DFAES 252, 225, 7049, 70/4/11
 UNS S30400, AISI 304
 Free of Cont. carbide network
 RA-53 RAM 304L
 ASTM F899 12b
 ASTM F899 12b
 1.4301 K2CrNi18-9 304
 Sol Ann 1900F min/WQ

----- MECHANICAL & OTHER TESTS -----
 Hardness as shipped (222 HB)
 Hardness as shipped 95 HRB
 Grain size 4.0
 Micro OK
 Intergranular corrosion OK
 Tensile strength, KSI (MPa) 108.5 (748)
 0.2% Yield Strngth, KSI (MPa) 97.3 (671)
 1% Yield Strength, KSI (MPa) 100.9 (696)
 Elongation % in 4D 48.0
 Elongation % in 5D 46.7
 Reduction of area % 70.2

-- Continued --



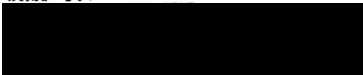
Certificate of Test TR#0526972 US

PRODEC QUALITY

Page: 2

HEAT E171238 ORDER 675603/ 01 BOL 0241966 * CERTIFICATION * 01/19/18

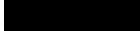
SHIP TO:



----- CHEMICAL COMPOSITION -----					
Carbon	(C)	.023	Manganese	(Mn)	1.860
Phosphorus	(P)	.036	Sulphur	(S)	.024
Silicon	(Si)	.280	Chromium	(Cr)	18.170
Nickel	(Ni)	8.180	Cobalt	(Co)	.187
Copper	(Cu)	.610	Moly	(Mo)	.420
Nitrogen	(N)	.077	Columbium	(Cb)	.030
Titanium	(Ti)	.002	Aluminum	(Al)	.006
Tin	(Sn)	.015	Boron	(B)	.002
Tantalum	(Ta)	.001	Vanadium	(V)	.070
Tungsten	(W)	.060			
Columbium/ Tantalum (Cb+Ta)		.031			
Iron	(Fe)	Balance			
Melt Practice		EAF			
Refining Practice		AOD			
De-long Ferrite					

Knowingly & willfully falsifying or concealing a material act on this form, or making false, fictitious or fraudulent statements or representations herein could constitute a felony punishable under federal statutes. We hereby certify that the test results shown in this report are correct and accurate as contained in the records of the company and are in compliance with the specifications, codes, and standards listed above.

M.F. Marcanio, Quality Manager



B.4: Stainless steel 304 rod, diameter of 0.25 in. and length of 1 ft.



Certificate of Test

PRODEC QUALITY

Page: 2

HEAT E180464 ORDER 683865/ 03 BOL 0245602 * CERTIFICATION * 12/17/18

SHIP TO:



		CHEMICAL COMPOSITION	
Carbon (C)	.022	Manganese (Mn)	1.910
Phosphorus (P)	.032	Sulphur (S)	.026
Silicon (Si)	.280	Chromium (Cr)	18.260
Nickel (Ni)	8.160	Cobalt (Co)	.283
Copper (Cu)	.710	Moly (Mo)	.470
Nitrogen (N)	.062	Columbium (Cb)	.030
Titanium (Ti)	.003	Aluminum (Al)	.006
Tin (Sn)	.010	Boron (B)	.001
Tantalum (Ta)	.002	Vanadium (V)	.070
Tungsten (W)	.057		
Columbium/ Tantalum (Cb+Ta)	.032		
Iron (Fe)	Balance		
Melt Practice	EAF		
Refining Practice	AOD		
De-long Ferrite			

Knowingly & willfully falsifying or concealing a material act on this form, or making false, fictitious or fraudulent statements or representations herein could constitute a felony punishable under federal statutes. We hereby certify that the test results shown in this report are correct and accurate as contained in the records of the company and are in compliance with the specifications, codes, and standards listed above.

M.F. Marciano, Quality Manager

Outokumpu Stainless Bar, LLC

CONTROLLED
BY ALLOYS

Receiving Inspection

By: [REDACTED]

Date: 12/17/18

HEAT # E180464



TRACER # 0556932US





Certificate of Test

PRODEC QUALITY

Page: 1

HEAT E180464 ORDER 683865/ 03 BOL 0245602 * CERTIFICATION * 12/17/18

SHIP TO:



----- YOUR ORDER & DATE -----
 0166593-STR 9/06/18 CUST# 0773001 CUST TAG#0009069

----- ITEM DESCRIPTION -----
 GRADE 304L/304 PRODEC QUALITY Ship Condition CONDA
 Size 304L RND CDA CONDA .5000 x 144.000 RL
 Country of Melt: UNITED KINGDOM Country of Mfg.: UNITED STATES
 No weld repair
 Free of mercury contamination, Free of radiation contamination
 No WEEE relevant substances; Meets RoHS-2011/65/EU and 2015/863

Total Bundles 5 Total Weight 10166 Approx. Hot Red. Ratio 133:1

WO 2087603 Bundles: 1A, 1B, 1G, 1H, 1J

----- SPECIFICATIONS -----
 MFG TO FINISHED BAR IN THE USA FROM BILLETS IMPORTED UNITED KINGDOM
 AMS 5639J, 5647K SAE AMS-QQ-S-763D
 ASME BPVC II.A-2017 SA-182 ASME SA-479 2017 Ed.
 ASME SA-484 2017 Ed. ASME SA-320 B8 CL1, 2017 Ed.
 ASME SA-193 B8 2017 Edition ASTM A182/A182M 18a
 ASTM A262 15 Practice A/E ASTM A276/A276M 17
 ASTM A314 15 ASTM A479/A479M 18
 ASTM A484/A484M 18a ASTM A320 17a B8 Class 1
 ASTM A193 16 B8 Solution Annealed Condition
 NACE MR0175-09, ISO 15156:09 DFARS 252.225-7009 10/4/11
 Federal Spec QQ-S-763F UNS S30400, AISI 304
 UNS S30403, AISI 304L Free of Cont. carbide network
 Prodec Quality RA-53 RAM 304L
 EN 10204 Type 3.1 Document ASTM F899 12b
 NACE MR0103-10 ASTM F899 12b
 QTC is a prolongation of bar 1.4301 X2CrNi18-9 304
 DFARS 225.7002-3(B)(1) No WEEE relevant substances
 Sol Ann 1900F min/WQ Bars are Eddy Current tested

----- MECHANICAL & OTHER TESTS -----
 Hardness as shipped 248 HB
 Hardness as shipped (99 HRB)
 Grain size 6.0 Tensile strength, KSI (MPa) 102.0 (703)
 Micro OK 0.2% Yield Strngth, KSI (MPa) 74.8 (516)
 Intergranular corrosion OK
 Elongation % in 4D 46.0
 Reduction of area % 74.2

-- Continued --

Outokumpu Stainless Bar, LLC

HEAT # E180464



TRACER # 0556932US



Appendix C: Calibration Reports for Laboratory Equipment

C.1: MR03-025 Force Sensor (Mark-10 Co., Copiague, USA)

Mark-10 Corporation

MARK-10

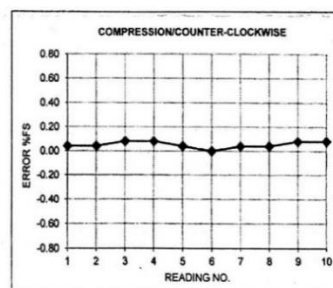
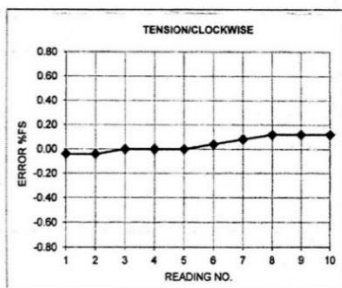
Tel: Fax:

CERTIFICATE OF CALIBRATION

MODEL NO. MR03-025
 SERIAL NO: 3550218
 DESCRIPTION: FORCE SENSOR
 CAPACITY: 0.25 LBF

RELATIVE HUMIDITY (%): 39%
 TEMPERATURE (°F): 70.0 °F
 TOLERANCE (±%FS): 0.15
 RESOLUTION: 0.0001

READING NUMBER	MASTER READING	TENSION/CLOCKWISE	ERROR %FS	COMPRESSION/COUNTER CLOCKWISE	ERROR %FS
1	0.0250	0.0249	-0.04	0.0251	0.04
2	0.0500	0.0499	-0.04	0.0501	0.04
3	0.0750	0.0750	0.00	0.0752	0.08
4	0.1000	0.1000	0.00	0.1002	0.08
5	0.1250	0.1250	0.00	0.1251	0.04
6	0.1500	0.1501	0.04	0.1500	0.00
7	0.1750	0.1752	0.08	0.1751	0.04
8	0.2000	0.2003	0.12	0.2001	0.04
9	0.2250	0.2253	0.12	0.2252	0.08
10	0.2500	0.2503	0.12	0.2502	0.08



We hereby certify that the above instrument was calibrated according to procedures traceable to the National Institute of Standards & Technology (NIST) utilizing calibration equipment traceable to the requirements of ISO 9001:2008, Registration No. 10001297 QM08, and ISO/IEC 17025:2005, Registration No. L1021-1. Applicable NIST traceability numbers: 90802-A02, 80234-G01, 00523-A01, 80324-H01, 00502-X01, 70708-A05, 91209-A01, 71030-X01, 1689182, 822/272801-06, 822/278785-10, L82707710408, 25430

By: _____

Date: 12/23/10

C.2: SPX123 Laboratory Balance (Ohaus Co., Parsippany, USA)



www.innocal.com

NIST Traceable Calibration Report



Reference Number: **996713**
PO Number: **70422N0021**

MRI Device Testing Inc (MRIDT)

Manufacturer: Ohaus
Model Number: SPX123
Description: Scale, Portable Balance 120g x 0.001g
Asset Number: CP263141
Serial Number: B649414665
Procedure: DS Universal Scale

Calibration Date: 04/26/2017
Calibration Due Date: 04/26/2018
Condition As Found: Initial Calibration
Condition As Left: In Tolerance, No adjustment

Remarks:

NIST-traceable calibration performed on the unit referenced above in accordance with customer requirements, published specifications and the lab's standard operating procedures. No adjustments were made to the unit.

Standards Utilized

Asset No.	Manufacturer	Model No.	Description	Cal. Date	Due Date
CP40273	Rice Lake Weighing Systems	11884	Mass, 1g- 20kg ASTM class 1 set	10/31/2016	04/30/2018

Calibration Data

FUNCTION TESTED	Nominal Value	As Found	Out of Tol	As Left	Out of Tol	CALIBRATION TOLERANCE
Zero Reference	0.000 g	0.000		Same		0.000 to 0.000 g
Weighing Accuracy	10.000 g	10.000		Same		9.983 to 10.017 g [EMU 580 µg]
	20.000 g	20.000		Same		19.983 to 20.017 g [EMU 580 µg]
	30.000 g	30.001		Same		29.983 to 30.017 g [EMU 590 µg]
	40.000 g	40.002		Same		39.983 to 40.017 g [EMU 590 µg]
	50.000 g	50.001		Same		49.983 to 50.017 g [EMU 600 µg]
	60.000 g	60.000		Same		59.983 to 60.017 g [EMU 600 µg]
	70.000 g	70.001		Same		69.983 to 70.017 g [EMU 600 µg]
	80.000 g	80.002		Same		79.983 to 80.017 g [EMU 610 µg]
	100.000 g	100.002		Same		99.983 to 100.017 g [EMU 660 µg]
	120.000 g	120.003		Same		119.983 to 120.017 g [EMU 660 µg]
Shift/Load Test Front Right	20.000 g	20.002		Same		19.983 to 20.017 g [EMU 580 µg]
Front Left	20.000 g	20.002		Same		19.983 to 20.017 g [EMU 580 µg]
Left Rear	20.000 g	20.003		Same		19.983 to 20.017 g [EMU 580 µg]
Right Rear	20.000 g	20.003		Same		19.983 to 20.017 g [EMU 580 µg]
Repeatability Test	Pass	PASS		Same		Pass/Fail



Temperature: 21° C
 Humidity: 63% RH
 Rpt. No.: 1151373

Calibration Performed By:				Quality Reviewer:	
Name	ID #	Title	Phone	Name	Date
Agosto, Axel	352	Metrologist	847-327-5339	Ziegler, Jeff	4/26/2017

This report may not be reproduced, except in full, without written permission of Innocot. The results stated in this report relate only to the items tested or calibrated. Measurements reported herein are traceable to SI units via national standards maintained by NIST and were performed in compliance with MIL-STD-45662A, ANSI/NCSS Z540-1-1994, 10CFR50, Appendix B, ISO 9002-94, and ISO 17025:2005. Guard Banding, if reported on this certificate, is applied at a Z-factor of 30% for test points with a test uncertainty ratio (TUR) below 4:1. The estimated measurement uncertainty (EMU), if reported on this certificate, is being reported at a confidence level of 95% or K=2 unless otherwise noted in the remarks section.

Report Number: 1151373

Ohaus / SPX123, Scale, Portable Balance 120g x 0.001g



Appendix D: Permission to Use Copyrighted Figures

D.1: Allen D. Elster of MRIquestions.com

Copyright Issues

During 30 years of radiology practice I have collected numerous cases, drawings, and illustrations relating to MR imaging and MR physics. Although most of these are of my own creation, a number of images, photographs, and graphic materials have come from colleagues in academics and industry. A number of these externally derived elements have been incorporated into this web site, and I have given full credit to these sources and/or obtained permission for their use when possible.

Unfortunately, the provenances surrounding some of these graphic elements collected over three decades have been lost or forgotten. It is not my intent to misuse anyone's copyrighted work, and I fully respect artist and content owner's rights. I pledge to fully comply with the [Digital Millenium Copyright Act of 1998](#), investigating any alleged infringement notices by the owner and removing any verified item or link promptly. To make such a notice, please click [here](#) and provide details. Alternatively, I would sincerely appreciate your allowing continued use of these materials on the site if you simply tell me how they should be credited.

In addition to graphic elements, this web site also contains links and pdfs to a number of scientific papers of which the original authors and publishers may retain copyrights. Many of these works are already widely available on the internet from the authors' own web sites or institutional repositories. A substantial number of papers and images are distributed under open access and Creative Commons licenses. Some very old works are now in the public domain. Others I have personally purchased or received as reprint gifts from authors over the years. As you read these papers on my web site, consider yourself as a student guest sitting in my private library that I maintain for teaching purposes. I would ask all readers of this site not to copy, repost, or distribute these works lest they be taken down and not available for the higher good of science education.

This web site has been created as a public service to the greater scientific community. I receive no compensation or external support for this endeavor and have personally assumed all costs of producing and maintaining this site. So, if an item is discovered that has unintentionally infringed on someone else's work, I ask understanding and forgiveness and promise to quickly make things right.

On the flip side, all other images and text on this website are my own creation, so any commercial use of this material without my express written consent is prohibited. However, **if you wish to use a small number of my images (in a non-commercial setting, such as for lectures, graduate theses, etc), feel free to do so, crediting them "Courtesy of Allen D. Elster, MRIquestions.com"**.

Allen Elster

D.2: Standards Council of Canada Letter of Agreement



Standards Council of Canada
Conseil canadien des normes

tel [REDACTED] fax [REDACTED] web www.scc.ca

2019-07-09

Xiao Fan Ding
[REDACTED]

Subject: Content Reproduction of ISO/TS 10974:2018 - (the "Publication(s)")

Dear Xiao Fan Ding,

In response to your recent request and based on the information that you have provided to us, the Standards Council of Canada is pleased to grant Xiao Fan Ding (the "Requestor") permission to reproduce the following:

- The specific content from the Publication(s) listed below;
- Reproduction of the content on/in 'Computational Methods for Assessing Static Field Induced Torque on Medical Implants in the MR Environment'
- Date of the reproduction: August 31, 2019

Please note that the following conditions apply, as per ISO's Policy for the Distribution, Sales and Reproduction of ISO Publications and the Protection of ISO's Copyright (ISO POCOSA) Agreement and/or IEC Sales Policy:

1. The content represents less than 10% of the total content of the Publication(s) referenced; and
2. These permissions are based on the condition that recognition will be given by the Requestor in all reproductions of the Content, by the inclusion of the attached notation:

"Copied by Xiao Fan Ding with the permission of the Standards Council of Canada (SCC) on behalf of ISO."; and

3. Include where the standard can be purchased.

Content:

ISO/TS 10974:2018: Figure 2 – Relationship between MR scanner output fields (RF, gradient, B_0) and hazards (test method clause numbers in parentheses)



Standards Council of Canada
Conseil canadien des normes

tel [redacted] fax [redacted] web www.scc.ca

Please confirm via signature below, your understanding and acceptance of the conditions and permissions outlined above.

Sincerely,

Pat Bonilla
2019.07.09 10:50:29 -04'00'

Pat Bonilla
Manager, Canadian Standards Development

Date

Requestor: I have read, understood, and will comply with the Conditions:

[redacted signature]

Xiao Fan Ding

19/07/09

Date

D.3: John Wiley and Sons License Terms and Conditions

8/6/2019

RightsLink - Your Account

JOHN WILEY AND SONS LICENSE TERMS AND CONDITIONS

Aug 06, 2019

This Agreement between Mr. Xiao Fan Ding – Xiao Fan Ding ("You") and John Wiley and Sons ("John Wiley and Sons") consists of your license details and the terms and conditions provided by John Wiley and Sons and Copyright Clearance Center.

License Number	4643221036929
License date	Aug 06, 2019
Licensed Content Publisher	John Wiley and Sons
Licensed Content Publication	Medical Physics
Licensed Content Title	The role of magnetic susceptibility in magnetic resonance imaging: MRI magnetic compatibility of the first and second kinds
Licensed Content Author	John F. Schenck
Licensed Content Date	Jun 4, 1998
Licensed Content Volume	23
Licensed Content Issue	6
Licensed Content Pages	36
Type of Use	Dissertation/Thesis
Requestor type	University/Academic
Format	Print and electronic
Portion	Figure/table
Number of figures/tables	1
Original Wiley figure/table number(s)	Figure 2
Will you be translating?	No
Title of your thesis / dissertation	Development of a Computational Method for Assessing Static Field Induced Torque on Medical Implants
Expected completion date	Aug 2019
Expected size (number of pages)	150
Requestor Location	Mr. Xiao Fan Ding [REDACTED]
	[REDACTED]
	Attn: Mr. Xiao Fan Ding
Publisher Tax ID	EU826007151
Total	0.00 USD
Terms and Conditions	

TERMS AND CONDITIONS

This copyrighted material is owned by or exclusively licensed to John Wiley & Sons, Inc. or one of its group companies (each a "Wiley Company") or handled on behalf of a society with which a Wiley Company has exclusive publishing rights in relation to a particular work (collectively "WILEY"). By clicking "accept" in connection with completing this licensing transaction, you agree that the following terms and conditions apply to this transaction (along with the billing and payment terms and conditions established by the Copyright Clearance Center Inc., ("CCC's Billing and Payment terms and conditions"), at the time that you opened your RightsLink account (these are available at any time at <http://myaccount.copyright.com>).

Terms and Conditions

- The materials you have requested permission to reproduce or reuse (the "Wiley Materials") are protected by copyright.
- You are hereby granted a personal, non-exclusive, non-sub licensable (on a stand-alone basis), non-transferable, worldwide, limited license to reproduce the Wiley Materials for the purpose specified in the licensing process. This license, **and any CONTENT (PDF or image file) purchased as part of your order**, is for a one-time use only and limited to any maximum distribution number specified in the license. The first instance of republication or reuse granted by this license must be completed within two years of the date of the grant of this license (although copies prepared before the end date may be distributed thereafter). The Wiley Materials shall not be used in any other manner or for any other purpose, beyond what is granted in the license. Permission is granted subject to an appropriate acknowledgement given to the author, title of the material/book/journal and the publisher. You shall also duplicate the copyright notice that appears in the Wiley publication in your use of the Wiley Material. Permission is also granted on the understanding that nowhere in the text is a previously published source acknowledged for all or part of this Wiley Material. Any third party content is expressly excluded from this permission.
- With respect to the Wiley Materials, all rights are reserved. Except as expressly granted by the terms of the license, no part of the Wiley Materials may be copied, modified, adapted (except for minor reformatting required by the new Publication), translated, reproduced, transferred or distributed, in any form or by any means, and no derivative works may be made based on the Wiley Materials without the prior permission of the respective copyright owner. **For STM Signatory Publishers clearing permission under the terms of the STM Permissions Guidelines only, the terms of the license are extended to include subsequent editions and for editions in other languages, provided such editions are for the work as a whole in situ and does not involve the separate exploitation of the permitted figures or extracts.** You may not alter, remove or suppress in any manner any copyright, trademark or other notices displayed by the Wiley Materials. You may not license, rent, sell, loan, lease, pledge, offer as security, transfer or assign the Wiley Materials on a stand-alone basis, or any of the rights granted to you hereunder to any other person.
- The Wiley Materials and all of the intellectual property rights therein shall at all times remain the exclusive property of John Wiley & Sons Inc, the Wiley Companies, or their respective licensors, and your interest therein is only that of having possession of and the right to reproduce the Wiley Materials pursuant to Section 2 herein during the continuance of this Agreement. You agree that you own no right, title or interest in or to the Wiley Materials or any of the intellectual property rights therein. You shall have no rights hereunder other than the license as provided for above in Section 2. No right, license or interest to any trademark, trade name, service mark or other branding ("Marks") of WILEY or its licensors is granted hereunder, and you agree that you shall not assert any such right, license or interest with respect thereto
- NEITHER WILEY NOR ITS LICENSORS MAKES ANY WARRANTY OR REPRESENTATION OF ANY KIND TO YOU OR ANY THIRD PARTY, EXPRESS, IMPLIED OR STATUTORY, WITH RESPECT TO THE MATERIALS OR THE ACCURACY OF ANY INFORMATION CONTAINED IN THE MATERIALS, INCLUDING, WITHOUT LIMITATION, ANY IMPLIED WARRANTY OF MERCHANTABILITY, ACCURACY, SATISFACTORY QUALITY, FITNESS FOR A PARTICULAR PURPOSE, USABILITY, INTEGRATION OR NON-INFRINGEMENT AND ALL SUCH WARRANTIES ARE HEREBY EXCLUDED BY WILEY AND ITS LICENSORS AND WAIVED BY YOU.
- WILEY shall have the right to terminate this Agreement immediately upon breach of this Agreement by you.
- You shall indemnify, defend and hold harmless WILEY, its Licensors and their respective directors, officers, agents and employees, from and against any actual or threatened claims, demands, causes of action or proceedings arising from any breach of this Agreement by you.
- IN NO EVENT SHALL WILEY OR ITS LICENSORS BE LIABLE TO YOU OR ANY OTHER PARTY OR ANY OTHER PERSON OR ENTITY FOR ANY SPECIAL, CONSEQUENTIAL, INCIDENTAL, INDIRECT, EXEMPLARY OR PUNITIVE DAMAGES, HOWEVER CAUSED, ARISING OUT OF OR IN CONNECTION WITH THE DOWNLOADING, PROVISIONING, VIEWING OR USE OF THE MATERIALS REGARDLESS OF THE FORM OF ACTION, WHETHER FOR BREACH OF CONTRACT, BREACH OF WARRANTY, TORT, NEGLIGENCE, INFRINGEMENT OR OTHERWISE (INCLUDING, WITHOUT LIMITATION, DAMAGES BASED ON LOSS OF PROFITS, DATA, FILES, USE, BUSINESS OPPORTUNITY OR CLAIMS OF THIRD PARTIES), AND WHETHER OR NOT THE PARTY HAS BEEN ADVISED OF THE POSSIBILITY OF SUCH DAMAGES. THIS LIMITATION SHALL APPLY NOTWITHSTANDING ANY FAILURE OF ESSENTIAL PURPOSE OF ANY LIMITED REMEDY PROVIDED HEREIN.
- Should any provision of this Agreement be held by a court of competent jurisdiction to be illegal, invalid, or unenforceable, that provision shall be deemed amended to achieve as nearly as possible the same economic effect as the original provision,

8/6/2019

RightsLink - Your Account

and the legality, validity and enforceability of the remaining provisions of this Agreement shall not be affected or impaired thereby.

- The failure of either party to enforce any term or condition of this Agreement shall not constitute a waiver of either party's right to enforce each and every term and condition of this Agreement. No breach under this agreement shall be deemed waived or excused by either party unless such waiver or consent is in writing signed by the party granting such waiver or consent. The waiver by or consent of a party to a breach of any provision of this Agreement shall not operate or be construed as a waiver of or consent to any other or subsequent breach by such other party.
- This Agreement may not be assigned (including by operation of law or otherwise) by you without WILEY's prior written consent.
- Any fee required for this permission shall be non-refundable after thirty (30) days from receipt by the CCC.
- These terms and conditions together with CCC's Billing and Payment terms and conditions (which are incorporated herein) form the entire agreement between you and WILEY concerning this licensing transaction and (in the absence of fraud) supersedes all prior agreements and representations of the parties, oral or written. This Agreement may not be amended except in writing signed by both parties. This Agreement shall be binding upon and inure to the benefit of the parties' successors, legal representatives, and authorized assigns.
- In the event of any conflict between your obligations established by these terms and conditions and those established by CCC's Billing and Payment terms and conditions, these terms and conditions shall prevail.
- WILEY expressly reserves all rights not specifically granted in the combination of (i) the license details provided by you and accepted in the course of this licensing transaction, (ii) these terms and conditions and (iii) CCC's Billing and Payment terms and conditions.
- This Agreement will be void if the Type of Use, Format, Circulation, or Requestor Type was misrepresented during the licensing process.
- This Agreement shall be governed by and construed in accordance with the laws of the State of New York, USA, without regards to such state's conflict of law rules. Any legal action, suit or proceeding arising out of or relating to these Terms and Conditions or the breach thereof shall be instituted in a court of competent jurisdiction in New York County in the State of New York in the United States of America and each party hereby consents and submits to the personal jurisdiction of such court, waives any objection to venue in such court and consents to service of process by registered or certified mail, return receipt requested, at the last known address of such party.

WILEY OPEN ACCESS TERMS AND CONDITIONS

Wiley Publishes Open Access Articles in fully Open Access Journals and in Subscription journals offering Online Open. Although most of the fully Open Access journals publish open access articles under the terms of the Creative Commons Attribution (CC BY) License only, the subscription journals and a few of the Open Access Journals offer a choice of Creative Commons Licenses. The license type is clearly identified on the article.

The Creative Commons Attribution License

The [Creative Commons Attribution License \(CC-BY\)](#) allows users to copy, distribute and transmit an article, adapt the article and make commercial use of the article. The CC-BY license permits commercial and non-

Creative Commons Attribution Non-Commercial License

The [Creative Commons Attribution Non-Commercial \(CC-BY-NC\) License](#) permits use, distribution and reproduction in any medium, provided the original work is properly cited and is not used for commercial purposes.(see below)

Creative Commons Attribution-Non-Commercial-NoDerivs License

The [Creative Commons Attribution Non-Commercial-NoDerivs License \(CC-BY-NC-ND\)](#) permits use, distribution and reproduction in any medium, provided the original work is properly cited, is not used for commercial purposes and no modifications or adaptations are made. (see below)

Use by commercial "for-profit" organizations

Use of Wiley Open Access articles for commercial, promotional, or marketing purposes requires further explicit permission from Wiley and will be subject to a fee.

Further details can be found on Wiley Online Library <http://olabout.wiley.com/WileyCDA/Section/id-410895.html>

Other Terms and Conditions:

<https://s100.copyright.com/MyAccount/web/jsp/viewprintablelicensefrommyorders.jsp?ref=eae2650d-a3fa-4967-88e4-1b25b3607240&email=>

3/4

8/6/2019

RightsLink - Your Account

v1.10 Last updated September 2015

Questions? customer-care@copyright.com or +1-855-239-3415 (toll free in the US) or +1-978-646-2777.

D.4: ASTM International License Terms and Conditions

8/9/2019

RightsLink - Your Account

ASTM INTERNATIONAL LICENSE TERMS AND CONDITIONS

Aug 09, 2019

This Agreement between Mr. Xiao Fan Ding -- Xiao Fan Ding ("You") and ASTM International ("ASTM International") consists of your license details and the terms and conditions provided by ASTM International and Copyright Clearance Center.

License Number	4644831390222
License date	Aug 09, 2019
Licensed Content Publisher	ASTM International
Licensed Content Publication	ASTM Standard
Licensed Content Title	ASTM F2213-17 Standard Test Method for Measurement of Magnetically Induced Torque on Medical Devices in the Magnetic Resonance Environment
Licensed Content Date	Sep 1, 2017
I would like to...	Thesis/Dissertation
Requestor type	Academic institution
Format	Print, Electronic
Portion	chart/graph/table/figure
Number of charts/graphs/tables/figures	2
Rights for	Main product
Duration of use	Current edition and up to 5 years
Creation of copies for the disabled	no
With minor editing privileges	no
For distribution to	Canada
In the following language(s)	Original language of publication
With incidental promotional use	no
The lifetime unit quantity of new product	0 to 499
Order reference number	
Title	Development of a Computational Method for Assessing Static Field Induced Torque on Medical Implants
Institution name	University of Western Ontario
Expected presentation date	Aug 2019
Portions	Figure 6 on Page 6 Figure 7 on Page 7
Requestor Location	Mr, Xiao Fan Ding [REDACTED]
	[REDACTED]
	Attn: Mr, Xiao Fan Ding
Billing Type	Invoice
Billing Address	Mr, Xiao Fan Ding [REDACTED]

8/9/2019

RightsLink - Your Account

Attn: Mr. Xiao Fan Ding

0,00 USD

Total

Terms and Conditions

Permissions Terms & Conditions

Introduction

The publisher for this copyrighted material is ASTM International ("ASTM"). By clicking "accept" in connection with completing this licensing transaction, you ("Licensee") agree that the following terms and conditions apply to this transaction (along with the Billing and Payment terms and conditions established by Copyright Clearance Center, Inc. ("CCC"), at the time that Licensee opened your CCC account.

Limited License:

ASTM hereby grants to Licensee a non-exclusive license to use this material. Licenses are for one-time use only with a maximum distribution equal to the number that Licensee identified in the licensing process. No emailing of ASTM documents is permitted. Licenses are for reproduction rights only and do not include a copy of the material.

It is the Licensee's responsibility to ensure that the material is original to ASTM's and does not contain the proprietary rights of another person or entity.

Altering/Modifying Material: Not Permitted

Licensee may not alter or modify the material in any manner. Licensee may not translate the material into another language.

Reservation of Rights:

ASTM reserves all rights not specifically granted in the combination of (i) the license details provided by Licensee and accepted in the course of this licensing transaction, (ii) these terms and conditions and (iii) CCC's Billing and Payment terms and conditions.

License Contingent on Payment:

While Licensee may exercise the rights licensed immediately upon issuance of the license at the end of the licensing process for the transaction, provided that Licensee have disclosed complete and accurate details of your proposed use, no license is finally effective unless and until full payment is received from Licensee (either by ASTM or by CCC) as provided in CCC's Billing and Payment terms and conditions. If full payment is not received on a timely basis, then any license preliminarily granted shall be deemed automatically revoked and shall be void as if never granted. Further, in the event that Licensee breach any of these terms and conditions or any of CCC's Billing and Payment terms and conditions, the license is automatically revoked and shall be void as if never granted. Use of materials as described in a revoked license, as well as any use of the materials beyond the scope of an unrevoked license, may constitute copyright infringement and ASTM reserves the right to take any and all action to protect its copyright in the materials.

Copyright Notice:

Licensee must include the following copyright and permission notice in connection with any reproduction of the licensed material: "Reproduced, with permission from [FULL CITATION], copyright ASTM International, 100 Barr Harbor Drive, West Conshohocken, PA 19428."

Disclaimer of Warranty:

Unless specified in this license, all express or implied conditions, representations and warranties, including any implied warranty of merchantability, fitness for a particular purpose or non-infringement are disclaimed, except to the extent that these disclaimers are held to be legally invalid.

Verification:

ASTM has the right to verify compliance with this license, at its expense, and at any time during the course of normal business hours. To do so, ASTM will engage an independent consultant, subject to a confidentiality agreement, to review your use of ASTM's material. Licensee agrees to permit access to its information and computer systems for this purpose. Verification will take place upon no less than 15 days notice, during normal business hours and in a manner that does not interfere unreasonably with Licensee's operations. If verification reveals unlicensed or prohibited use of the ASTM material, Licensee agrees to reimburse ASTM for the costs incurred in verification and reimburse ASTM for any unlicensed/prohibited uses. By invoking this procedure, ASTM does not waive any of its rights to enforce this Agreement or to protect its intellectual property by any other means permitted by law.

Limitation of Liability:

To the extent not prohibited by law, in no event will ASTM and CCC be liable for any loss, damage, lost data or for special, indirect, consequential or punitive damages, however caused regardless of the theory of liability, arising out of or related to the use of ASTM material. In no event will ASTM's and CCC's liability exceed the amount paid by Licensee under this License Agreement.

No Transfer of License:

This license is personal to you and may not be sublicensed, assigned, or transferred by you to any other person without publisher's written permission.

Governing Law, Venue, and Jurisdiction:

This license shall be interpreted and construed in accordance with the laws of the Commonwealth of Pennsylvania. Licensee agrees to submit to jurisdiction and venue in the state and federal courts of Pennsylvania for any dispute which may arise under this license. Licensee also agrees to waive any claim of immunity it may possess.

8/9/2019

RightsLink - Your Account

Integration

ASTM hereby objects to any terms contained in any purchase order, acknowledgment, check endorsement or other writing prepared by Licensee, which terms are inconsistent with these terms and conditions or CCC's Billing and Payment terms and conditions. These terms and conditions, together with CCC's Billing and Payment terms and conditions (which are incorporated herein), comprise the entire agreement between Licensee and ASTM International (and CCC) concerning this licensing transaction. In the event of any conflict between your obligations established by these terms and conditions and those established by CCC's Billing and Payment terms and conditions, these terms and conditions shall control. No modification of this license will be binding, unless in writing and signed by an authorized representative of each party (or, in the case of ASTM, by CCC on ASTM's behalf).

Licensee acknowledges and agrees that the adoption, enactment, reference, or incorporation of any of the ASTM material by any government or agency has not and will not effect, transfer, modify or alter the ASTM Rights in the ASTM materials in any way.

There are additional terms and conditions, established by Copyright Clearance Center, Inc. ("CCC") as the administrator of this licensing service that relate to billing and payment for licenses provided through this service. Those terms and conditions apply to each transaction as if they were restated here. As a user of this service, you agreed to those terms and conditions at the time that you established your account, and you may see them again at any time at <http://myaccount.copyright.com>.

Content Services:

Subject to these terms of use, any terms set forth on the particular order, and payment of the applicable fee, Licensee may make the following uses of the ordered materials:

Content Rental: Licensee may access and view a single electronic copy of the materials ordered for the time period designated at the time the order is placed. Access to the materials will be provided through a dedicated content viewer or other portal, and access will be discontinued upon expiration of the designated time period. An order for Content Rental does not include any rights to print, download, save, create additional copies, to distribute or to reuse in any way the full text or parts of the materials.

The materials may be accessed and used only by the person who placed the Order or the person on whose behalf the order was placed and only in accordance with the terms included in the particular order.

Licensee acknowledges and agrees that the adoption, enactment, reference, or incorporation of any of the ASTM material by any government or agency has not and will not effect, transfer, modify or alter the ASTM Rights in the ASTM materials in any way.

There are additional terms and conditions, established by Copyright Clearance Center, Inc. ("CCC") as the administrator of this licensing service that relate to billing and payment for licenses provided through this service. Those terms and conditions apply to each transaction as if they were restated here. As a user of this service, you agreed to those terms and conditions at the time that you established your account, and you may see them again at any time at <http://myaccount.copyright.com>.

Other Terms and Conditions:

v1.1

Questions? customercare@copyright.com or +1-855-239-3415 (toll free in the US) or +1-978-646-2777.

8/9/2019

RightsLink - Your Account

ASTM INTERNATIONAL LICENSE TERMS AND CONDITIONS

Aug 09, 2019

This Agreement between Mr. Xiao Fan Ding -- Xiao Fan Ding ("You") and ASTM International ("ASTM International") consists of your license details and the terms and conditions provided by ASTM International and Copyright Clearance Center.

License Number	4644831450434
License date	Aug 09, 2019
Licensed Content Publisher	ASTM International
Licensed Content Publication	ASTM Standard
Licensed Content Title	ASTM F2503-13 Standard Practice for Marking Medical Devices and Other Items for Safety in the Magnetic Resonance Environment
Licensed Content Date	Jun 1, 2013
I would like to...	Thesis/Dissertation
Requestor type	Academic institution
Format	Print, Electronic
Portion	chart/graph/table/figure
Number of charts/graphs/tables/figures	1
Rights for	Main product
Duration of use	Current edition and up to 5 years
Creation of copies for the disabled	no
With minor editing privileges	no
For distribution to	Canada
In the following language(s)	Original language of publication
With incidental promotional use	no
The lifetime unit quantity of new product	0 to 499
Order reference number	
Title	Development of a Computational Method for Assessing Static Field Induced Torque on Medical Implants
Institution name	University of Western Ontario
Expected presentation date	Aug 2019
Portions	Table 1 on Page 3
Requestor Location	Mr, Xiao Fan Ding [REDACTED] [REDACTED] [REDACTED]
Billing Type	Attn: Mr, Xiao Fan Ding Invoice
Billing Address	Mr, Xiao Fan Ding [REDACTED]

8/9/2019

RightsLink - Your Account



Attn: Mr. Xiao Fan Ding

0,00 USD[Total](#)[Terms and Conditions](#)**Permissions Terms & Conditions****Introduction**

The publisher for this copyrighted material is ASTM International ("ASTM"). By clicking "accept" in connection with completing this licensing transaction, you ("Licensee") agree that the following terms and conditions apply to this transaction (along with the Billing and Payment terms and conditions established by Copyright Clearance Center, Inc. ("CCC"), at the time that Licensee opened your CCC account.

Limited License:

ASTM hereby grants to Licensee a non-exclusive license to use this material. Licenses are for one-time use only with a maximum distribution equal to the number that Licensee identified in the licensing process. No emailing of ASTM documents is permitted. Licenses are for reproduction rights only and do not include a copy of the material.

It is the Licensee's responsibility to ensure that the material is original to ASTM's and does not contain the proprietary rights of another person or entity.

Altering/Modifying Material: Not Permitted

Licensee may not alter or modify the material in any manner. Licensee may not translate the material into another language.

Reservation of Rights:

ASTM reserves all rights not specifically granted in the combination of (i) the license details provided by Licensee and accepted in the course of this licensing transaction, (ii) these terms and conditions and (iii) CCC's Billing and Payment terms and conditions.

License Contingent on Payment:

While Licensee may exercise the rights licensed immediately upon issuance of the license at the end of the licensing process for the transaction, provided that Licensee have disclosed complete and accurate details of your proposed use, no license is finally effective unless and until full payment is received from Licensee (either by ASTM or by CCC) as provided in CCC's Billing and Payment terms and conditions. If full payment is not received on a timely basis, then any license preliminarily granted shall be deemed automatically revoked and shall be void as if never granted. Further, in the event that Licensee breach any of these terms and conditions or any of CCC's Billing and Payment terms and conditions, the license is automatically revoked and shall be void as if never granted. Use of materials as described in a revoked license, as well as any use of the materials beyond the scope of an unrevoked license, may constitute copyright infringement and ASTM reserves the right to take any and all action to protect its copyright in the materials.

Copyright Notice:

Licensee must include the following copyright and permission notice in connection with any reproduction of the licensed material: "Reproduced, with permission from [FULL CITATION], copyright ASTM International, 100 Barr Harbor Drive, West Conshohocken, PA 19428."

Disclaimer of Warranty:

Unless specified in this license, all express or implied conditions, representations and warranties, including any implied warranty of merchantability, fitness for a particular purpose or non-infringement are disclaimed, except to the extent that these disclaimers are held to be legally invalid.

Verification:

ASTM has the right to verify compliance with this license, at its expense, and at any time during the course of normal business hours. To do so, ASTM will engage an independent consultant, subject to a confidentiality agreement, to review your use of ASTM's material. Licensee agrees to permit access to its information and computer systems for this purpose. Verification will take place upon no less than 15 days notice, during normal business hours and in a manner that does not interfere unreasonably with Licensee's operations. If verification reveals unlicensed or prohibited use of the ASTM material, Licensee agrees to reimburse ASTM for the costs incurred in verification and reimburse ASTM for any unlicensed/prohibited uses. By invoking this procedure, ASTM does not waive any of its rights to enforce this Agreement or to protect its intellectual property by any other means permitted by law.

Limitation of Liability:

To the extent not prohibited by law, in no event will ASTM and CCC be liable for any loss, damage, lost data or for special, indirect, consequential or punitive damages, however caused regardless of the theory of liability, arising out of or related to the use of ASTM material. In no event will ASTM's and CCC's liability exceed the amount paid by Licensee under this License Agreement.

No Transfer of License:

This license is personal to you and may not be sublicensed, assigned, or transferred by you to any other person without publisher's written permission.

Governing Law, Venue, and Jurisdiction:

This license shall be interpreted and construed in accordance with the laws of the Commonwealth of Pennsylvania. Licensee agrees to submit to jurisdiction and venue in the state and federal courts of Pennsylvania for any dispute which may arise under this license. Licensee also agrees to waive any claim of immunity it may possess.

8/9/2019

RightsLink - Your Account

Integration

ASTM hereby objects to any terms contained in any purchase order, acknowledgment, check endorsement or other writing prepared by Licensee, which terms are inconsistent with these terms and conditions or CCC's Billing and Payment terms and conditions. These terms and conditions, together with CCC's Billing and Payment terms and conditions (which are incorporated herein), comprise the entire agreement between Licensee and ASTM International (and CCC) concerning this licensing transaction. In the event of any conflict between your obligations established by these terms and conditions and those established by CCC's Billing and Payment terms and conditions, these terms and conditions shall control. No modification of this license will be binding, unless in writing and signed by an authorized representative of each party (or, in the case of ASTM, by CCC on ASTM's behalf).

Licensee acknowledges and agrees that the adoption, enactment, reference, or incorporation of any of the ASTM material by any government or agency has not and will not effect, transfer, modify or alter the ASTM Rights in the ASTM materials in any way.

There are additional terms and conditions, established by Copyright Clearance Center, Inc. ("CCC") as the administrator of this licensing service that relate to billing and payment for licenses provided through this service. Those terms and conditions apply to each transaction as if they were restated here. As a user of this service, you agreed to those terms and conditions at the time that you established your account, and you may see them again at <http://myaccount.copyright.com>.

Content Services:

Subject to these terms of use, any terms set forth on the particular order, and payment of the applicable fee, Licensee may make the following uses of the ordered materials:

Content Rental: Licensee may access and view a single electronic copy of the materials ordered for the time period designated at the time the order is placed. Access to the materials will be provided through a dedicated content viewer or other portal, and access will be discontinued upon expiration of the designated time period. An order for Content Rental does not include any rights to print, download, save, create additional copies, to distribute or to reuse in any way the full text or parts of the materials.

The materials may be accessed and used only by the person who placed the Order or the person on whose behalf the order was placed and only in accordance with the terms included in the particular order.

Licensee acknowledges and agrees that the adoption, enactment, reference, or incorporation of any of the ASTM material by any government or agency has not and will not effect, transfer, modify or alter the ASTM Rights in the ASTM materials in any way.

There are additional terms and conditions, established by Copyright Clearance Center, Inc. ("CCC") as the administrator of this licensing service that relate to billing and payment for licenses provided through this service. Those terms and conditions apply to each transaction as if they were restated here. As a user of this service, you agreed to those terms and conditions at the time that you established your account, and you may see them again at any time at <http://myaccount.copyright.com>.

Other Terms and Conditions:

v1.1

Questions? customercare@copyright.com or +1-855-239-3415 (toll free in the US) or +1-978-646-2777.

D.5: Cambridge University Press License Cover Sheet

PLS Clear

PARTIES:

1. **Cambridge University Press** [CompanyNumber] (Licensor); and
2. **Xiao Fan Ding** (Licensee).

Thank you for your recent permission request. Some permission requests for use of material published by the Licensor, such as this one, are now being facilitated by PLSclear.

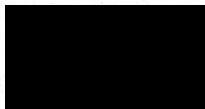
Set out in this licence cover sheet (the **Licence Cover Sheet**) are the principal terms under which Licensor has agreed to license certain Licensed Material (as defined below) to Licensee. The terms in this Licence Cover Sheet are subject to the attached General Terms and Conditions, which together with this Licence Cover Sheet constitute the licence agreement (the **Licence**) between Licensor and Licensee as regards the Licensed Material. The terms set out in this Licence Cover Sheet take precedence over any conflicting provision in the General Terms and Conditions.

Free Of Charge Licence Terms

Licence Date: 08/08/2019
 PLSclear Ref No: 17085

The Licensor

Company name: Cambridge University Press
 Address:



The Licensee

Licensee Contact Name: Xiao Fan Ding
 Licensee Address:



Licensed Material

title: MRI FROM PICTURE TO PROTON
 ISBN: 9780521818599
 publisher: Cambridge University Press

figure number & title / caption	Figure 9.12
Are you requesting permission to reuse your own work?	No. I am NOT the author
page number	180
Are you using the content as a prop?	content will NOT be used as a prop
reproduction colour	Full Colour
reproduction size	Thumbnail
positioning	inside or later pages
will it be cropped	Yes
figure number & title / caption	Figure 9.13
Are you requesting permission to reuse your own work?	No. I am NOT the author
page number	180
Are you using the content as a prop?	content will NOT be used as a prop
reproduction colour	Full Colour
reproduction size	Thumbnail
positioning	inside or later pages

For Use In Licensee's Publication(s)

usage type	Book, Journal, Magazine or Academic Paper...-Thesis
language	English
publication title	Development of a Computational Method for Assessing Static Field Induced Torque on Medical Implants
type of document	Thesis

Rights Granted

Exclusivity:	Non-Exclusive
Format:	Thesis
Language:	English
Territory:	
Duration:	Lifetime of Licensee's Edition
Maximum Circulation:	0

GENERAL TERMS AND CONDITIONS

1. Definitions and Interpretation

1.1 Capitalised words and expressions in these General Terms and Conditions have the meanings given to them in the Licence Cover Sheet.

1.2 In this Licence any references (express or implied) to statutes or provisions are references to those statutes or provisions as amended or re-enacted from time to time. The term including will be construed as illustrative, without limiting the sense or scope of the words preceding it. A reference to in writing or written includes faxes and email. The singular includes the plural and vice versa.

2. Grant of Rights

2.1 The Licensor grants to Licensee the non-exclusive right to use the Licensed Material as specified in the Licence Cover Sheet.

2.2 The rights licensed to Licensee under this Licence do not include the right to use any third party copyright material incorporated in the Licensed Material. Licensee should check the Licensed Material carefully and seek permission for the use of any such third party copyright material from the relevant copyright owner(s).

2.3 Unless otherwise stated in the Licence Cover Sheet, the Licensed Material may be:

2.3.1 subjected to minor editing, including for the purposes of creating alternative formats to provide access for a beneficiary person (provided that any such editing does not amount to derogatory treatment); and/or

2.3.2 used for incidental promotional use (such as online retail providers' search facilities).

2.4 Save as expressly permitted in this Licence or as otherwise permitted by law, no use or modification of the Licensed Material may be made by Licensee without Licensor's prior written permission.

3. Copyright Notice and Acknowledgement

3.1 Licensee must ensure that the following notices and acknowledgements are reproduced prominently alongside each reproduction by Licensee of the Licensed Material:

3.1.1 the title and author of the Licensed Material;

3.1.2 the copyright notice included in the Licensed Material; and

3.1.3 the statement "Reproduced with permission of The Licensor through PLSclear."

4. Reversion of Rights

4.1 The rights licensed to Licensee under this Licence will terminate immediately and automatically upon the earliest of the following events to occur:

4.1.1 the Licensed Material not being used by Licensee within 18 months of the Licence Date;

4.1.2 expiry of the Licence Duration; or

4.1.3 the Maximum Circulation being reached.

5. Miscellaneous

5.1 By using the Licensed Material, Licensee will be deemed to have accepted all the terms and conditions contained in this Licence.

5.2 This Licence contains the entire understanding and agreement of the parties relating to its subject matter and supersedes in all respects any previous or other existing arrangements, agreements or understandings between the parties whether oral or written in relation to its subject matter.

5.3 Licensee may not assign this Licence or any of its rights or obligations hereunder to any third party without Licensor's prior written consent.

5.4 This Licence is governed by and shall be construed in accordance with the laws of England and Wales and the parties hereby irrevocably submit to the non-exclusive jurisdiction of the Courts of England and Wales as regards any claim, dispute or matter arising under or in relation to this Licence.

Curriculum Vitae

Name: Xiao Fan Ding

Education: **M.Sc. Medical Biophysics**
Western University
London, Ontario, Canada
Supervisor: Dr. Blaine Chronik
2017-Present

B.Sc. Biology – Biophysics (Honours) with Distinction
Ryerson University
Toronto, Ontario, Canada
2013-2017

Honours and Awards: **ISMIRM Educational Stipend**
2018-Present

Western Graduate Research Scholarship
2017-Present

Dean's Honour List
2015-2017

Related Work Experience: **Volunteer (Mobile App Promoter)**
London Health Research Day, Lawson Health Research
Institute
London, Ontario, Canada
2019

Graduate Research Assistant
Department of Physics and Astronomy, Western University
London, Ontario, Canada
Supervisor: Dr. Blaine Chronik
2017-Present

Graduate Teaching Assistant
Department of Physics and Astronomy, Western University
London, Ontario, Canada
2017-2019

Pitch Presenter

OxiLight, Ryerson Biomedical Zone, Ryerson University
 Toronto, Ontario, Canada
 2016

Tutor (Grade 12 Biology and Physics)

Everest Academy
 Toronto, Ontario, Canada
 2015-2017

Group Leader

Student Spaceflight Experiment Program, Faculty of Science,
 Ryerson University
 Toronto, Ontario, Canada
 2015

**Conference
Presentations:**

Ding X., Handler W. B., Chronik B.A.
 “Uncertainty Analysis of Torque Measurement Methods
 Described in ASTM F2213-17”
 Abstract 1441, Digital Poster Presentation
 ISMRM 27th Annual Meeting
 Montreal, Canada (May 2019)

Ding X., Handler W. B., Chronik B.A.
 “Uncertainty Analysis of Torque Measurement Methods
 Described in ASTM F2213-17”
 Abstract 13, Poster Presentation
 Imaging Network Ontario 17th Annual Symposium
 London, Ontario, Canada (March 2019)